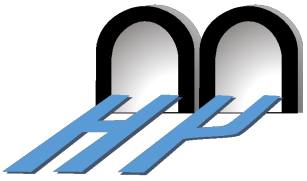

Pre-normative research for safety of hydrogen driven vehicles and transport through tunnels and similar confined spaces

Fuel Cells and Hydrogen Joint Undertaking (FCH JU)
Grant Agreement Number 826193

# Deliverable 5.3
# Report on QRA methodology for tunnels and similar confined spaces

Lead authors: URS (P. Russo),
Contributing authors: DTU (F. Markert)
UU (S. Kashkarov, S. Sivaraman,
D. Makarov, V. Molkov)
KIT (M. Kuznetsov)

Version: 220227
Delivery date for internal review: 18 February 2022
Due date: 28 February 2022
Dissemination level: Public


FUEL CELLS AND HYDROGEN
JOINT UNDERTAKING

| Deliverable administration | | | | | |
|---|---|---|---|---|---|
| Work Package | WP5. First responders' intervention strategies and tactics for hydrogen accidents in underground transportation systems and risk assessment | | | | |
| N. and title | D5.3. Report on QRA methodology for tunnels and similar confined spaces | | | | |
| Type | Report | | | | |
| Status | Draft/Working/**Released** | Due | M36 | Date | 28-02-2022 |
| Comments | | | | | |

| Development and revision | | | |
|---|---|---|---|
| Version N. | Date | Authors | Description |
| 210908 | 08 Sept 2021 | P.Russo, URS; F. Markert, DTU | 1st draft ToC |
| 211130 | 30 Nov 2021 | P.Russo, URS; F. Markert, DTU; S. Kashkarov, UU | Description of road and railway tunnel case studies (M5.4) |
| 211207 | 07 Dec 2021 | M. Kuznetsov, KIT | DDT model for road tunnel case study |
| 220203 | 03 Feb 2022 | S. Kashkarov, UU | UU methodology-draft |
| 220207 | 07 Feb 2022 | F. Markert, DTU | Underground car park case study-draft |
| 220208 | 08 Feb 2022 | M. Kuznetsov, KIT | DDT model for railway tunnel case study |
| 220212 | 12 Feb 2022 | S. Kashkarov, UU | UU methodology revised |
| 220214 | 14 Feb 2022 | F. Markert, DTU | Underground car park case revised |
| 220222 | 22 Feb 2022 | S. Giannissi, NCSRD | Deliverable review |
| 250222 | 22 Feb 2022 | S. Kashkarov, UU | Deliverable review |

## Disclaimer



## Acknowledgments

This project has received funding from the Fuel Cells and Hydrogen 2 Joint Undertaking (JU) under grant agreement No 826193. The JU receives support from the European Union's Horizon 2020 research and innovation programme and United Kingdom, Germany, Greece, Denmark, Spain, Italy, Netherlands, Belgium, France, Norway, Switzerland.


FUEL CELLS AND HYDROGEN
JOINT UNDERTAKING

## Summary

The HyTunnel-CS project aims to conduct internationally leading pre-normative research (PNR) to close knowledge gaps and technological bottlenecks in the provision of safety and acceptable level of risk in the use of hydrogen and fuel cell cars as well as hydrogen delivery transport in underground transportation systems. Work Package 5 (WP5) of HyTunnel-CS focus on first responders' intervention strategies and tactics for hydrogen accidents in underground transportation systems and risk assessment.

This document presents the deliverable (D5.3) on the QRA methodologies developed by the task partners and on the results of application of these methodologies to selected scenarios as consequence of release of hydrogen in road and railway tunnels, and underground car parks.

## Keywords

QRA; risk assessment; hydrogen safety; hazards; consequence assessment; unignited release; jet fire; deflagration; detonation; quantitative risk assessment; hydrogen in tunnel; explosion; mitigation; engineering correlation; numerical simulation; experiment; tunnel safety; ventilation; hydrogen vehicle; hydrogen dispersion; hydrogen combustion; car park.

# Table of contents

# Nomenclature and abbreviation

| | |
|---|---|
| $E$ | Energy (J) |
| $EP$ | Escalation probability (-) |
| $F$ | Frequency (accident/$10^6$ vehicle-mile/year; rupture/vehicle/year) |
| $HRR/A$ | Fire specific heat release rate (W/m$^2$) |
| $L$ | Length (m) |
| $m$ | Mass (kg) |
| $N$ | Number of individuals affected (fatality/rupture) |
| $P$ | Probability (-); pressure (Pa) |
| $Risk$ | Risk (fatality/vehicle/year; £/accident) |
| $V$ | Tank volume (m$^3$) |

**Subscripts**

| | |
|---|---|
| $ch$ | Chemical (energy) |
| $fat.$ | Fatality |
| $fire\ init.$ | Initiation of a fire |
| $H2$ | Hydrogen |
| $loc.fire$ | Localised fire |
| $m$ | Mechanical (energy) |
| $no\ leak$ | No hydrogen leak |
| $p-crash\ fire$ | Post-crash fire |
| $sev.accident$ | Severe accident |
| $ser.injury$ | Serious injury |
| $sl.injury$ | Slight injury |
| $tot$ | Total |
| $TPRD\ fail.$ | Failure of TPRD |
| $tun.accident$ | Accident in a tunnel |
| $t.rupt.$ | Hydrogen tank rupture |

**Abbreviations**

| | |
|---|---|
| AADT | Annual average daily traffic |
| DDT | Deflagration-to-Detonation Transition |
| EP | Escalating probability |
| ETA | Event Tree Analysis |
| FRR | fire-resistance rating |
| GTR#13 | Global Technical Regulation No.13 |
| $H_2$ | Hydrogen |
| HFCV | Hydrogen fuel cell vehicle |
| HGV | Heavy good vehicle |
| HRR | Heat release rate |
| HRR/A | Specific heat release rate |
| LFL | Lower Flammability Limit |
| µLNB | Microleak-no-burst |
| MIE | Minimum Ignition Energy |
| NTP | Normal Temperature and Pressure |
| NWP | Nominal working pressure |
| OEM | Original equipment manufacturer |

| | |
|---|---|
| PIARC | Permanent International Association of Road Congresses |
| PNR | Pre-Normative Research |
| PPP | Pressure Peaking Phenomena |
| PRD | Pressure relief device |
| QRA | Quantitative risk assessment |
| SOC | State of charge |
| TNT | Trinitrotoluene |
| TPRD | Thermally activated pressure relief device. |
| UFL | Upper Flammability Limit |
| UIC | International Union of Railways |

## Definitions

**Accident** is an unforeseen and unplanned event or circumstance causing loss or injury.

**Flammability range** is the range of concentrations between the lower and the upper flammability limits. *The lower flammability limit* (LFL) is the lowest concentration of a combustible substance in a gaseous oxidizer that will propagate a flame. *The upper flammability limit* (UFL) is the highest concentration of a combustible substance in a gaseous oxidizer that will propagate a flame.

**Deflagration** is the phenomenon of combustion zone propagation at the velocity lower than the speed of sound (sub-sonic) into a fresh, unburned mixture.

**Detonation** is the process of combustion zone propagating at the velocity higher than the speed of sound (supersonic) in the unreacted mixture

**Fire resistance rating** is a measure of time for which a passive fire protection system can withstand a standard fire resistance test.

**F-N curves** are curves relating the probability per year of causing N or more fatalities (F) to N. Such curves may be used to express societal risk criteria and to describe the safety levels of particular facilities.

**Harm** is physical injury or damage to health.

**Hazard** is any potential source or condition that has the potential for causing damage to people, property and the environment.

**Hazard distance** is a distance from the (source of) hazard to a determined (by physical or numerical modelling, or by a regulation) physical effect value (normally, thermal or pressure) that may lead to a harm condition (ranging from “no harm” to “max harm”) to people, equipment or environment.

**Hydrogen safety engineering** is application of scientific and engineering principles to the protection of life, property and environment from adverse effects of incidents/accidents involving hydrogen.

**Incident** is something that occurs casually in connection with something else.

**Normal temperature and pressure** (NTP) conditions are: temperature 293.15 K and pressure 101.325 kPa.

**State of Charge** (SoC) is the ratio of hydrogen density in the compressed hydrogen storage system (CHSS) to the density at nominal working pressure (NWP) rated at the standard temperature 15 °C

**Separation distance** is the minimum separation between a hazard source and an object (human, equipment or environment) which will mitigate the effect of a likely foreseeable incident and prevent a minor incident escalating into a larger incident.

**Risk** is the combination of the probability of an event and its consequence.

# List of figures

## List of tables

# 1 Introduction and scope

Hydrogen energy is recognized by many European governments as an important part of the development to achieve a more sustainable energy infrastructure. Great efforts are spent to build up a hydrogen supply chain to support the increasing number of hydrogen electrical fuel cell vehicles. This includes an increasing production and transport of bulk amounts of hydrogen by tankers and other means. Naturally, both the vehicles and tankers will use the common infrastructures established for traffic. Thus, it has to be ensured that the traffic infrastructures are capable to withstand the potential specific risks that may arise from these new technologies. Hereunder, the safe transport using ordinary FCH vehicles and smaller vans through tunnels is a very important question.

For the vehicles private transport and to answer these questions the FCH2-JU is funding the Horizon 2020 project "Pre-normative research for safety of hydrogen driven vehicles and transport through tunnels and similar confined spaces" (project no. 826193) – the HyTunnel-CS project.

Due to sustainability and environmental aspects, more tunnels are being established worldwide, as they potentially reduce travelling distances and protect neighbours from traffic emissions and noise. New hydrogen vehicles such as cars, busses and heavy goods trucks will also use such infrastructures and therefore the risks in case of a serious accident have to be estimated to ensure the safety of the tunnel users and the tunnel structure.

In order to have an appropriate assessment tool for hydrogen vehicles transport through tunnels a new QRA methodology is developed and presented here.

A quantitative risk assessment is a logical and systematic approach to estimate the risk level associated with certain hazardous events scenarios. It is an assessment that uses special quantitative tools and techniques to establish the risk to people from defined scenarios with a given set of parameters. It involves estimating the likelihood and consequences of hazardous events and expressing the findings as risk to people.

A prior literature review revealed a number of risk assessment models and tools, as e.g. QRAM, (Caliendo and De Guglielmo, 2017; Caliendo and Genovese, 2020), TUNRIM RWS, IRAM, QRAFT, BASt and the PIARC (PIARC 2012; Rázga et al., 2015; Zulauf *et al.*, 2012; ). These models and tools are evaluated concerning four major points:

1) inclusion of hydrogen as a dangerous substance,
2) description of the implemented models,
3) their respective potential for analysis of "low frequency – high consequence" events,
4) how they treat typical thermal and pressure hazards and the applied thresholds for humans and structures.

From the analysis it can be concluded that either they do not include hydrogen as a dangerous substance (i.e., QRAM, TUNRIM RWS, IRAM, QRAFT, BASt and the PIARC), or the "low frequency – high consequence" events are not analysed (i.e., QRA developed by Erhart et al., 2019).

The overall conclusion was that a new methodology is needed to embrace all the safety risks imposed by the increasing number of hydrogen vehicles in tunnels. While most of the proposed models for the QRA in tunnels focused on the societal risk with respect to evaluating the safety

issues and safety measures of the tunnel, a QRA methodology for a tunnel considering the safety issues and safety measures of the vehicle itself is a lack.

Indeed, when it comes to the first responders' intervention strategies and tactics for hydrogen accidents in a tunnel, a probabilistic indicator like the "societal risk" being visualized in FN curves may not provide sufficient decision support within the scope of any actual emergency situation. QRA evaluations should be used in the pre-planning phase only, but they still provide valuable information for risk-based dimensioning of the emergency service and training scenarios. Therefore, other indicators should be provided as well, e.g. to address the definition of appropriate safety distances and to enable actual, real-time assessment of the potential hazard of the various accident scenarios. This is of utmost importance for the individual safety of the emergency staff. Such could be e.g. based on indicators could be the localized individual risk IR, potential loss of live PLL, Fatality accident rate FAR and others (Zulauf *et al.*, 2012; Benekos and Diamantidis, 2017).

In Europe, the PIARC is very common approach. It is therefore chosen as a starting point for the new methodology (Zulauf *et al.*, 2012).The PIARC methodology provides already mean data as traffic statistics, accident frequencies, tunnel geometries including certain prevention and protection measures, as e.g. means of traffic control, monitoring, ventilation systems, protection of escape routes, and emergency procedures. This approach will be enhanced by allowing better identification of hazards and their respective sources for hydrogen vehicles. It will facilitate a detailed analysis of the accident scenarios that are unique for hydrogen vehicles hereunder the initiating events, severity of collision types that may result in a release of hydrogen gas in a tunnel and the location of such an accident.

The new methodologies will in particular enable the assessment and evaluation of scenarios involving external fires or vehicles that burst into fire as a result of an accident or other fire sources. Hereunder the heat impact on the hydrogen storage system is of great importance as it includes the potentially very severe tank rupture and gas cloud explosion scenarios. The consequence analysis will therefore also include the hazards from blast waves, hydrogen jet fires, DDT (see e.g. Molkov and Saffers, 2013; Li, 2019; Otxoterena et al., 2020).

In particular, the QRA methodology proposed by URS and DTU enables the calculation of the individual risk (IR), i.e. annual fatality probability, risk of structural failure and hazard distance associated with a hydrogen powered vehicle accident in a confined space like a tunnel (road or railway) and underground parking. But further applications include other confined spaces like ship's hold. It provides the likelihood of all the possible scenarios and the consequence analysis includes the hazards from blast waves, DDT, hydrogen jet fires.

The QRA methodology developed by UU is focused on low-frequency high consequence events, i.e. the rupture of a tank in a fire with the consequent blast wave and fireball. It is an extension to tunnel of the QRA previously developed for onboard hydrogen storage of hydrogen-powered vehicles applied to roads in London (Dadashzadeh et al. (2018). The QRA output for hydrogen-powered vehicles in tunnels is a value of risk in terms of human fatality per vehicle per year (for vehicles having entered a tunnel) and in terms of monetary losses of human lives per an accident.

The outcome will be usable in terms of decision support to establish appropriate safety distances and to support for risk based dimensioning of the emergency services, e.g., the preparation of emergency plans for the emergency services including fire fighters, police and ambulances.

This document reports first a description of the methodologies developed and then the application of the QRA methodology proposed by URS and DTU to the examples of a road tunnel in Italy, a railway tunnel in the UK and an underground car park in Denmark. Next, the application of QRA methodology developed by UU for an accident with onboard hydrogen storage tank inside a road tunnel in the UK is shown. Finally, the results and the main conclusions derived from the analysis of the case studies are reported.

# 2 The QRA methodology flow diagram

The QRA methodology for "quantitative tunnel and car park risk analysis" is an analytic method that fundamentally is facilitating to find the answers to the following main questions:

- What could happen inside the system?
- What is the probability of occurrence of the event?
- Having established that the event occurs, what are its possible consequences?

The risk analysis process is divided into several phases as shown in Figure *1*, according to PIARC (2008), and an analytical model can correspond to each phase.

The QRA methodology proposed in HyTunnel-CS includes incident and fire frequencies, traffic statistics, tunnel geometries, including certain prevention and protection measures such as e.g. means of traffic control, monitoring, ventilation and emergency procedures that can control and extinguish the fire. It is aiming to ensure the safety of the tunnel users and the tunnel structure.

# 3 Definition of the system

The first step of the QRA methodology is the definition of the system. For each of the respective systems, i.e. road tunnel, railway tunnel and car park, this will include the topics:

| | |
|---|---|
| Type of Structure | Materials used, underground, under sea, etc |
| Type of traffic-environment | Road with dangerous goods transport, rail, public or private car parks |
| Type of Safety measures implemented | Passive fire safety, sectioning, fire doors, fire ventilation, sprinkler, etc. |

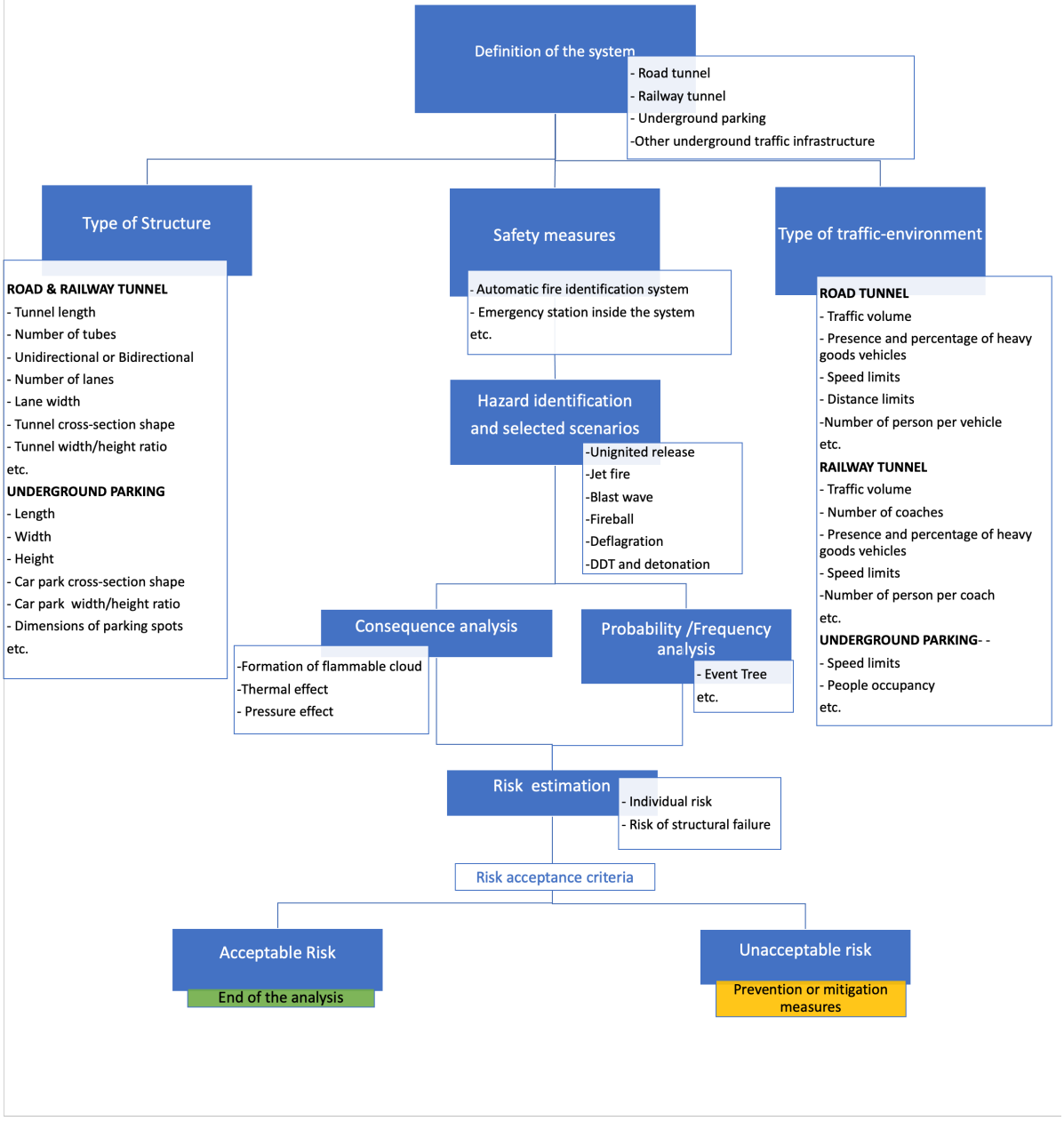


*Figure 1 Phases of risk assessment procedure*

Elements of tunnel design identified as relevant to the outcome of an accident involving a FCH vehicle are listed in Table 1.

*Table 1 Elements for the risk analysis*

| **Type of Structure** | **Type of traffic-environment** | **Safety measures** | **Characteristics of the access roads** |
|---|---|---|---|
| ***Road & Railway Tunnel*** | ***Road Tunnel*** | | |
| Tunnel length | Traffic volume | Automatic fire identification system | Geographical and meteorological environment |
| Number of tubes | Presence and percentage of heavy goods vehicles | Emergency station inside the system | etc. |
| Number of lanes | Speed limits | etc. | |
| Lane width | Distance limits | | |
| Traffic direction | Number of person per vehicle | | |
| Tunnel Cross-section shape | ***Railway Tunnel*** | | |
| Tunnel width/height ratio | Traffic volume | | |
| Vertical alignment; | Number of coaches | | |
| Horizontal alignment. | Presence and percentage of heavy goods vehicle | | |
| | Speed limits | | |
| | Number of person per coach | | |
| **Underground Parking** | **Underground Parking** | | |
| Car park length | Speed limits | | |
| Car park width | People occupancy | | |
| Car park height | etc. | | |
| Car park cross-section shape | | | |
| Car park width/height ratio | | | |
| Dimensions of parking spots | | | |
| etc. | | | |

# 4 Hazard identification and selected scenarios

The scope of our methodology is to assess the hazard due to normal traffic situations and therefore it does not consider the bulk transport of hazardous goods (i.e. LPG, gasoline, $H_2$).

In order to identify the possible hazard in a gaseous hydrogen vehicle a sketch of a car is shown in Figure 2 and relative safety features are given in Table 2. The vehicles from the different manufactures may differ in a number of details, such as the number of tanks and their sizes; but the separation of the gas tanks place in the rear region of the vehicles and having the fuel cell and the electric motor in front is similar on most of the vehicles. Different is the layout though in busses Figure 3 and trains Figure 5 and Figure 6, which also have larger quantities of hydrogen on-board.

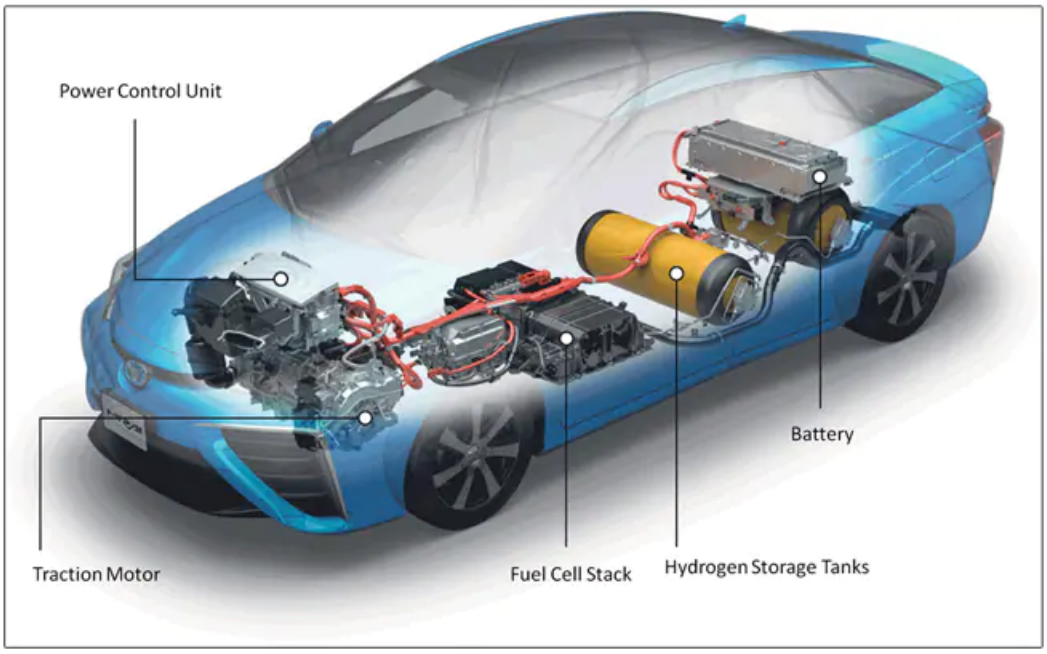


*Figure 2*. Simplified sketch of a FCEV showing the principal layout of such types of cars.

In addition to car homologation (e.g. several normalized full-scale tests: crash, fire…) and a design compliant with many codes and standards, many mitigation barriers are presently based on risk analysis (Table 2).

*Table 2 Safety features for FCEV.*

| What? | Where? | For what? |
|---|---|---|
| TPRD | Connected to 700-bar $H_2$ composite cylinders<br>Located at the bottom of the car, and downward directed | Avoid the pressurization and the burst of the cylinder in case of fire |
| Thermal insulation | Around the gas storage | Delay warming of gas storage |
| $H_2$ detection | Close to the $H_2$ storage tanks<br>In the car cockpit | Activate warning, and shutdown valves |
| Automatic shut-off valve | Between $H_2$ storage tanks and fuel cell | Limit $H_2$ inventory in case of accidental release |
| Very short high pressure line | Between $H_2$ storage tanks and fuel cell | Limit $H_2$ inventory in case of accidental release |
| Low medium pressure (10 bar or less) | Between $H_2$ storage tanks and fuel cell | Limit $H_2$ inventory in case of accidental release |
| Excess flow valve | on the low pressure piping | Limit flowrate in case of release or piping rupture |
| Shock detector | In the car | Close $H_2$ feeding valve |
| Shock absorbing shielding | around the gas storage | Protect from mechanical aggression for avoiding potential leaks |
| Electrical grounding | Car refuelling nozzle | Prevent sparks caused by static electricity during refuelling |

## *4.1* Hydrogen fuel cell bus

Main characteristics of the fuel cell buses is that hydrogen tanks and fuel cell are set up on the roof of the bus (Figure 3 and Figure 4). The pressure of storage in the tanks is 350 bar. The mains safety features for a FC bus are reported in Table 3.

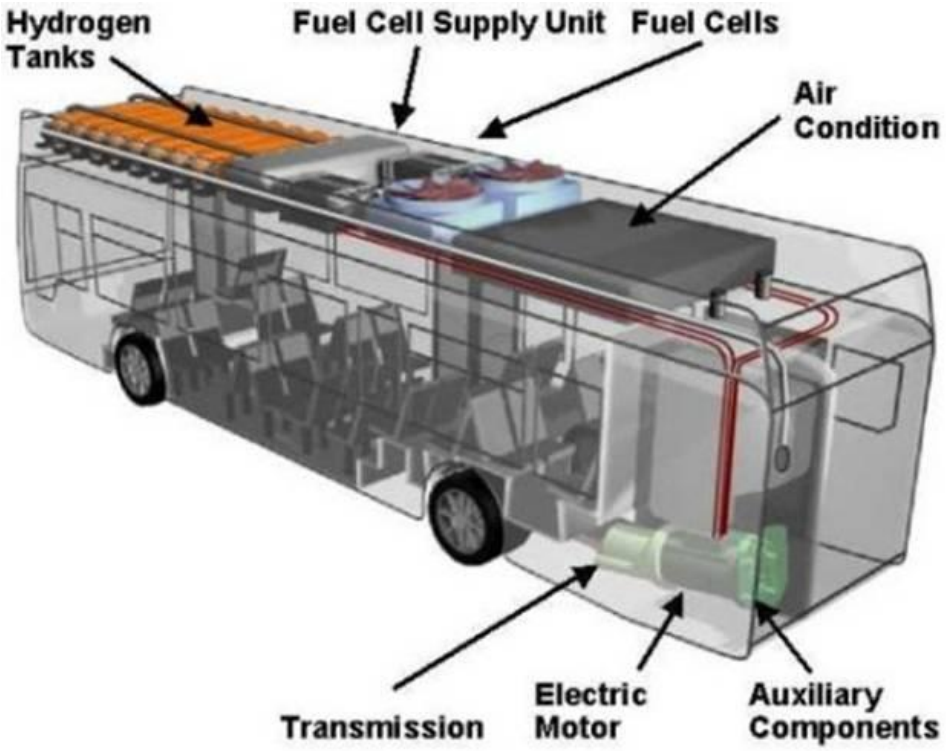


*Figure 3 Simplified sketch of a FC bus (HyResponder, 2021).*

*Figure 4. FC bus. Left: H2 storage, right: fuel cell system (HyResponder, 2021) .*

*Table 3.* Safety features for FC buses

| What? | Where? | For what? |
|---|---|---|
| TPRD | Connected to 350-bar $H_2$ composite cylinders<br>Located on the roof of the bus, and upward directed | Avoid the pressurization and the burst of the cylinder in case of fire |
| $H_2$ detection for some models | Close to the $H_2$ storage tanks<br>Close to the fuel cell | Activate warning, and shutdown valves |
| Shutdown valves | Between $H_2$ storage tanks and fuel cell | Limit $H_2$ inventory in case of accidental release |
| Electrical grounding | Bus refuelling nozzle | prevent sparks caused by static electricity |

## *4.2* Hydrogen fuel cell train

As shown in Figure 5 and Figure 6, hydrogen storage and fuel cell are on the roof of the train. Pressure in the storage tanks is 350 bar. An evolution of the pressure of storage for fuel cell trains could be 700 bar.

*Figure 5* ALSTOM CORADIA iLINT FC train (Germany) *(HyResponder, 2021).*

Electricity for the traction and on-board equipment is generated by a fuel cell, stored in battery and recovered during braking.

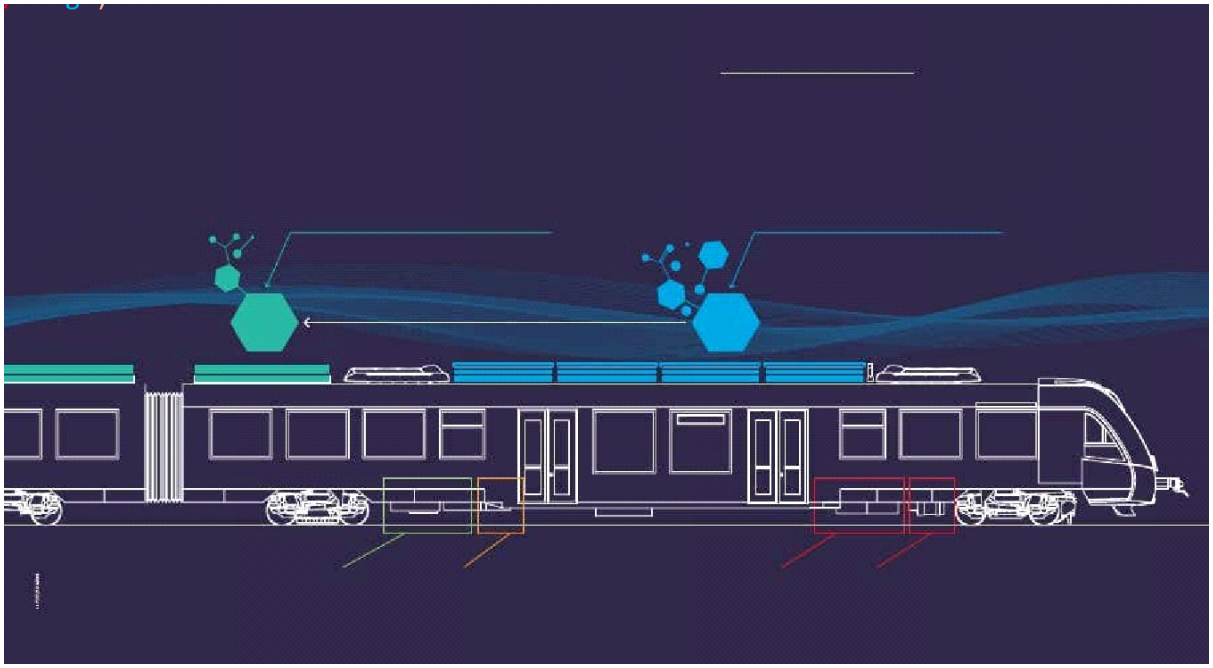

*Figure 6* ALSTOM CORADIA iLINT FC train concept *(HyResponder, 2021)*

The mains safety features for a FC train are reported in

Table 4. Safety features for FC trains.

*Table 4*. Safety features for FC trains.

| **What?** | **Where?** | **For what?** |
|---|---|---|
| TPRD | Connected to 350-bar (or 700-bar) $H_2$ composite cylinders<br>Located on the roof of the train, and upward directed | Avoid the pressurization and the burst of the cylinder in case of fire |
| $H_2$ detection for some models | Close to the $H_2$ storage tanks<br>Close to the fuel cell | Activate warning, and shutdown valves |
| Pressure monitoring | On medium and high pressure lines between fuel cell and storage tanks | Detect hydrogen leaks |
| Shutdown valves | Between $H_2$ storage tanks and fuel cell | Limit $H_2$ inventory in case of accidental release |
| Electrical grounding | Train refuelling nozzle | prevent sparks caused by static electricity |

# 5 Quantitative risk assessment methodology for hydrogen vehicles in confined space (Task 5.3; URS, DTU)

## 5.1 Selected scenarios

The HyTunnel-CS deliverable D1.3 (2019) established the state of the art and knowledge gaps in hydrogen technologies.

In particular, the factors contributing to the extent and severity of an accident involving a FCH vehicle in a tunnel or a similar confined space were assessed. The accident scenarios used as the basis of the approach undertaken by the HyTunnel-CS project were then identified. For these scenarios, the consequences in a tunnel or confined space were identified during the HyTunnel-CS project and established the difference to a comparable accident in an open environment. Based on these findings, safety strategies and engineering solutions were identified to support inherently safer deployment and use of hydrogen vehicles in tunnels, underground parking, garages, etc. The outcome was a list of potential scenarios that need more consideration (Table 5).

Ten typical accident scenarios have been identified. Each scenario is described in terms of fixed factors and accident variables that are combined to describe the scope and range of the scenario. The transportation modes that are likely to see the greatest deployment of FCH technology are cars, buses and trains. These transportation modes also include a wide range of quantities of hydrogen storage on board (5 to 400 kg hydrogen) which, once fully evaluated, allowed a thorough understanding of the consequences.

In particular, activation of the TPRD by fire may, in the worst case, lead to the simultaneous discharge of the entire hydrogen inventory. Specifically, where the TPRDs are interconnected prolonged discharge through a common vent may occur. These large quantities of hydrogen release were taken into account in environments with differing geometries (i.e. trains and railway tunnels)

The detailed description of the scenarios is reported in deliverable D1.3.

*Table 5 List of addressed scenarios*

| | |
|---|---|
| | **Unignited scenarios:** |
| 1. | Unignited hydrogen release and dispersion in a confined space with mechanical ventilation |
| 2. | Unignited hydrogen release in confined spaces with limited ventilation |
| 3. | Unignited hydrogen release in a tunnel with natural/mechanical ventilation |
| | **Immediate ignition scenarios:** |
| 4. | Hydrogen jet fire in confined spaces with limited ventilation |
| 5. | Hydrogen jet fire and vehicle fire in a mechanically ventilated confined space (maintenance shop/ underground parking) |
| 6. | Hydrogen jet fire impingement on a tunnel |
| 7. | Hydrogen jet fire and vehicle fire in a tunnel |
| 8. | Fire spread in underground parking |
| | **Burst scenario:** |
| 9. | Hydrogen storage vessel rupture in a tunnel |
| | **Delayed ignition scenario:** |
| 10. | Hydrogen storage vessel blowdown with delayed ignition in a tunnel |

These scenarios have been adopted in the QRA methodology and will be our base scenarios that the methodology is capable of analysing.

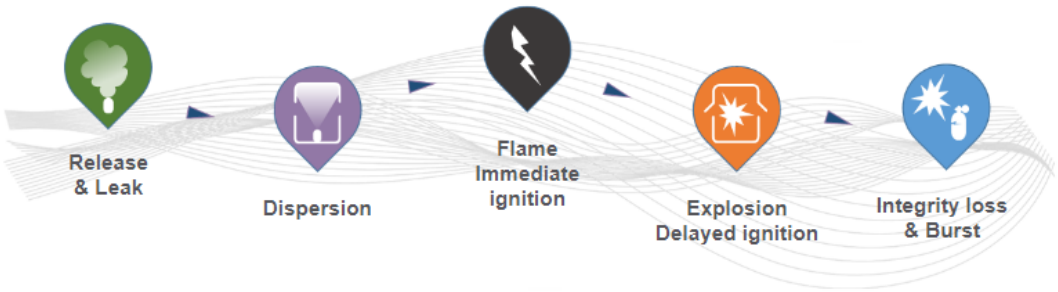


*Figure 7. Overview of the accidental kindling chain for gaseous hydrogen (HyResponder, 2021)*

It has to underline that in the following we will consider only the scenarios that are consequence of a crash. In the case of a crash, hydrogen is released because of component failure (i.e., valves, connections, flanges) due to the impact of the crash.

When the accidental leakage arises because of a collision, it can lead to massive leakage (>100 NL/min) (Gentilhomme et al, 2012). Once released hydrogen can be not ignited, immediately ignited or ignited after a delay (La Fleur et al., 2017) (Figure 7).

With reference to the unignited hydrogen release scenarios (1, 2, 3 in Table 5) they may occur when there is not an ignition source as a fire post-crash (event chain B in the event tree reported in Figure 10) or the hydrogen jet release from TPRD (i.e., vertical downwards backwards for passenger cars; upwards backwards for buses and trains) is not get into contact with the ignition source (event chain G in the event tree).

Accordingly, the scenarios 1 to 3 (Table 5) are included in the event tree.

Regarding to the immediate ignition scenarios, scenario 4 (Table 5) refers to hydrogen jet fire in confined spaces with limited ventilation and it is related to 1-2 cars garages, case study which is not considered here because a severe crash is not expected inside a garage.

Regarding to the other immediate ignition scenarios, jet fires are considered occurring in car park, road and rail tunnels (scenarios 5 to 7) and fire spread in underground parking (scenario 8) (Table 5).

The scenarios 5 to 7 correspond to event chain C, H and J in the event tree. Among them, the event chain H refers to a TPRD hydrogen release ignited by a fire post-crash, therefore it is defined in size (0.5-5 mm depending on the transportation type) and direction (i.e. vertical downwards or upwards, 45° downwards). While event chain C and J are consequence of a component failure with random hole sizes and directions, in dependence of the type of vehicles and manufacturer.

The scenario 8 (Fire spread in underground parking) is not taken into account in the analysis in spite of the fact that there have been very severe fires in car parks involving a great number of cars. Scenarios could be imagined where a number of TPRD's are activated giving rise to a hydrogen gas cloud that potentially could lead to an explosion. Nevertheless, for this type of scenarios neither statistical data nor proper consequence models are presently available. This knowledge gap should be addressed in the future.

The burst scenario 9 (Hydrogen storage vessel rupture in a tunnel) it is expected to occur as consequence of a fire post-crash and the TPRD failure "Not open" on demand. In this case after

a certain exposure time to fire, hydrogen tank rupture can occur. More details of this scenario are reported in the paragraph 5.1.1. This is defined as event chain F in the event tree.

Finally, the delayed ignition scenario 10 (Hydrogen storage vessel blowdown with delayed ignition in a tunnel) has been considered.

The release of hydrogen from vehicles (i.e. bus and train) also those with a smaller inventory (i.e, cars) can deflagrate when is not immediately ignite. In this case a flammable cloud of $H_2$-air mixture may be formed which can give rise to a deflagration that eventually develops into detonation during accidents because the hydrogen has shorter DDT distance with respect to other fuel (Li, 2019; Li et al., 2021). If the hydrogen is with better mixing with the ambient air, for example, the ignition is delayed, or the combustion is enhanced by some external obstacles, the combustion could develop into detonation under certain circumstance creating significant pressure impulse to the surrounding structures, vehicles or human being.

Researches were conducted for the hydrogen detonation in a confined space focusing on the threshold for onset of detonation and the resulting overpressure (Groethe et al., 2007; Kuznetsov et al., 2015) but the results vary with the experiment conditions. For instance, the maximum over pressure of 1.5 bar was measured at the outlet of the tunnel for an experiment in a sub-scaled tunnel with the hydrogen premixed with air and confined in a plastic film barrier (Groethe et al., 2007). Another experiment is conducted in a flat semi-confined layer with gradient hydrogen concentration and the measured over pressure was in the order of magnitude of 10 bar (Kuznetsov et al., 2015).

Hence a detonation case is here taken into account to evaluate the consequence of the hydrogen detonation in the tunnel; it is assumed to be the consequence of the release of hydrogen from TPRD, when TPRD is activated by a fire (chain event I), and a strong ignition at the top of the tunnel at an unfavourable time and location. The pressure loads are calculated to evaluate the consequence of the hazard.

A delayed ignition scenario may also occur if a leakage from the system takes place directly in the engine compartment, in this case the resulting hydrogen-air mixture may encounter an ignition source and it was found that pressure effects will be negligible if the averaged concentration is less than 10% v/v $H_2$. Based on dispersion experiments carried out by the DRIVE project, using a transparent rig fully representative of an engine compartment in windless conditions, this concentration will not be exceeded if the leakage flow rate is less than 10 NL/min, but an accidental leakage after a crash could easily reach this maximum tolerable value (Gentilhomme et al., 2012). Similar results were obtained from hydrogen accumulation tests on the front-crashed vehicle (DOT, 2013), where low leak rates (up to 15 L/min) in trunk or passenger compartment resulted in random, but sometimes detectably flammable, levels of hydrogen.

This scenario is taken into account in the event tree and corresponds to the event chains D and K. These event chains are consequence of a component failure with random hole sizes and directions, because are dependent on the type of vehicles and manufacturer, so their consequences can be properly quantified if this information is available.

Very few researches were conducted to analyse the effect of this release on the vehicle and on people in or outside the vehicles (SAE Technical Paper Series 2006-01-0126, SAE Technical Paper Series 2007-01-0428). In details, the results of experimental campaign carried out by U.S. Department of Transportation are the following (DOT, 2013):

Altogether, eight ignition tests were conducted on the intact or front-, rear-, or side-impact vehicles. Two types of ignition tests were conducted: (1) at the in-going potential standard leak rate of 118 lpm for a duration of 1.5 min, which introduced a just-flammable ~5 percent hydrogen inside the car if distributed evenly; and (2) at the lowest leak rate experimentally possible (3 lpm) over 60 min, which resulted in accumulated hydrogen (~5%) that could be ignited by sparking at the top of the passenger compartment (leaking 3 lpm for 60 min was near-equivalent to the volume of hydrogen leaking at 118 lpm for 1.5 min).

With regard to achieving the objective of determining a minimum allowable post-crash leak rate, tests indicated that leak rate is not defining metric. Instead, the critical information was whether hydrogen, if allowed to leak into a car compartment, could accumulate anywhere locally to ~5 percent, just above the lower flammability limit of hydrogen (~4%). Tests indicated that flammable concentrations of hydrogen could accumulate in different locations within passenger compartments, either at low leak rates after long times or at high leak rates after short times.

Fire effects varied in terms of peak thermal flux, overpressure, and internal vehicular damage. Aftereffects ranged from window fogging (condensation from hydrogen combustion) to structural damage (deformed doors, broken windows) to second-degree burns and eardrum rupture.

One additional significant finding was a propensity for secondary fire after sparking and hydrogen ignition, which was replicated. These secondary fires, that consumed flammable material inside the vehicles, occurred in the intact and front and side-impact cars. The origin of these secondary fires, that erupted within minutes after initial sparking and severely damaged the vehicles, appeared to be flammable material inside the trunk (spare tire) or cabin (headliner).

### 5.1.1 Hydrogen storage vessel rupture in a tunnel

This scenario is strictly related to the type of $H_2$ container present on the vehicle. There are four different types of $H_2$ containers depending on the material which satisfy the specification reported in (UNECE, 2014):

1. Metal container and cylinder (metal, Type I).
2. Metal container that is, aside from the bottom and neck, wrapped in sheets of composite materials (hoop wrapped, Type II).
3. Metal container that is entirely wrapped in sheets of composite materials (fully wrapped, Type III).
4. Plastic container that is entirely wrapped in sheets of composite materials (all composite, Type IV).

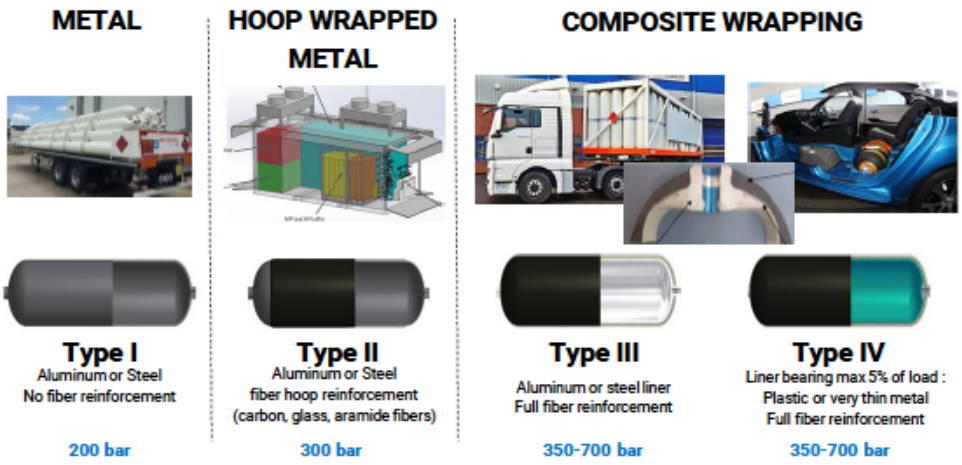


*Figure 8. $H_2$ containers (HyResponder, 2021)*

Within the automotive application, mainly high-pressure composite cylinders (Type IV and Type III) are used for the on-board storage of the hydrogen fuel. The strength of these types of cylinders is fully (for Type IV) or mostly (for Type III) determined by composite material made of wrapped carbon fibre in an epoxy resin matrix. The hydrogen storage pressure is either 35 or 70 MPa; however, most of the car makers focus their activities on the 70 MPa technology because of the major advantage with regard to higher storage density per required mass or volume (FireComp, 2014). The dimensions of automotive cylinders seem to have a large variety in the range of 20L to 150L. In the large end of the range, the cylinder might become either long and slim or short and fat depending on the orientation of the cylinder on-board. However, when evaluating the integration of hydrogen storage cylinders for Fuel Cell Vehicles, there are various aspects that need to be considered (FireComp, 2014).

Different situations of tank exposure are available: full engulfed fire, and localized fire. According to the literature (Ruban et al, 2012), the reviews of the accident literature on the CNG and $H_2$ composite cylinder showed that the cause of accidental burst of cylinders was mainly a localized fire or a wrong design of the size of the TPRD orifice. Then, overpressure and fragments from the burst cylinder could have catastrophic consequences (Perrette and Wiedemann, 2007; Zalosh, 2008)

Furthermore, experience shows that fire-protected tanks may not survive some of the aforementioned attacks indicating that PRD's efficiency is limited. This limitation should be recognized. Indeed as reported by Perrette and Wiedemann (2007), protected tanks can not survive an impinging jet flame and fail within a couple of minutes. With regard to localised fire, it could be expected that no thermal fuses will intervene and that the tank will fail depending on the distance between the local flires and the PRD.

On the contrary PRDs are useful for an engulfing flame which is the less serious case for the protected integrity of the tank. This test is part of the certifying process of protected tanks as mentioned before (UNECE, 2014).

This problem is also addressed by Dadashzadeh et al. (2018) who recognized that the installation of TPRD on the on-board $H_2$ tanks is required for hydrogen vehicles by EU Regulations. This allows the $H_2$ content to be released in the event of a fire and thus prevents catastrophic rupture of the tank. But in some scenarios such as a localized fire or the blocking of the TPRD sensing element due to an accident, the activation of TPRD may fail. In these cases, a tank can experience a strong and rapid thermal load from a fire and thus a progressive

degradation of the composite tank wall. This is probably the most important current safety issue.

Explosion-free in a fire composite tank (infinite FRR), which is currently under development at Ulster University, would be a solution to drastically increase safety of hydrogen vehicles and gain public acceptance of the technology.

## 5.2 Event Tree Analysis for hydrogen release in the event of a crash

A risk analysis was performed to define realistic accident scenarios for hydrogen release in the event of a crash.

The method is shown to be applicable for a worst case scenario in a road tunnel as shown in Figure 9 which is assumed to be a collision of a heavy vehicle at high speed into the last vehicle in a queuing situation. This is assumed to lead to mechanical rupture of FCEV and a potential fire scenario.

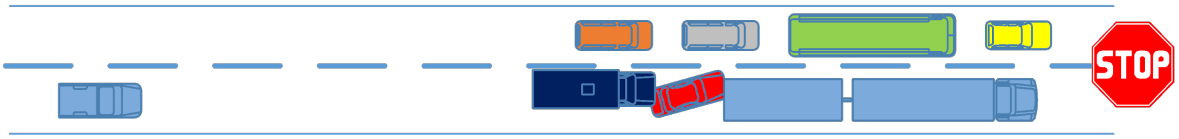


*Figure 9. Worst case situation like front rear crash of a large vehicle in case of a traffic jam situation*

Event Tree Analysis (ETA) is the technique used to estimate the event frequencies. It is a common and widely used technique and tool in industry to enable event frequencies to be estimated from numerical data such as accident/event data, failure rates and probabilities.

The event tree begins with an initiating event and illustrates the chronological sequence of events involving the successes and/or failures of the system components. Each bifurcation is assigned a probability of occurrence and thus the probability of various possible outcomes (event chain) can be calculated. The total for each event chain (branch frequency) is the combination of all the probabilities leading to that event chain multiplied by the frequency of the accidental (initiating) event.

Event trees were developed to graphically illustrate all possible outcomes following an accident involving a $H_2$ vehicle. It depicts the chronological sequence of events that could occur following the initiating accident including escalations and mitigations (e.g. first responder's intervention). In particular, the new methodology enables the assessment and evaluation of scenarios involving external fires or vehicles that burst into fire as a result of an accident or other fire sources. Hereunder the heat impact to the hydrogen storage system is of great importance because of the risks of largest consequences scenarios leading to gas cloud explosions and tank rupture.

As an example, event tree developed within this assessment and applied to quantify the risk of hydrogen vehicles accidents in a tunnel is reported in Figure 10.

The initiating event is an accident involving a hydrogen vehicle in a tunnel but it can refer also to other confined spaces (i.e. underground car park). Since there are currently no statistical data available for accidents involving a hydrogen vehicle, due to the small number of this type of vehicle in circulation on the roads, this analysis uses the generic accident rate for tunnels conservatively (paragraph 5.2.1).

If a fire does not occur, the next event tree branch analyses whether hydrogen is released from all components of the hydrogen system in a crash. Published crash test data for hydrogen vehicles were used for this evaluation even if they are very scarce (just five), and in all five tests there was not enough damage to the system for it to leak or release hydrogen (event chain A) (paragraph 5.2.2).

The next bifurcation in the diagram is whether the hydrogen released from the hydrogen system will ignite. La Fleur et al. (2017) proposed ignition probabilities for hydrogen releases according to a step function with 3 levels for both immediate and delayed ignition. The relationship depends only on the initial release rate and does not consider gas accumulation by confinement or extensive congestion. The total ignition probability is the sum of the average probabilities for immediate and delayed ignition. In the case after the release, hydrogen does not ignite then there is only dispersion of the substance into the atmosphere (event chain B). On the contrary, once hydrogen escapes from the fuel system, if it ignites immediately generates a jet fire (event chain C), while if its ignition is delayed a deflagration may occur (event chain D). The deflagration can also concern only a layer of $H_2$-air mixture accumulated under the ceiling of the tunnel.

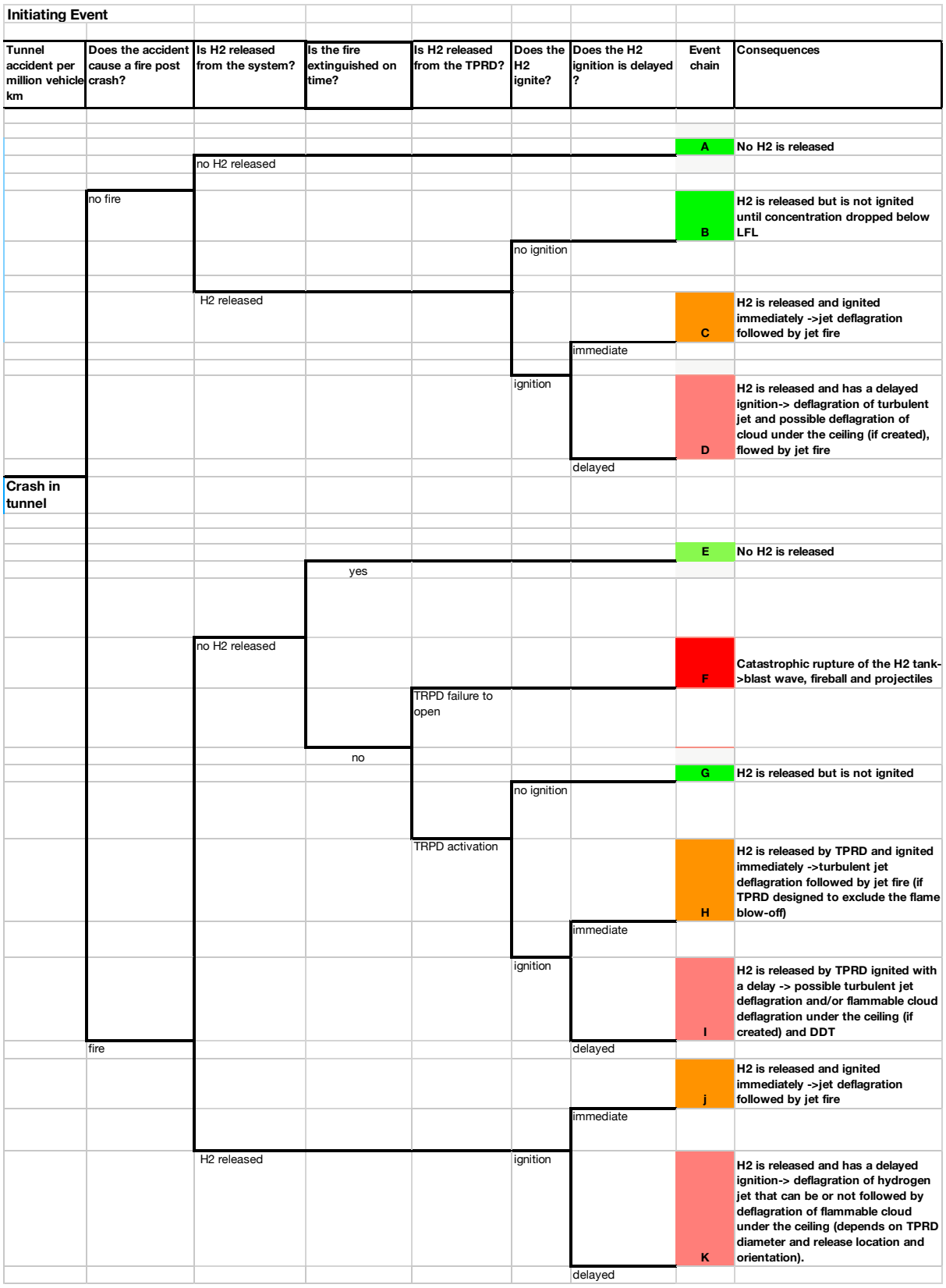


*Figure 10. Event tree for crash scenarios involving hydrogen vehicles*

If the car catches fire after the accident, the consequences will depend on whether or not the fire reaches the fuel tank and affects the TPRD. A branch is added here to take into account the option that fire is extinguished on time, i.e. before tank rupture occurs (event chain E) (paragraph 5.2.3).

In case that the fire is close to the tank, a new tree branch has to consider the probability of failure of the TPRD. Indeed, the likelihood of catastrophic tank rupture scenario is closely linked with the failure rate on demand for the installed TPRD's. Unfortunately, no specific data for TPRD failure are available in the literature. There are only very limited literature data available in FireComp risk assessment study (Saw et al., 2016) and in the SANDIA publication (Ehrhart et al., 2020). TPRD failure probability due to accident/fire for both engulfed fire and localized fire scenarios were taken into account in the analysis (paragraph 5.2.4).

If the TPRD is not activated the consequence will be a catastrophic rupture of the hydrogen tank with the consequent blast wave and fireball and projectiles formation (event chain F). On the contrary if the TPRD is activated, $H_2$ is released but is not ignited (event chain G) or it is ignited immediately giving a jet fire (event chain H) or alternatively it is ignited with a delay. In this latter case a deflagration may occur, or a deflagration and DDT if it involves a flammable cloud that is accumulated on the top of the tunnel under the ceiling (event chain H). In the case of $H_2$ release from TPRD the ignition probability is calculated as function of $H_2$ flow rate from TPRD (i.e., SOC of tank and TPRD orifice size) (Aarskog et al., 2020).

Finally, if the $H_2$ is released from the system as consequence of the crash, and the car catches fire, it can be ignited immediately or with delay with consequent jet fire or deflagration scenario, respectively (event chain J and K, respectively).

### 5.2.1 Statistics of accidents and fires in road tunnel

The first data required for the risk analysis is the frequency of occurrence of the initial event. This initial event is considered the collision of a hydrogen vehicle against another vehicle.

Most papers are related to accidents occurring on open roads, while accidents occurring in road tunnels have been less investigated. Driving in road tunnels often causes anxiety in drivers because tunnels are dark, narrow, and monotonous. As a result, driving behaviour in road tunnels is different when compared to that on open roads. Also the change in light conditions (e.g., the so-called ‘‘black hole effect’’ when entering the tunnel), the disturbing effects on driving due to the tunnel wall (which is too close to the traffic lane), and the excessive stiffness of the tunnel wall (which in absence of safety barriers with re-directive profile is not able to reduce the severity level of the impact when vehicles collide against it) can contribute to more fatalities and/or injuries when compared to those on open roads.

The accident rate in tunnels is measured as the number of accidents per million vehicles per km (per mvk). The road accident rate is independent of the type of supply of carriers, whose significant statistic is related to vehicles powered by traditional fuels. This accident rate was defined by a recent report where the frequency data of tunnel accidents were reported for different countries from which the average global accident frequency in tunnels was obtained equal to 0.19 accidents per million vehicles km (Bassan, 2016). This is a lower value than the mean value of 0.35 per million vehicles-kilometers reported by La Fleur et al. (2017) obtained over a 3-year period for 10 different countries.

In Italy, where they count hundreds of tunnels (for a total of 954 km), the accidents in tunnel are listed and statistics are established by the ANAS expressed in million vehicles-kilometers (ANAS, 2009). The rates correspond to road tunnels in non-urban and urban zones and

accidents with material damage only and those with people damage. The result is an average tunnel accident rate of 0.46 per million vehicles-kilometers.

*Table 6.Accident rate in Italian tunnels (ANAS, 2009)*

| **Accidents with material damage only** | **Rate per million vehicles-km** |
|---|---|
| **Urban Tunnels** | from 0.40 to 1.50 |
| **Motorway Tunnels** | from 0.30 to 0.80 |
| **Accidents with people damage** | |
| **Urban Tunnels** | from 0.10 to 0.50 |
| **Motorway Tunnels** | from 0 to 0.15 |

The database of crashes collecting data from 252 Italian tunnels (226 two-lane and 26 three-lane) over a monitoring period of 4 years (2006–2009) that result in both severe and non-severe crashes was recently analysed (Caliendo et al., 2022). Only motorway tunnels were considered in the analysis. Results are the following: 2280 accidents are accounted, 757 of which are severe accidents. In two-lane tunnels, 1930 accidents are counted (665 of which are severe accidents), while in three-lane tunnels 350 accidents are registered (92 of which are severe crashes). A decreasing trend in the aforementioned three crash types over time is also observed. The length of the tunnels varies from 0.39 to 3.25 km. Unidirectional traffic flow is expressed in terms of the average annual daily traffic AADT per lane, and it ranges between 2250 and 20,380 vehicles/day per lane. The percentage of trucks (i.e., vehicles with weight C >30 kN) ranges from 15.0 to 31.2%.

The second step in the ETA is the calculation of the probability of a fire in tunnel. This probability is determined as the ratio of the number of tunnel fires to the total number of accidents occurring.

The European Union directive on minimum safety requirements for tunnels in the trans-European road network (2014) requires (article 15) member states to publish fire incident statistics for their road tunnel assets every two years (Council of the European Union).

In Austria ASFiNAG, the Austrian state owned highway operator, collected breakdown and fire incident data between May 2006 and January 2013 (Rattei et al., 2014). The work identified 67 road tunnel fires. Approximately 90% of the fires derived from technical issues with only 7% the result of collisions, heavy goods vehicles were overrepresented as they were the source of 44% of fires. Finally, a rate of vehicle fires of 6.5 fires per billion vehicle kilometres travelled (VKT) is reported. In France, the Centre for Tunnel Studies (CETU) collected statistics related to breakdown, accidents and fires in road tunnels from 2002 to 2011 (Willmann, eta al., 2016). The data are collected for 96 tunnels (70% of all French tunnels above 300 m in length). It is reported a rate of vehicle fires of 1.1 fires per billion VKT. Only 10% of these fires were caused by ‘accidents’ or ’collisions’. In Australian a similar work has been compiled through the Austroads Tunnel Task Force (ATTF) (Casey, 2020). All of the tunnels in the dataset are in urban locations with some on major freight routes. It is reported a fire frequency of 8 fires per billion VKT. From the breakdown of vehicle fire incidents by vehicle type (Table 7), it results that over 25% of the fires were on heavy vehicles (HVs) although the percentage of HVs in the tunnel fleet is likely to be less than 10%. Fires on HVs therefore occur significantly more frequently than fires in passenger cars per kilometre travelled by those vehicle classes in tunnels.

*Table 7. Classification of fires by vehicle type in major Australian road tunnels*

| **Type of vehicle** | **Passenger car** | **Length Duty vehicle** | **Heavy vehicle** | **Multiple vehicle** |
|---|---|---|---|---|
| n. of fires | 41 | 14 | 20 | 1 |
| Percentage of total | 53.9 | 18.4 | 26.3 | 1.3 |

The World Road Association has issued a report which identifies and compares road tunnel fire incident data for various countries (PIARC, 2017). For 12 countries, the report includes comprehensive information on tunnel fires, with the aim to present statistical data on fire incidents in tunnels from different countries and other information which may be useful to describe the characteristics of real tunnel fires.

The two types of tunnel fires are distinguished: triggered by a collision or a vehicle defect (e.g. a result of technical, electrical or mechanical defaults). The majority of vehicle fires occur as a result of vehicle defects. Fires resulting from vehicle defect typically start in engine, exhaust system, wheels or brakes; seldom in the load. However, fires caused by collisions can have severe consequences as they may develop more rapidly and often involve persons who are unable to escape from the burning vehicle.

The following influencing factors are identified as relevant in determining the likelihood or frequency of fire:

• Collision rates

• Percentage of HGV traffic (because there may be a difference in the fire rates of HGVs and passenger cars)

• Inclination in the tunnel and the length of the inclination.

• Inclination on the routes leading towards the tunnel

• Combination of tunnel length and gradient

• Traffic composition / age and technical standard of the vehicles, as well as maintenance of heavy vehicles

The fire rates are presented in terms of rates per billion vehicle-km, which has made it necessary to collect also the traffic volume in tunnels for the relevant period and the geographical area covered by the data collection.

Data for 12 countries are used for the calculation of average fire rates reported in Figure 11.

| TABLE 6 AVERAGE FIRE RATES FOR ROAD TUNNELS IN VARIOUS COUNTRIES | |
|---|---|
| **Country** | **Fire rate all vehicles (per $10^9$ veh. Km)** |
| Norway | 15.0 |
| Netherlands | 3.2 |
| Austria | 6.5 |
| Germany° | 25.7 |
| Italy | 5.6 |
| Spain | 3.5 |
| France | 10.6 |
| United Kingdom# | Insufficient data (10 – 20) |
| Czech Republic | 17 - 25 |
| Japan^ | (38) |
| South Korea | 6.4 |
| Vietnam* | 560 |

Notes : # Value from the UKs in parenthesis is a rough estimate.
^ The tunnels cover four tunnels with fire events only – the rate is an upper value for Japan.
* The statistics only cover one single tunnel.
° The available data covers only the 28 German TERN tunnels – also small fires are included
Background data concerning fire rates see *appendix 4.1*

*Figure 11. Average fire rates for road tunnel in various countries (Piarc, 2017)*

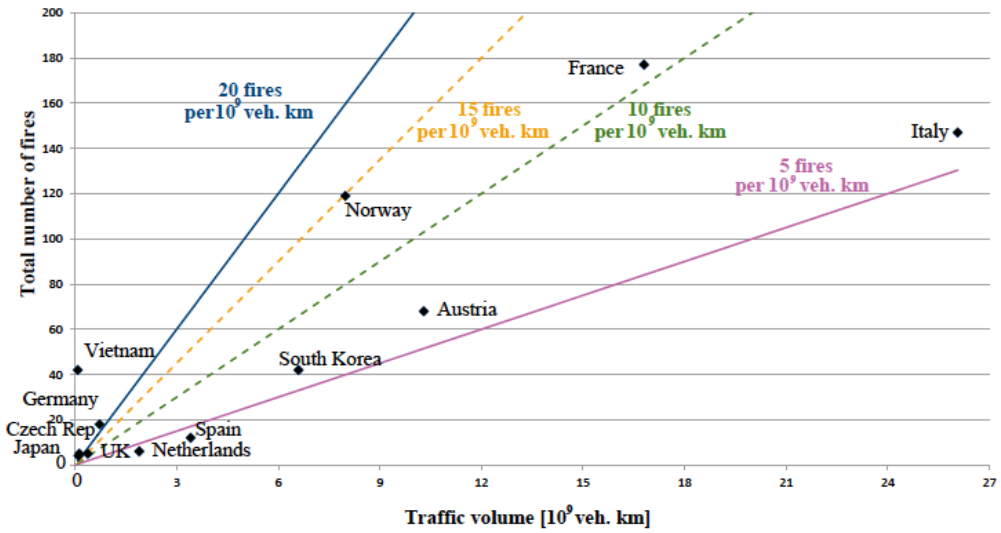


*Figure 12. Total number of fires vs the corresponding traffic for various countries. Reference lines for fire rates. (PIARC, 2017)*

The fire rates are also reported in Figure 12 where the total number of fires is shown in relation to the corresponding tunnel-traffic volume for each of the countries: the fire rates are generally within the interval 5 – 15 fires per billion vehicle-km.

The data collection of fire events is serving as basis for the fire rates and for the risk analyses, which in turn may lead to the decision of safety measures in tunnels. Therefore, it is important that reliable data are collected in the future for a large number of tunnels, so that the statistical basis can be improved in the coming years.

### 5.2.2 Probability of $H_2$ release post-accident

Published crash test data for hydrogen vehicles are very scarce (just five), and in all five tests there was not enough damage to the system for it to leak or release hydrogen. A gamma distribution conjugate prior was used to account for a half of an event (0.5, 5.5) (Lafleur *et al.*, 2017), which corresponds to a **10% probability of a release** and a 90% probability of not releasing hydrogen. In this latter case the vehicle is involved in a tunnel accident which, however, causes neither fires nor the release of hydrogen into the atmosphere.

### 5.2.3 Probability of fire extinguishment

Fixed Fire Fighting Systems (FFFS) have been routinely used in road tunnels in countries such as Japan and Australia for decades, and there is increased interest in the use of FFFS in parts of Europe, North America and Asia. FFFS are increasingly seen as a method that can deliver user safety and infrastructure protection and can be used as a risk reduction measure. However, their use is not widespread for various political, economic, technical and social reasons. It is still recognised that FFFS may not be the most appropriate measure to adopt in all circumstances or in all locations.

The World Road Association confirms regarding fixed firefighting (deluge) systems in tunnel that "*their installation provides the fixed infrastructure within a tunnel to enable fires to be addressed more quickly and more easily than if incident responders had to provide and deliver alternate systems to the fire site to respond to the event by other means*". "*Where FFFS are installed, it is recommended that they are activated in the early stages of a fire to minimise fire growth and to provide the desired effectiveness"* (PIARC (2016)).

The analysis of fire accidents in Australian road tunnels reported by Casey (2020) showed that portable fire extinguishers, both those installed in the tunnel or those carried in vehicles, were used to extinguish over 40% of the fires; other extinguishment means include: drive through, hose reels, fixed firefighting (deluge) systems. In response to 78 fires, operators deployed deluge on 30 occasions (38%). For most of the fires (62%), the operators determined that the use of the deluge system was not needed as the risk from the fire was low. Of the 30 fires where deluge was deployed, the system extinguished 16 (20%). The emergency services (fire brigade) extinguished 15 fires (18%) using a hydrant system.

In addition, the reported data include the recorded duration of fire incidents as shown in Table 8. Of the 71 fires in the dataset, seven fires are identified as 'drive through' fires where the vehicle went through the tunnel without stopping and thus the fires were not extinguished in the tunnel. Of all fires, 48% were declared extinguished within 10 min while 98.5% were declared extinguished within 50 min.

*Table 8. Recorded time from fire detected to fire declared extinguished (Casey, 2020)*

| **Duration (min)** | **<5** | **<10** | **<20** | **<30** | **<40** | **<50** | **<60** | **>60** |
|---|---|---|---|---|---|---|---|---|
| n. of fires | 15 | 34 | 54 | 66 | 69 | 70 | 70 | 71 |
| % | 21 | 48 | 76 | 93 | 97.2 | 98.5 | 98.5 | 100 |

The duration of vehicle fire is measured from detection to the time the fire is declared extinguished (Casey, 2020). The data were fitted by a cumulative gamma distribution (a=1.6 and b= 8.5), the mean is 13.6 min ± 10.8 min (*Figure 13*). Mean for gamma= a·b, Sigma for gamma= $\sqrt{a \cdot b^2}$

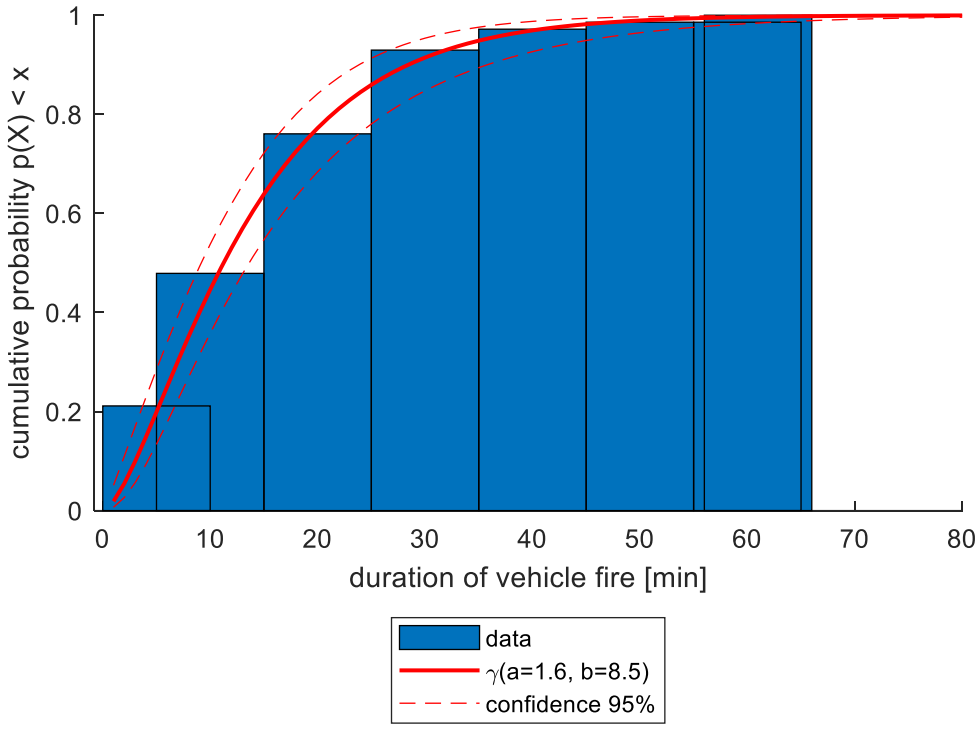


*Figure 13 Duration of vehicle fires in Australian road tunnels.*

Based on these data the probability that a fire will be extinguished on time is assessed. In particular, in order to avoid the tank rupture, the extinction must be faster than the time of failure of the tank in the event of exposure to a fire (Fire Resistance rate, min). According to the CFD simulations carried out by Ulster University, for a 62.4 L tank exposed to a fire of 1 MW/m$^2$, and with a state of charge of 100%, the fire resistance rate is 8 min (Makarov et al., 2016). Only an extinction time of this value can avoid the escalation of this scenario.

From the Table 8, **the probability that a fire is extinguished** in a time <10 min is evaluated **equal to 48%.**

### 5.2.4 Probability of TPRD failure

The reliability of the TPRDs is not reported sufficiently. Thermally activated PRDs exist in neither public nor AIR LIQUIDE internal database (Saw et al., 2016). There are only very limited literature data available in the FireComp risk assessment study (Saw *et al*., 2016) and the SANDIA publication (Ehrhart *et al*., 2020).

The value proposed in the FireComp project (Saw et al, 2016) for TPRD failure in the case of engulfed fire is $6.04\times10^{-3}$. It is estimated from failure of rupture disc PRDs data from database NPRD (Reliability Analysis Center, 1991). But thermally activated Pressure Relief Devices are a technology completely different from pressure-activated rupture discs or safety valves. Based on their knowledge of TPRDs and pressure safety discs, Air Liquide believes the probability of failure to open on demand of a TPRD when exposed to a fire is lower than the probability of failure on the same demand of a disc (Saw et al, 2016).

Dadashzadeh et al. (2018) used as failure probability of a TPRD the value of 6.04 $10^{-3}$ reported in FireComp project. On the contrary, Ehrhart *et al*. (2020) do not use this value commenting as follows:

"*However, this value was not used in the analysis because it may not be applicable to crash conditions. The reliability data used in its derivation does not explicitly define mechanical failure, so the data may represent TPRD leak, rather than failure of the TPRD to release pressure."*

Further values for the random mechanical failure probability of pressure relief device (PRD) are proposed in the literature:

- a probability of $2.22\times10^{-5}$ is found in report of Khalil et al. (2020) on the analysis of hydrogen storage;
- failure rate of $2\times10^{-5}$ is recommended for pressure relief devices in risk assessment in Purple Book (TNO);
- Sun and Li (2019) proposed a conservative value of $3\times10^{-5}$

As a conservative value, **$6.04\times10^{-3}$ is** adopted as **the probability of TPRD failure** in the event of an **engulfed fire** in the QRA analysis.

For localised fire, Saw et al. (2016) give a value of 50% efficiency for vehicles, "for illustrative purposes", but do not justify this data, therefore it is not considered in our methodology.

Ehrhart *et al*. (2020) proceeded by using statistics of the results of fire test on pressurized hydrogen tank to evaluate the failure rate of TPRDs, as explained in the following*:*

*"A literature review was performed on pressurized hydrogen tank fire testing. Experiments that included TPRDs, of any design, were included. Experiments that did not include TPRDs were excluded. Generally, the experiments reviewed were designed to test the hydrogen tank structures rather than the TPRDs themselves and the TPRDs were included in the experimental design as a safety measure. However, this means that each experiment represents a condition in which a demand was made on a TPRD and it either functioned as designed or did not. This data, shown in Table 2, was assumed to be representative of the actual TPRD failure-to-operate probability. This assumption may not hold if there are significant differences between the designs of the TPRDs used in experiments and those in operation in FCEVs."*

Also, in this case the authors assumed a Jeffrey's beta prior distribution, which from the available data resulted in a Beta (0.5, 16.5) distribution.

Based on these results, in the ET analysis for **localised fire** it is assumed as value for **TPRD failure probability of 0.03** which is evaluated as mean of the beta distribution (0.5, 16.5).

### 5.2.5 Probability of $H_2$ ignition

Ignition probabilities for hydrogen releases are proposed in the literature according to a step function with 3 levels for both immediate and delayed ignition (

Table 9) (La Fleur et al., 2017). The relationship depends only on the initial release rate and does not consider gas accumulation by confinement or extensive congestion. The **total ignition probability** is then the sum of the average probabilities for immediate and delayed ignition and is estimated to be **14.7%.** This value is used for release of hydrogen from the system where the diameter are dependent from the car design. This provides a complementary 85.3% chance of not igniting. In this latter case after release, the hydrogen does not ignite and therefore there is only dispersion of the substance into the atmosphere. On the contrary, once hydrogen escapes from the fuel system, the likelihood of an **immediate ignition is 66.7%,** generating a jet fire, while a **delayed ignition has a probability of 33.3%,** with a consequent deflagration and eventually a DDT.

*Table 9. Hydrogen ignition probability*

| **$H_2$ release rate (kg/s)** | **<0.125** | **0.125-6.25** | **>6.25** | **Average** |
|---|---|---|---|---|
| Immediate Ignition Probability | 0.008 | 0.053 | 0.23 | 0.098 |
| Immediate Ignition Probability | 0.004 | 0.027 | 0.12 | 0.049 |

Alternatively, a continuous model for ignition probability of hydrogen jet release is proposed according to the following equation (Aarskog et al., 2020):

$$P_{ign\_H2\_jet} = minimum(1.0; 0.55 \times rate^{0.87}; 0.267 \times rate^{0.52})$$

It gives 3 times higher ignition probability per cloud size for releases less than 125 g/s, 30% ignition probability for a 1.25 kg/s release, and 100% probability for ignition for releases above 12.5 kg/s.

In the case of hydrogen jet release from a TPRD the mass flow rate depends on the TPRD diameter and on the pressure tank. The TPRD release diameter for current hydrogen-powered vehicles is in the range of 2 mm to 6 mm. The use of smaller than 2 mm size of TPRD is preferable. The values of initial mass flow rate are reported for car (700 bar tank) and bus/train (350 bar tank) in Table 10. These values were calculated through the adiabatic model of blowdown of storage tank available on the free online e-Laboratory of Hydrogen Safety (https://elab.hysafer.ulster.ac.uk/) .

*Table 10. Initial mass flow rate of H2 jet from TPRD for cars and bus/train*

| **TPRD diameter (mm)** | **Initial mass flow rates (kg/s), for:** | |
|---|---|---|
| | Car (700 bar tank) | Bus/train (350 bar tank) |
| 0.5 | 0.0067 | 0.0038 |
| 1 | 0.0268 | 0.0150 |
| 2 | 0.1072 | 0.0601 |
| 3 | 0.2412 | 0.1353 |
| 4 | 0.4289 | 0.2405 |
| 5 | 0.6701 | 0.3757 |
| 6 | 0.9649 | 0.5410 |

Assuming a TPRD diameter for cars equal to 2 mm an initial flow rate of 0.1072 kg/s is evaluated to which corresponds an ignition probability of 8%. Similarly, for bus and train for which is assumed a TPRD diameter of 5 mm, the initial flow rate is 0.3757 kg/s and the ignition probability is 20%.

Concluding the **total probability of ignition of $H_2$ released from TPRD** is estimated here to be **8% for car and 20% for bus/train**. While the probability of an **immediate ignition** is 66.67%, and the complimentary probability of delayed ignition is 33.33%.

## 5.3 Consequence analysis

The consequence analysis includes the hazard from unignited release, hydrogen jet deflagration and fire, deflagrations/DDT/detonations of flammable cloud under a ceiling if it is created, blast wave and fireball after hydrogen storage tank rupture in a fire, etc. The pressure peaking phenomenon could hardly be relevant for hydrogen releases in tunnels and thus not included in ETA. For jet fire, the flame length, which depends on the storage pressure and release orifice diameter, can be calculated using the dimensionless correlation for hydrogen jet flames (Molkov and Saffers, 2013) that is available on the free online e-Laboratory of Hydrogen Safety (https://elab.hysafer.ulster.ac.uk/). The correlation is for free jets and applies to hydrogen temperatures down to cryogenic (Cirrone et al., 2019). Unfortunately, there are no engineering tools for the assessment of hazards of attached or impinging jets at the moment. In the case of TPDR releases, impinging jet will be shorter due to loss of momentum and follow-up effect of buoyancy than free jet and therefore the correlation can be considered as a conservative estimate. To assess the effect of radiation from a jet fire the radiative heat flux may be calculated. Radiant heat flux predictions derived from conventional single point source models have been observed to underpredict measured values by 40% or more, particularly in the near-field (Ekoto et al., 2012, 2014). On the contrary, weighted source flame radiation models have demonstrated substantial improvement in the heat flux predictions, particularly in the near-field of the hydrogen jet flame. Radiative heat fluxes are also considered in Computational Fluid Dynamics (CFD) software like FireFoam, Andrea-HF, Fluent, etc.

For the blast wave in tunnels, the engineering tool for the calculation of the hazard distances (Molkov and Dery, 2020) was employed for the consequence analysis. For fireball after high-pressure hydrogen tank rupture in a fire the engineering correlations for assessment of hazard distance (defined by the fireball size) are available both for stand-alone and under-vehicle tanks rupture in the open atmosphere, but not in confined spaces (Makarov et al., 2021). The HyTunnel-CS research demonstrated the higher hazard of fireball in a tunnel compared to the open atmosphere, i.e. propagation of fireball along the tunnel with velocity up to 20-25 m/s depending on the location of tank rupture in a fire. No correlation for fireball hazards in a tunnel is developed yet to be used in QRA.

Prediction of the consequences of hydrogen detonation is important for hydrogen safety assessment in confined spaces. Partner KIT (Li et al., 2021) calculated the hydrogen dispersion in the tunnel to evaluate the risk of flame acceleration and the DDT. The detonation in the tunnel is calculated by assuming a strong ignition at the top of the tunnel at an unfavourable time and location. The pressure loads are calculated to evaluate the consequence of the hazard.

Below are models and tools for hydrogen safety engineering of systems, e.g. vehicles, which were used for the assessment of hazards and associated risks in underground traffic infrastructure. The models and tools enable the assessment of hazards, the consequences of incidents and could facilitate the development of prevention and mitigation strategies and innovative engineering solutions.

### 5.3.1 Unignited release

Unignited hydrogen releases in the enclosures may accumulate and form a flammable cloud that may potentially burn if there is an ignition source, followed by thermal effects and a

dangerous overpressure; asphyxiation in case hydrogen release causes oxygen depletion is also potential hazard.

In the case of upward unobstructed release from TPRD at any angle, the similarity law, described in (Molkov, 2012) can be used to determine the concentration decay up to the ceiling. If hydrogen concentration under the ceiling is below LFL, the formation and build-up of flammable hydrogen-air cloud there can be excluded. Hydrogen at concentrations below LFL disperses further in the air and does not represent hazards in tunnels and underground parking. Care should be taken for small scale enclosures to exclude accumulation. The validated CFD models accounting for complex geometry and distributed over walls and ceiling vents can be applied for hydrogen safety engineering in such scenarios.

As an example, to determine the maximum distance at which LFL is reached ADREA-HF CFD code was used by NCSRD performing simulations of $H_2$ dispersion in different conditions (i.e. TPRD diameter, ventilation velocity). The CFD simulations (HyTunnel-CS, D2.3, 2022) performed for scenarios inside a tunnel, with and without inclination, showed that:

- Release through TPRD diameter in the range 2-4 mm leads to the formation of flammable volume that increases with the increase of TPRD diameter. However, TPRD with a smaller diameter might exhibit higher hydrogen cloud volumes of 10-75% vol. after a certain time due to the longer release duration.
- For the vertically downwards release the flammable cloud did not reach a distance of 4 m behind the car. The hazard distance and associated risk, however, increase with the increasing TPRD diameter.
- The ventilation inside a tunnel has a strong effect on the flammable cloud. The total flammable cloud and its dispersion towards the direction from which ventilation occurs is reduced significantly. However, the ventilation does not seem to have a significant effect on the total volume of the more hazardous fast-burning nearly-stoichiometric mixture because it is located for under-expanded jets in the momentum-dominated area of the jet. To exclude the formation of fast-burning mixture under the vehicle, it is wise to direct the release out of this area.
- Hydrogen tends to rise by buoyancy under the ceiling regardless of the release orientation. However, proper design of TPRD diameter and release direction could help ensure that hydrogen under the ceiling is at concentrations below the lower flammability limit and thus does not pose any hazard.

### 5.3.2 Jet fire

The dimensionless hydrogen flame length correlation (Molkov and Saffers, 2013) can be used to assess hazard distances for unobstructed hydrogen jet fires. It is valid for laminar and turbulent flames, buoyancy-controlled fire plumes and momentum-dominated jet fires, expanded (subsonic and sonic) and under-expanded (sonic and supersonic) hydrogen jet fires. The tool is freely available online and allows to calculate a flame length and three hazard distances (fatality, injury and no-harm) for free jets (https://elab.hysafer.ulster.ac.uk/).

The flame length at the storage pressure of 35 and 70 MPa, and TPRD orifice sizes typical for $H_2$ vehicles are reported in Figure 14 together with the hazard distances.

For the evaluation of hazard distances, the following harm criteria for people are considered:

- Temperature 70°C is taken as “no harm” criterion in this study.
- Temperature 115°C is assumed as the acceptance criteria for pain limit in hot air when considering an escape from an elevated temperature gas flow generated by a hydrogen jet fire.

- Temperature 309ºC is assumed as the acceptance criteria for "death" limit, causing third degree burns for a 20 seconds exposure, causing burns to larynx after a few minutes, escape improbable.

It should be noted that this correlation is for free jets and there are no engineering tools for attached jets at the moment. In the case of TPRD releases the direction of the jet may be considered vertical upward and downward or within an angle of 45° backward downward. This impinging jet will be shorter than free jet and therefore it can be considered a very conservative estimation.

To overcome the problem of the lack of engineering tools to model impinging jet, CFD calculations can be done. Radiative heat fluxes are also considered in Computational Fluid Dynamics (CFD) software like FireFoam, Andrea-HF, Fluent, etc

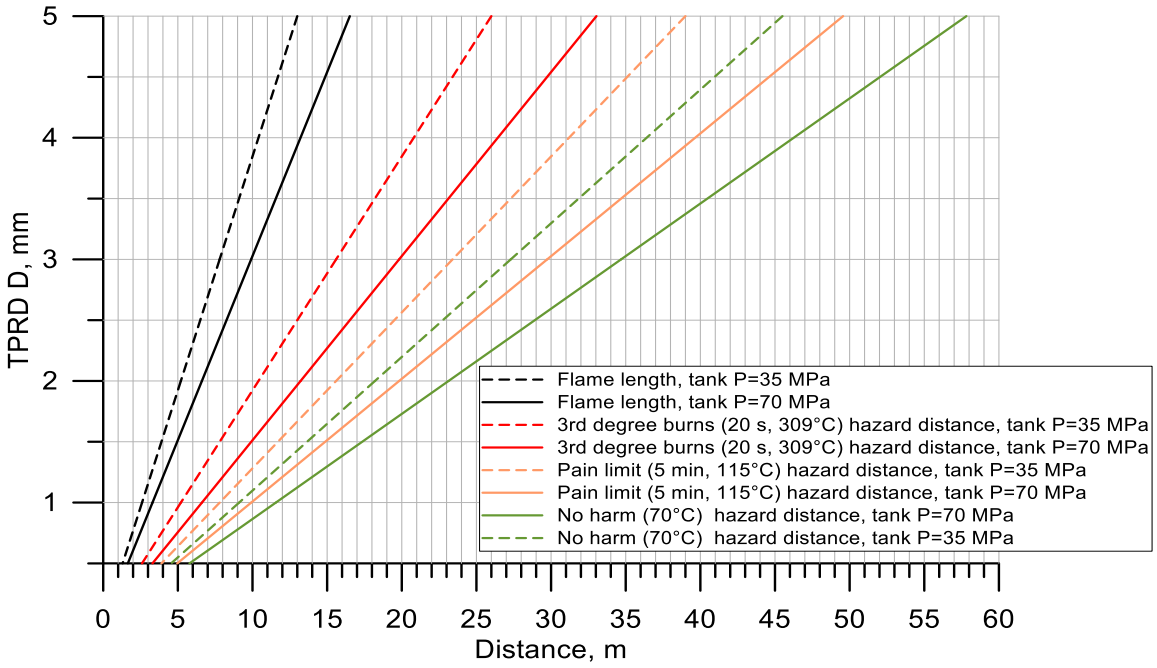


*Figure 14. Calculations of flame lengths and three hazard distances for free hydrogen jet fires.*

### 5.3.3 Tank rupture

The rupture of the hydrogen tank in a tunnel generates a blast wave, which has little decay with distance due to the one-dimensional character of the problem, a fireball that propagates with velocity up to 20-25 m/s in a tunnel behind the shock wave, and the projection of flying fragments.

For the prediction of the blast wave generated by catastrophic tank rupture the universal correlation of blast wave attenuation in a tunnel proposed by Molkov and Dery (2020) was employed (Figure 15). In Figure 15 the blast wave overpressure parameter ($\bar{P}_T$) defined as follows:

$$\bar{P}_T = \frac{\Delta P}{P_o \bar{L}_T}$$

is reported as function of the dimensionless tunnel length ($\bar{L}_T$)

$$L_T = \frac{P_o L A_T}{E A R^{0.5}} \left(\frac{fL}{D_T}\right)$$

where: $\Delta P$ is the blast wave overpressure (Pa), $P_0$ is the atmospheric pressure (Pa), L is the distance (m), $A_T$ is the tunnel cross-section area ($m^2$), $f$ is the friction factor, AR is the tunnel aspect ratio (width-to-height ratio) and $D_T$ is the tunnel hydraulic diameter (m)

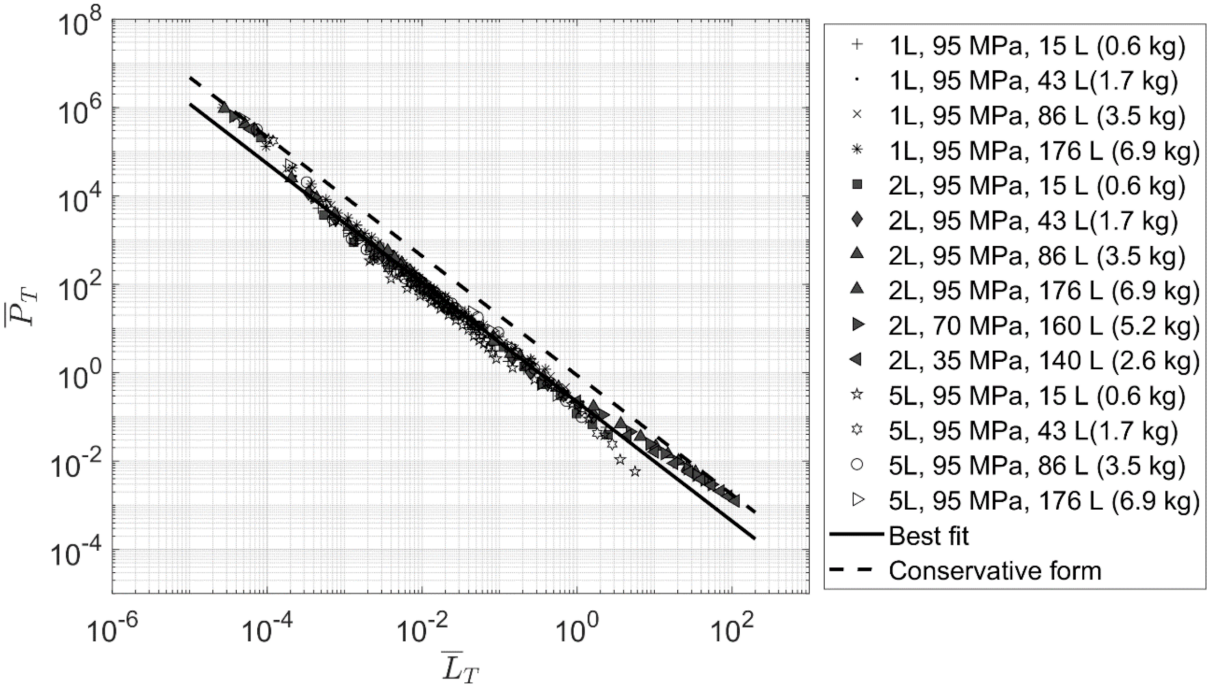


*Figure 15. Universal correlation for the blast wave decay after a hydrogen tank rupture in a tunnel fire ( Molkov and Dery, 2020) .*

For fireball after high-pressure hydrogen tank rupture in a fire, engineering correlations for assessment of hazard distance (defined by a size of the fireball) are available both for stand-alone and under-vehicle tanks rupture in the open atmosphere, but not in confined spaces (Makarov et al., 2021).

### 5.3.4 Deflagration/DDT

The delayed ignition of a highly turbulent under-expanded hydrogen jet causes a deflagration, and eventually a Deflagration-Detonation Transition (DDT), which can harm people and damage civil structures.

Predicting of the consequences of hydrogen deflagration and DDT is also important for hydrogen safety assessment, and for ensuring the safety of installations during accidents. Li et al. (2021) calculated the hydrogen dispersion in a tunnel to evaluate the risk of flame acceleration and the DDT. The detonation in the tunnel is calculated by assuming a strong ignition at the top of the tunnel at an unfavorable time and location. The pressure loads are calculated to evaluate the consequence of the hazard.

The evaluation of flame propagation and eventual DDT was performed by the partners of the project KIT through the method of flame propagation regime evaluation which is based on the so called sigma-criterion for flame acceleration, lambda criterion and run-up distance criterion for detonability evaluation. A detailed description of the method is reported in Li et al. (2021).

More details of the correlation developed by KIT for flame propagation and DDT in horizontal and vertical ventilation systems with non-uniform hydrogen-air mixtures in the presence of obstacles are reported in Appendix A1.

## 5.4 Harm to humans and structures

The generally applied method to estimate the level of harm to humans and structures uses the Probit (Probability unit) functions, which characterize the dose–effect relationship. A Probit Function transforms a dose to a probability of injury or fatality.
The dose is a concentration times duration of exposure, but the concentrations may be replaced by heat radiation flux, pressure load, etc.
In the case of a fire scenario a Probit function translates a thermal dose level to a probability of injury or fatality. Several Probit functions are available to evaluate the probability of injury or fatality as a function of thermal dose. Unfortunately, there is no Probit function that has been generated specifically for hydrogen fires. According to LaChance et al. (2011) the Eisenberg Probit function is likely the most appropriate Probit function in the harm predictions from radiant heat fluxes.

People involved in an explosion can suffer from harm due to the high level of overpressure. Direct and indirect effects are generally distinguished. On the one hand, pressure-sensitive organs (e.g., lungs and ears) can be damaged by a change in pressure. On the other hand, a person can be indirectly involved in the explosion and suffer from indirect damage, such as the impact from flying fragments generated by structure damage or collapse. In addition, people can be thrown away from the overpressure, with a possible subsequent impact. All these effects must be viewed in order to establish the risk to which a person may be exposed (Russo et al., 2020). Generally, a harm criterion is used to transform the consequences of an accident into a probability of harm to people. For people, both damage in terms of either injury or fatality are considered.

In the case of a catastrophic tank rupture possible consequences on humans and structures or equipment include blast wave overpressure effects, impact effects, impact from fragments generated by the explosion, the collapse of buildings, and the heat effects from subsequent fire balls. Only the blast wave effects on humans and structures are here considered.

The direct effect of explosion overpressure is normally displayed in the form of lethality as a function of overpressure and duration of the blast wave. Persons who are exposed to explosion overpressures have no time to react or take shelter; thus, time does not enter into the relationship. Probit functions are available to predict the level of harm to people and structures from the impact of blast overpressures (HyTunnel-CS, Deliverable 1.2, 2019)

The HSE report on methods of approximation and determination of human vulnerability for offshore major suggests a Probit relationship for blast over pressure fatality. Among the models available in the literature, the HSE model provides the most conservative results for low peak overpressures even if it provides lower probabilities than other models at higher overpressures (LaChance et al., 2011). The equation of Probit function suggested by HSEis the following:

$Y = 5.13 + 1.37 \ln (P)$ Pressure in barg units

where 1% fatality corresponds to 0.17 barg, 50% fatality to 0.90 barg and 95% fatality 3.00 barg.

Regarding the structural failure, the Eisenberg model (LaChance et al., 2011) is chosen as it provides results that agree reasonably well with the data reported by American Institute of Chemical Engineers (1998). The equation of Probit function for structural failure used is the following:

$Y= 23.8 + 2.92 \ln (P)$ Pressure in Pa

## 5.5 Risk evaluation

Whereas risk analysis is a scientific process of assessment and/or quantifying the probabilities and the expected consequences of identified risks, risk evaluation is a socio-political process in which judgements are made on the acceptability of those risks.

The risk evaluation is directed towards the question of acceptability and must answer the question "Is the estimated risk acceptable?" For a systematic and operable risk evaluation, risk criteria must be defined and whether a certain level of risk is acceptable or not must be determined. For the purpose of risk evaluation, different types of risk criteria are available. For example, for a system-based risk analysis, like the QRA proposed here, criteria expressed in terms of individual risk (e.g. probability of death per year for a specific person exposed to a risk) or societal risk (e.g. reference line in a FN diagram) can be applied (PIARC, 2012). Among them, individual risk was used as risk criterion in the QRA presented here.

There are no anthropic or natural activities which can be considered absolutely safe or risk-free, risk prevention and/or mitigation means that the risk value can be lowered below certain thresholds of societal acceptance (Figure 16)

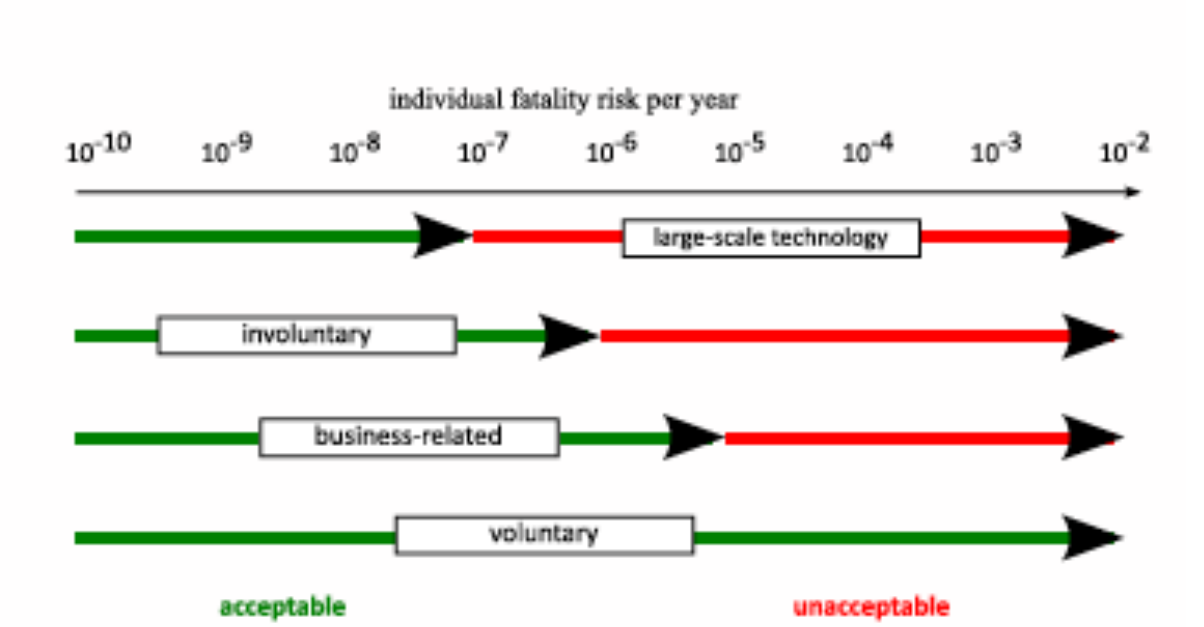


*Figure 16. Thresholds of societal acceptance of individual risk for different activities*

In our knowledge, specific acceptance criteria for users of road or railway tunnels, and underground car parks in the presence of the $H_2$ vehicle are not present in the literature. Selection of individual risk guidelines should be based on sound arguments and reflect the consensus of all stakeholders. Ideally, the risk associated with the utilization of hydrogen should not substantially increase the injury or fatality risk of an individual. This concept is based on Minimum Endogenous Mortality (MEM) which is a method to derive absolute values for risk acceptance, i.e. it is an equity-based risk acceptance criteria (EN 50126, 2000). MEM rule states that a new system should not lead to a significant increase in the risk exposure for the population with the lowest endogenous mortality. The rate of natural deaths is then a reference point for acceptability. It is mainly used within Germany to transport systems.

This principle has been derived as follows: Deaths due to "technological facts" (includes, e.g., work, machines, transport, do-it-yourself activities, entertainment and sport etc.) is called "Endogenous Mortality," R. In developed countries, this risk is lowest for the age group 5-15

years. This risk level is called the "minimum endogenous mortality," Rm. The principle is that Rm should not increase significantly as a result of a new transport system. Rm is $6\times10^{-5}$ fatalities/per person per year (in Germany) (source: Sterbetafel, Statistisches Bundesamt). As each individual is exposed to more than one risk, a value ≤MEM/20 should not be exceeded by a new technology (EN 50126, 2000). Thus, acceptable individual fatal risk: ≤ $3x10^{-6}$/yr.

As reported by LaChance et al. (2009): "*several groups have adopted this approach for hydrogen safety applications. This includes the EIGA [15] and the European Integrated Hydrogen Project (EIHP) [19]. The fraction of the fatality rate used by these two groups to establish a risk criterion ranges from 1% (EIHP) to 17.5% (EIGA). Recent data [20] suggest that the individual fatality risk from unintentional injuries in the United States is on the order of 3.8 x10$^{-4}$/yr (the cited rate in other countries is approximately 2 x 10$^{-4}$/yr [15]). Thus, the fatality risk criterion proposed by EIHP and EIGA are 2x10$^{-6}$/yr and 3.5 x 10$^{-5}$/yr, respectively.*"

For $H_2$ refuelling stations EIHP (Haugom et al., 2003) has established different types of criteria for all groups of people that are exposed to accidents.

- $10^{-6}$ per year for third party: "people living and working in the vicinity of the refuelling station or visiting/travelling through the neighbourhood of the refuelling station;
- $10^{-4}$ per year for second party: "people will be exposed to the risks at the refuelling station for a limited period of time, while visiting the facilities", or
- $10^{-4}$ per year for first party: "personnel involved in operation, inspection and maintenance of the hydrogen and/or the conventional re-fuelling station".

On the basis of the previous consideration, two risk acceptance criteria values were defined and utilised in the QRA as $10^{-5}$ and $10^{-6}$ fatalities per year.

### 5.5.1 Number of people in road tunnel after a crash

To define the number of people involved in an incident, it is necessary to identify the length of the queue (Lq) generated when the vehicles are stopped due to the car crash. This length is calculated as the product of queue formation speed ($v$) and the time of queue formation (t). The length of the queue in the tunnel is calculated as follows:

$$\mathrm{Lq} = v * \mathrm{t}$$

Queue formation speed is analytically calculated with the following formula proposed by Borghetti et al. (2019) as follows:

$$v = \frac{QBi - QAi}{\mathrm{KBi} - \mathrm{KAi}}$$

where $QA_i$ is the flow of vehicles interrupted due to the crash (post event) and $QB_i$ is the normally free flow condition in the i-*th* lane (before the event), both expressed as vehicles/h while $KA_i$ and $KB_i$ (vehicles/km) are respectively the vehicle density in the interrupted flow and in the free flow.

Considering the following assumptions:

- $QB_i = 0$;
- $QA_i = Q_i$ = the average daily traffic ADT, vehicles/h;
- $KB_i$ = density of the queue $D_{queue}$, vehicles/km;
- $KA_i = \frac{QAi}{v_{FL}} = \frac{Qi}{v_{FL}}$

- $v_{FL}$ = speed in the free flow conditions, km/h;

the queue formation speed equation becomes as follows:

$$v = \frac{-\mathrm{Q}i}{\mathrm{Dqueue} - \frac{Qi}{v_{FL}}}$$

where density of the queue, Dqueue, is calculated by the following equation:

$$Dqueue = \frac{1000 + dveic}{(lLV * \mathrm{LV\%} + lHV * \mathrm{HV\%} + dveic)}$$

*lLV*, *lHV* are respectively the average lengths of the light vehicles, heavy vehicles and *dveic* is the average safety distance between the vehicles stopped in the queue.

The purpose of this calculation is to define the number of people involved in a crash. Therefore, by multiplying the length of queue (km) and the density of vehicles (vehicles/km) the number of vehicles present in the tunnel after the crash was evaluated, and assuming a certain occupancy of the vehicle (i.e., 2 people per car) the number of people potentially exposed in the tunnel was obtained.

# 6 QRA methodology for an accident with onboard hydrogen storage tank inside a road tunnel (Task 5.3, lead - URS)

Many countries in the world are deploying hydrogen fuel cell vehicles (HFCV) such as passenger cars, buses, trucks, trains, marine vessels and aeroplanes. A fire incident with such a vehicle may involve a flammable liquid spill, hydrogen jet fire, smouldering fire, and the fact that the fire may affect an onboard hydrogen storage tank. The current onboard composite high-pressure tanks have a low fire-resistance rating (FRR) of 4-12 min (Kashkarov et al., 2021). Such FRR would be characteristic, for instance, for gasoline/diesel/hydrogen fires with intensity of specific heat release rate (HRR), i.e. ratio of the total fire HRR over the fire source area, A, HRR/A=1~4 MW/m$^2$. An incident in a tunnel with HFCV could escalate to fire and lead to a catastrophic onboard tank rupture with severe consequences for life, property and the built environment. The severity of an incident and risk will depend on the storage tank volume and pressure, tunnel and traffic parameters.

While the models for the quantitative risk assessment (QRA) in tunnels (Ehrhart et al., 2020) focus on the societal risk and safety measures of the tunnel, a QRA methodology in a tunnel considering the safety issues relevant to HFCV is lacking. The study (Dadashzadeh et al., 2018) has shown that increasing the FRR of onboard storage can reduce the risk to the acceptable level of $10^{-5}$ fatality/vehicle/year using innovative engineering solutions.

One of the reasons for the scatter of the hydrogen tanks' FRR values is the present fire test protocol of GTR#13 (UNECE, 2013) with no specified control of HRR/A. Other factors influencing the FRR are the tank design and the state of charge (SoC). A vehicle driving (or sailing) in-between fuellings would be always characterised by the SoC below 100%. It was observed for the selection of 17 hydrogen-powered cars where the SoCs before refuelling of the tanks varied from 17% to 59% on average (Mattelaer, 2020). Hence, looking at consequence analysis of a tank with SoC=100% would be a worst-case scenario. With the decrease of SoC to a certain level, e.g. in the numerical study (Kashkarov et al., 2021) the SoC below 54% was shown to be safe, the tank does not rupture in a fire, but leaks.

The detailed comprehensive analysis of different hazards, including jet fires from thermally activated pressure relief devices (TPRD), possible pressure and thermal effects from deflagrations and detonations, and projectiles emanating from a tank explosion, is out of the scope of this study. This QRA study is performed to address the risk associated with the blast waves after the tank rupture in the tunnels. The QRA methodology is demonstrated on a typical road tunnel to calculate the blast wave decay and define hazard distances for fatality, injury and no-harm. The risk in terms of fatalities per vehicle per year and the cost per accident (accounting for the loss of human lives only) are assessed for the hydrogen tank rupture at SoC=59% (assuming a realistic situation of a car driving some distance after refuelling).

## 6.1 The QRA for fuel cell vehicles in road tunnels (5.3, UU)

A flowchart of the QRA methodology is shown in Figure 17. The risk in terms of fatalities per vehicle per year (Figure 17a) is calculated based on the consequence analysis of hydrogen tank rupture and the frequency of ruptures per vehicle per year in road tunnels. Following a similar consequence analysis procedure, the risk in terms of cost per accident (Figure 17b) is evaluated using the tank rupture probability with an additional extension to account for losses of human lives in the incident scenario.

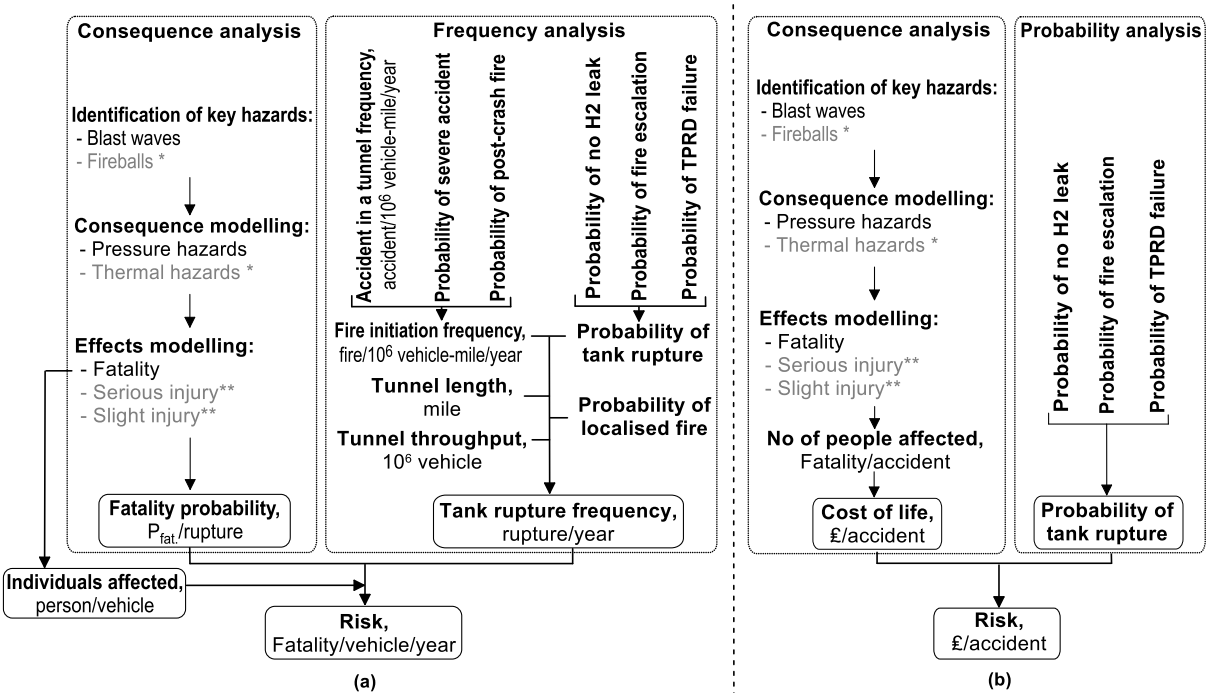


*Figure 17. The QRA methodology flowchart for HFCV in a tunnel: (a) risk in terms of fatality per vehicle per year; (b) risk in terms of monetary losses per accident.*

Notes: * fireball and thermal hazards are excluded from consideration in this study due to the current unavailability of the tool of fireball propagation inside tunnels; ** serious and light injury are excluded from consideration in this study; only fatalities are taken into account.

The main hazards after tank rupture in a tunnel are considered to be the blast wave, which has little decay with distance due to the one-dimensional character of the problem, and the fireball (not taken into account in this study), which propagates with velocity up to 20-25 m/s in a tunnel behind the shock wave based on a preliminary computational study.

The harmful effects on humans from the blast wave inside the tunnel (see Figure 18) are based on the pre-defined harm criteria (Kashkarov et al., 2020):

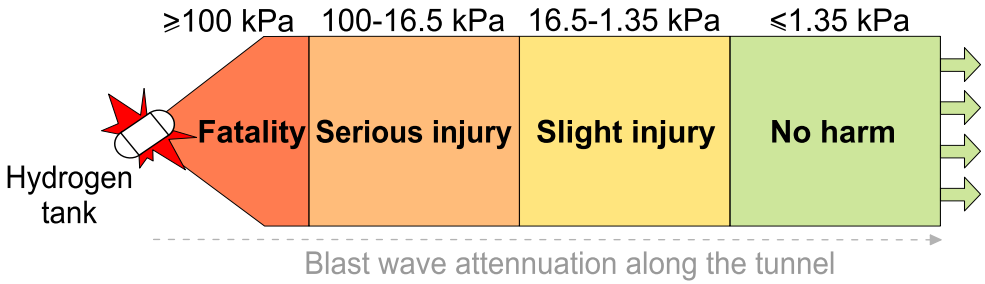


*Figure 18. Schematic representation of possible overpressure thresholds inside a tunnel and hazard zones.*

The frequency analysis (see Figure 17) includes the estimation of the tank rupture frequency (rupture/year) by multiplying the following parameters:

- the fire initiation frequency,
- the probability of tank rupture,

- tunnel parameters, i.e.
  - tunnel length and
  - tunnel throughput and
- the probability of a localised fire mode (among all the fires occurred).

Here the fire initiation frequency is calculated by multiplying:

- accident in a tunnel frequency,
- severe accident probability and
- post-crash fire probability.

The probability of tank rupture includes:

- the probability of no hydrogen leak (as no leak is considered before the tank rupture), following (LaFleur et al., 2017),
- the probability of fire escalation and
- the TPRD failure probability.

There is no, and probably cannot be, any statistics on a probability of localised (in sense on affecting or not the TPRD) fire among all fires. Indeed, each fire could be both a localised fire, e.g. when an edge of a liquid spill is affecting a tank, or a fire engulfing the tank fully. Moreover, the fire could start as localised due to small initial portion of combustion area and develop to engulfing fire (as per the GTR#13 fire test protocol). Thus, in our study we assume that half of all fires would affect the storage tank as an engulfing fire and half as a localised fire. Therefore, the probability of a localised fire, $P_{loc.fire}$, is taken as 0.5.

The consequence analysis includes the estimation of the fatality probability ($P_{fat.}$/rupture) and the individuals, i.e. passengers of the vehicles (person/vehicle).

Finally, the risk in terms of fatality/vehicle/year is calculated as a product of the fatality probability, the tank rupture frequency and the individuals affected (by fatality effect) inside the tunnel (see Figure 17a).

The risk in terms of cost per an accident is estimated as a product of the cost of life (based on the individuals affected) and the tank rupture probability. The latter is calculated by multiplying the no hydrogen leak probability, the fire escalation probability and the TPRD failure probability.

# 7 Examples of QRA of selected scenarios (Task 5.4; lead URS)

The QRA methodology for $H_2$ vehicles in confined spaces proposed by URS and DTU enables the calculation of the individual risk (IR), i.e. annual fatality probability, risk of structural failure and hazard distance associated with a hydrogen powered vehicle accident in a confined space like a tunnel (road or railway) and an underground car park. But further applications include other confined spaces like ship's hold. It provides the likelihood of all the possible scenarios and the consequence analysis includes the hazards from blast waves, DDT, hydrogen jet fires. The application of this QRA methodology developed by URS and DTU to the examples of a road tunnel in Italy, a railway tunnel in UK and an underground car park in Denmark is reported in this paragraph.

The QRA methodology developed by UU is focused on low frequency high consequence events, i.e. the rupture of a tank in a fire with the consequent blast wave and fireball. The QRA output for hydrogen powered vehicles in tunnels is a value of risk in terms of human fatality per vehicle per year (for vehicles having entered a tunnel) and in terms of monetary losses of human lives per an accident. The application of QRA methodology developed by UU for an accident with onboard hydrogen storage tank inside a road tunnel in UK is shown.

## 7.1 QRA of hydrogen vehicle in a road tunnel: Varano tunnel (Italy) (Task 5.4; URS, DTU)

As an example of the QRA methodology application to road tunnels, an Italian tunnel was considered. The investigated tunnel is the Varano tunnel. The investigated tunnel is located in Southern Italy along a rural road (S.S.145) between the cities of Castellamare di Stabia and Sorrento. It is a curved bi-directional road tunnel, 1.2 km long, 10.5 m wide and 5.5 m high, with an almost uniform upward slope of 2%. The tunnel has a rectangular cross-section with two lanes. The annual average daily traffic (AADT) is more than 10,000 vehicles per day for each traffic direction, with a percentage of heavy vehicles (HDV) slightly less than 5%. The speed limit for vehicles is 50 km/h.

The tunnel is equipped with a ventilation system constituted by eight pairs of axial jet fans fixed on the ceiling. In ordinary traffic conditions the first pair of fans is active for providing a minimum level of ventilation (air average velocity of 2–2.5 m/s), while in the case of fire emergency the activation of all fans supplied an air flow at the velocity of 9 m/s in order to remove and control smoke and toxic gases generated by fire. The emergency ventilation system is activated by a linear heat detection system when the temperature is above 68 °C (Caliendo et al., 2012, 2013), blocking both lanes of the tubes (Figure 19).

The scenario under congested traffic is assumed as follows: an HGV collides at high speed into the last vehicle (a FCEV) in a queuing situation, at the tunnel centre (600 m from the exit), blocking both lanes of the tube. In each lane of the tube, cars (carrying two persons per car) are supposed to queue up and stop, maintaining a minimum distance from the vehicle in front of about 2 m, up to the tunnel downstream portal, which is reached by the queue after about 10 min from the accident. People caught up in the traffic jam downstream of the HGV can be considered as being unable to leave the tunnel by car. From the middle of the tunnel length, the maximum distance to walk to reach exit B is 600 m. It is assumed that the car has two onboard storage tanks, whereas only the rupture on the larger tank of 62.4 L, NWP=70 MPa (Yamashita et al., 2015) is considered. Considering the onboard hydrogen tank's state of charge (SoC) will normally not be 100% (immediately after fuelling), but rather 40% on average (Mattelaer, 2020) after driving before refuelling, the value of SoC=40% (giving tank pressure of 24.4 MPa

at 20°C, as calculated using Abel-Noble real gas EoS) is selected for the consequence analysis. The value of SoC=100% is also selected as worst-case scenario.

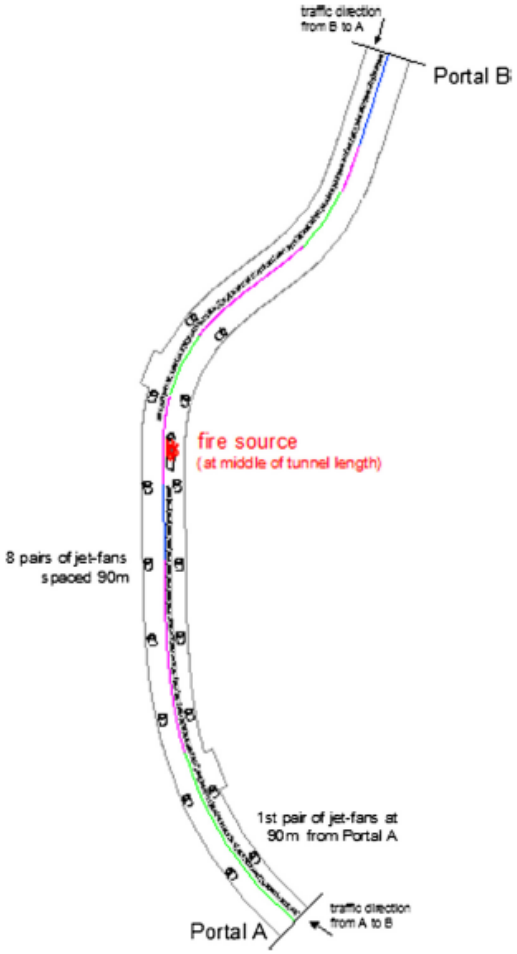


*Figure 19. A sketch of the tunnel with position of the accident and formation of the queues.*

### 7.1.1 Event tree

The event tree analysis for the case study of the Varano tunnel is reported in Figure 20.

The first step consists on the definition of a relevant accidental (initial) event that may give rise to unwanted consequences, which is defined here as an HGV colliding at high speed into the last vehicle (a fuel cell car) in a queuing situation.

For the calculation of the probability of different scenarios, an average tunnel accident rate of 0.46 per $10^6$ vehicle-km is used as reported by ANAS (2009) for Italian tunnels, and an average fire rate of $5.6\times10^{-3}$ per $10^6$ vehicle-km as reported by PIARC (2017) for tunnels in Italy. This latter corresponds to a probability that an accident in tunnels results in a fire of 1.2%.

As consequence of a crash hydrogen may be released from all the components of the hydrogen system which has the aim to supply hydrogen stably and safely such as magnetic valves, pressure regulator, pressure sensors, pressure relief valve, excess flow valve, etc. This is shown in the event sequence diagram with 90% probability of not releasing hydrogen and a 10% probability of a release (Lafleur et al., 2017; DOT, 2015; Pape and Cox, 2105). Once hydrogen is released from the hydrogen system it may ignite or not. The total probability of ignition is the sum of the averaged probabilities for immediate and delayed ignition, and is estimated to

be 14.7% (Lafleur et al., 2017). This provides a complementary 85.3% chance of not igniting. Then, if it ignites immediately (66.7%), generates a jet fire, while if its ignition is delayed (33.3%) a deflagration of turbulent jet can occur or possible deflagration of cloud under the ceiling (if it is formed).

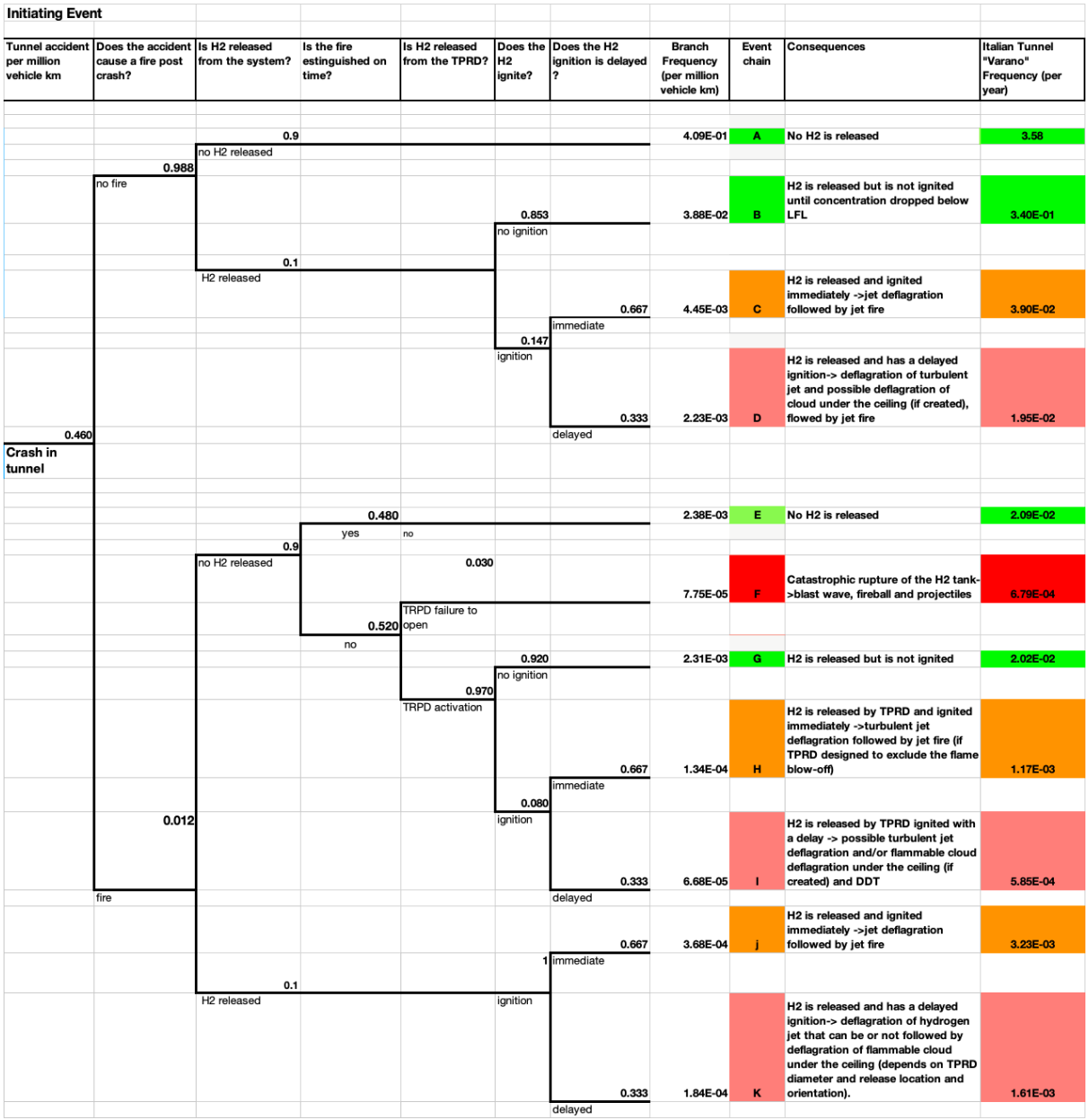


*Figure 20. Event tree for crash scenarios involving hydrogen vehicles (case of SoC=100%) in Varano road tunnel (case of localised fire).*

If the car catches fire after the crash, the consequence will depend on whether or not the fire reaches the fuel tank and affects the TPRD. If the fire is extinguished on time, $H_2$ is not released from TPRD. The probability that a fire can be extinguished on time, is obtained by comparing the time to fire extinguishment with the fire resistance rate of $H_2$ tank. According to the CFD simulation carried out by Kashkarov et al. (2021), for a 62.4 L tank type IV exposed to a fire of 1 MW/m$^2$, the fire resistance rate for a SOC of 100% is 8 min and it increases decreasing the SoC. It is here considered a time <10 min from fire detected to fire declared extinguished. According to the literature the probability that a fire is extinguished in a time <10 min is 48% (Casey, 2020). This provides a complementary 52% chance of not extinguishing. When the fire

is not extinguished on time, the tank is exposed to the fire and the TPRD may activate or not. The probability of failure of the TPRD is assumed to be 6.04 x $10^{-3}$ for engulfed fire (Saw et al., 2016) and 0.03 for localized fire (Ehrhart et al., 2019). In the following a localized fire is assumed as conservative approach.

If TPRD is not activated a catastrophic tank rupture may occur with fireball and blast wave as consequences. On the contrary, if TPRD is activated, $H_2$ is released, and it can be ignited with a probability of 8% for SoC=100% (3% for SoC=40%). This probability value is calculated for a TPRD orifice size of 2 mm and for SoC=100% (SoC=40%), which corresponds to an initial mass flow rate of 0.107 kg/s (0.040 kg/s) from the tank @700 bar (225 bar). This mass flow rate gives 8% (3%) probability of ignition (Aarskog et al., 2020). This provides a complementary 92% chance of not igniting. Then, if $H_2$ released by TPRD ignites immediately (66.7%), it generates a jet fire, while if its ignition is delayed (33.3%) it is possible turbulent jet deflagration and/or flammable cloud deflagration under the ceiling (if created) and DDT.

The branch frequency (events per $10^6$ vehicle-km) of each event chain is obtained by the combination of all the probabilities leading to that event chain multiplied by the frequency of the initiating event (event per $10^6$ vehicle-km). Then the likelihood of each event chain (events per year) is obtained by multiplying the branch frequency (events per $10^6$ vehicle-km) by the annual average daily traffic AADT ($10^6$ vehicle per day) by the number of days in a year (days per year) and the length of tunnel (km).

The results of the analysis show that the most likely consequence includes scenarios with no release of hydrogen (3.6 events per year) or hydrogen release without ignition (0.36 events per year). When the hydrogen does ignite, it is most likely a jet fire from the hydrogen system ($4.2\times10^{-2}$ events per year) than from a TPRD ($1.2\times10^{-3}$ events per year for SoC=100% and $4.4\times10^{-4}$ events per year for SoC=40%). If hydrogen-air flammable cloud is accumulated under the ceiling, it is more unlikely that deflagration of the cloud occurs ($5.8\times10^{-4}$ events per year for SoC=99% and $2.2\times10^{-4}$ events per year for SoC=40%).

### 7.1.2 Consequence analysis

#### *7.1.2.1 Jet fire*

In the case of release and subsequent ignition, a jet fire from TPRD is the most likely scenario. In this event, flame length and hazard distances are calculated thanks to the dedicated tool available in hydrogen e-laboratory (https://hyresponder.eu/e-platform/e-laboratory). In Table 11 the input data and the results in terms flame length and hazard distances are reported.

*Table 11. Input data and results for jet fire from 2mm-TPRD*

| **INPUT DATA** | | | | | |
|---|---|---|---|---|---|
| SOC (%) | $H_2$ pressure in reservoir (bar) | $H_2$ temperature in reservoir (°C) | Orifice diameter (mm) | Ambient pressure (atm) | Ambient temperature (°C) |
| 40 | 225 | 15 | 2 | 1 | 15 |
| 99 | 700 | 15 | 2 | 1 | 15 |
| **RESULTS** | | | | | |
| Flame length (m) | No harm (70°C) separation distance (m) | Pain limit (5 mins, 115°C) separation distance (m) | | Third degree burns (20 sec, 309°C) separation distance (m) | |
| 4.37 | 15.30 | 13.12 | | 8.74 | |
| 6.59 | 23.07 | 19.77 | | 13.18 | |

#### *7.1.2.2 Tank rupture*

In the presence of a localised fire, if the TPRD is not affected by a fire, or engulfing fire when fails to open, or is blocked from a fire during an incident, the catastrophic hydrogen tank rupture is the most likely scenario ($6.8\times10^{-4}$ events per year). For this worst-case tunnel scenario, the overpressures along the tunnel at different distances from the tunnel centre, where an accident occurs, are calculated through the universal correlation for the blast wave decay after a hydrogen tank rupture in a tunnel fire (Molkov and Dery, 2020).

The overpressures calculated along the Varano tunnel at different distances from tunnel centre as consequence of catastrophic tank rupture are reported Figure 21.

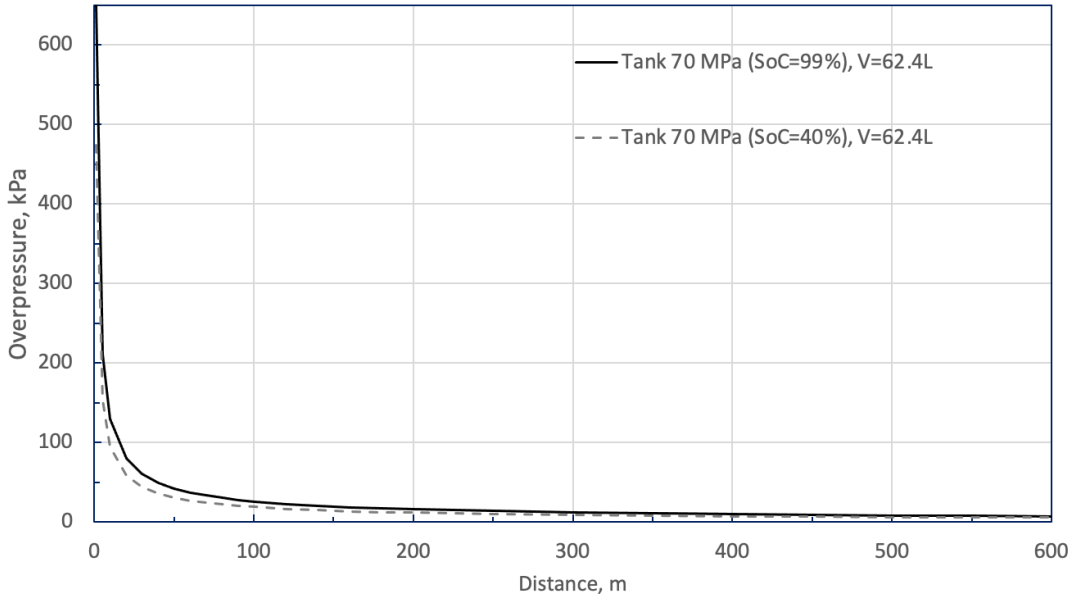


*Figure 21. Blast wave decay vs distance in Varano tunnel for the tank of 62.4 L: SoC=99% and SoC=40%.*

The probability of fatality at different distances from the tunnel centre is predicted using the Probit function using the HSE model (LaChance *et al*., 2011). Results in terms of fatality probability are reported in Figure 22 for the tank type IV of 62.4 L and two different SoC (99% and 40%).

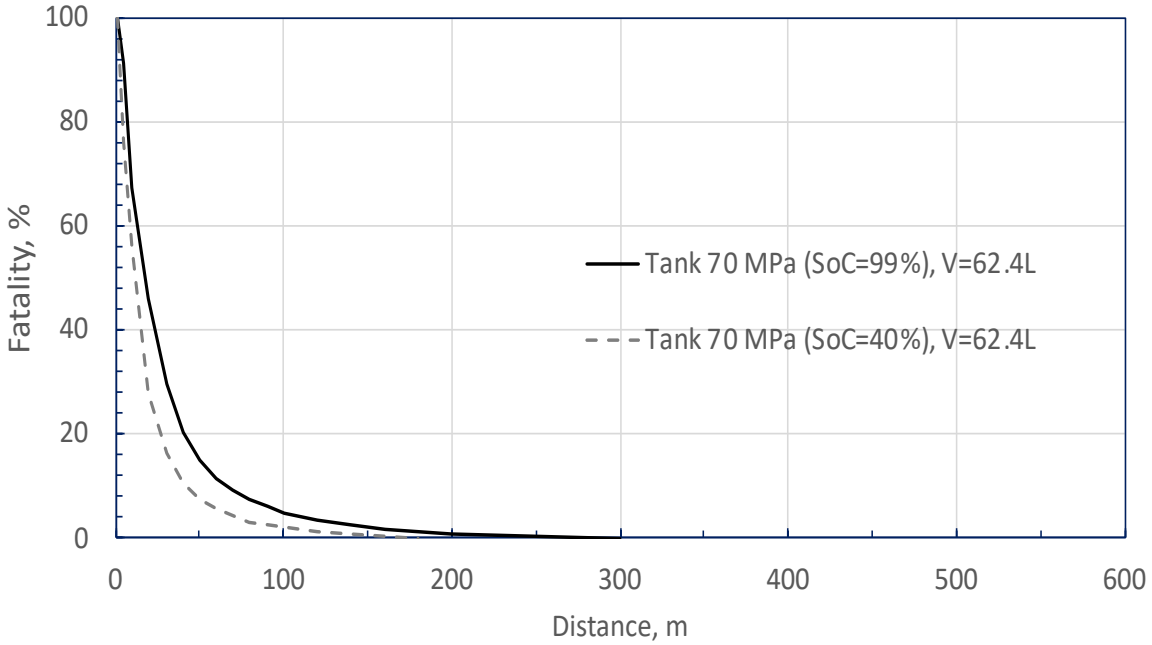


*Figure 22. Probability of fatality along the Varano tunnel at different distances from tunnel centre as consequence of catastrophic tank rupture (tank of 62.4 L: SoC=99% and SoC=40%).*

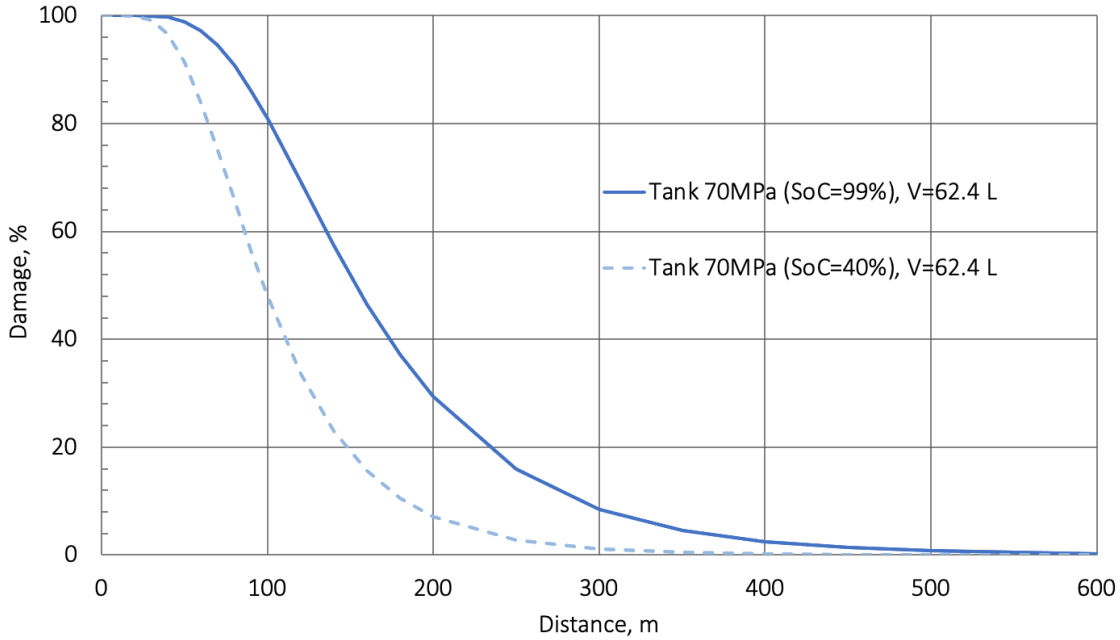


*Figure 23. Probability of structural failure along the Varano tunnel at different distances from tunnel centre as consequence of catastrophic tank rupture (tank of 62.4 L: SoC=99% and SoC=40%).*

It is observed that the probability of fatality is 100% at the tunnel centre. It decreases to 50% probability of fatality at a distance of 17 m and 10 m from the tunnel centre respectively for SoC=99% and SoC=40%, and to 1% at 190 m and 120 m from the tunnel centre for SoC=99% and SoC=40%, respectively.

The probability of failure of the tunnel structure is evaluated at different distances from the tunnel centre using the Eisenberg model (American Institute of Chemical Engineers, 1998). The Eisenberg probit provides as result a probability of tunnel failure of 100% up to a distance of 50 m and 30 m from the tunnel centre for SoC=99% and SoC=40%, respectively. It decreases to 50 % probability of failure at a distance of 154 m and 98 m from the tunnel centre respectively for SoC=99% and SoC=40%.

The comparison of the data provided in Figure 22 and Figure 23 shows that the human body is relatively resistant to static overpressure compared to rigid structures such as buildings. In this area of the tunnel failure fatality are also expected for indirect effect of the explosion.

#### *7.1.2.3 Deflagration/DDT*

In the case of hydrogen release and accumulation under the ceiling, four cases of hydrogen cloud formation in a tunnel cross-section were analysed for car and bus accidents, as shown in Figure 24:

- Case 1: Uniform hydrogen concentration distributed over the full tunnel cross-section for the given hydrogen inventory;
- Case 2: Uniform hydrogen concentration distributed inside a layer of hydrogen-air mixture for the given hydrogen inventory;
- Case 3: Stratified layer of hydrogen-air mixture for the given hydrogen inventory;
- Case 4: Stratified hydrogen-air mixture filled the whole tunnel cross-section for the given hydrogen inventory.

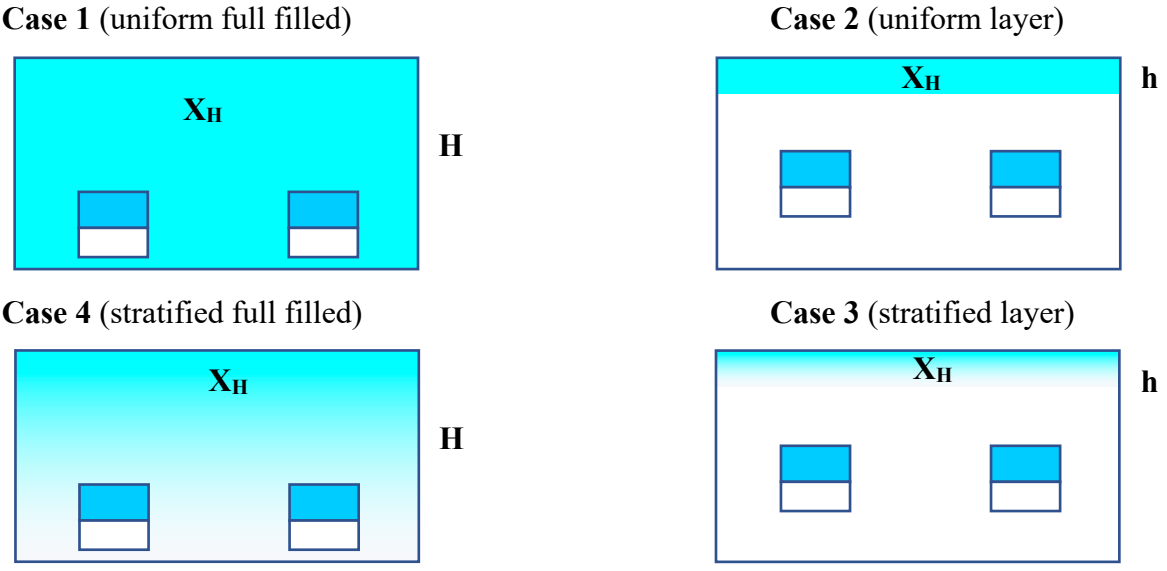


*Figure 24. Hydrogen distribution profiles in a tunnel.*

Then, if hydrogen cloud is ignited with delay, a deflagration or DDT may occur. The evaluation of flame propagation and eventual DDT is performed by the method of flame propagation regime evaluation developed by KIT which is based on the so called sigma-criterion for flame acceleration, lambda criterion and run-up distance criterion for detonability evaluation. A detailed description of the method and its application to the Varano tunnel is reported in Appendix A1.

Different amounts of hydrogen inventory from 2.48 kg for car accident and to 41.64 kg for bus accident could lead to different size of hydrogen-air flammable cloud. The traffic and hydrogen cloud characteristics considered in the model are reported in the following Tables 4-5 and 6-7 for car's accident (I) and buses accident (II), respectively.

*Table 12. Traffic characterisation for car accident (I).*

| Title | Value | Units |
|---|---|---|
| Cars in queue lane 1 | 125 | - |
| Cars in queue lane 2 | 125 | - |
| Car density | 10000 | vehicles/day |
| Car height | 1.7 | m |
| Car width | 1.8 | m |
| Car cross-section area | 3.06 | m2 |
| Car length | 6 | m |
| Parking distance | 2 | m |
| Distance between cars (front to front) | 8 | m |
| Blockage ratio BR (single lane) | 0.052987 | - |
| Blockage ratio BR (double lane) | 0.105974 | - |

*Table 13. Hydrogen cloud characterisation for car accident (I).*

| Title | Value | Units |
|---|---|---|
| Tank pressure | 700 | bar |
| Hydrogen inventory cars | 62.4 | Liter |
| Mass of hydrogen | 2.48 | kg |
| Volume of hydrogen (STP conditions) | 30.0 | $m^3$ |

*Table 14. Traffic characterisation for bus accident (II).*

| Title | Value | Units |
|---|---|---|
| Buses in queue lane 1 | 1 | - |
| Buses in queue lane 2 | 1 | - |
| Bus height | 3.1 | m |
| Bus width | 2.5 | m |
| Bus cross-section area | 7.75 | $m^2$ |
| Bus length | 12 | m |
| Parking distance | 2 | m |
| Distance between buses (front to front) | 14 | m |
| Blockage ratio BR (single lane) | 0.1342 | - |
| Blockage ratio BR (double lane) | 0.2684 | - |

*Table 15. Hydrogen cloud characterisation for bus accident (II).*

| Title | Value | Units |
|---|---|---|
| Tank pressure | 350 | bar |
| Amount of tanks | 8 | tanks |
| Hydrogen inventory buses | 200 | Liter/tank |
| Mass of hydrogen | 41.64 | kg |
| Volume of hydrogen (STP conditions) | 503.5 | $m^3$ |
| TPRD vent size | 5 | mm |

Table *16* shows the calculated release time for the car accident in a tunnel depending on TPRD orifice diameter from 1 mm to 5 mm in the case of accident (speed of sound 1909 m/s).

*Table 16. Calculated hydrogen release time for tank 70 MPa, 62.4 L.*

| **TPRD orifice diameter, mm** | **1** | **2** | **3** | **5** |
|---|---|---|---|---|
| Characteristic release time, $t_{ch}$, s | 41.6 | 10.4 | 4.6 | 1.7 |
| Total release time, $t$, s | 166 | 42 | 18 | 6.7 |

Table 17 shows the calculated release time for the bus accident in a tunnel depending on TPRD orifice diameter from 1 mm to 5 mm. The difference with previous Table 16 is the hydrogen tank volume and pressure (speed of sound 1614 m/s).

*Table 17. Calculated hydrogen release time for tank 35 MPa, 200 L.*

| **TPRD orifice diameter, mm** | **1** | **2** | **3** | **5** |
|---|---|---|---|---|
| Characteristic release time, $t_{ch}$, s | 157.8 | 39.4 | 17.5 | 6.3 |
| Total release time, $t$, s | 631 | 158 | 70 | 25 |

The case of hydrogen car accident in a tunnel with tank of 70 MPa and TPRD=5 mm was numerically simulated using GASFLOW-MPI CFD code (Li et al., 2019, 2021). A semiconfined layer of hydrogen-air mixture at the ceiling of the tunnel of about 1 m thickness is formed in 4 s (Figure 25a-b, snapshots 1 s and 4 s) without any tunnel ventilation i.e. a still atmosphere, velocity of 0 m/s. (stagnant air gives a conservative case). Then, it develops along the ceiling at almost constant thickness of 1m with longitudinal velocity starting from 2 m/s and approaching the velocity of 0.3 m/s after 8 s (Figure 30c, snapshot 8 s). In parallel, the average hydrogen concentration reduces inversely proportional to the time. At time 16 s (Figure 30d), a layer of 25-m length will be formed in the tunnel with a maximum hydrogen concentration of 15-20% vol. at the ceiling (Li et al., 2019, 2021).

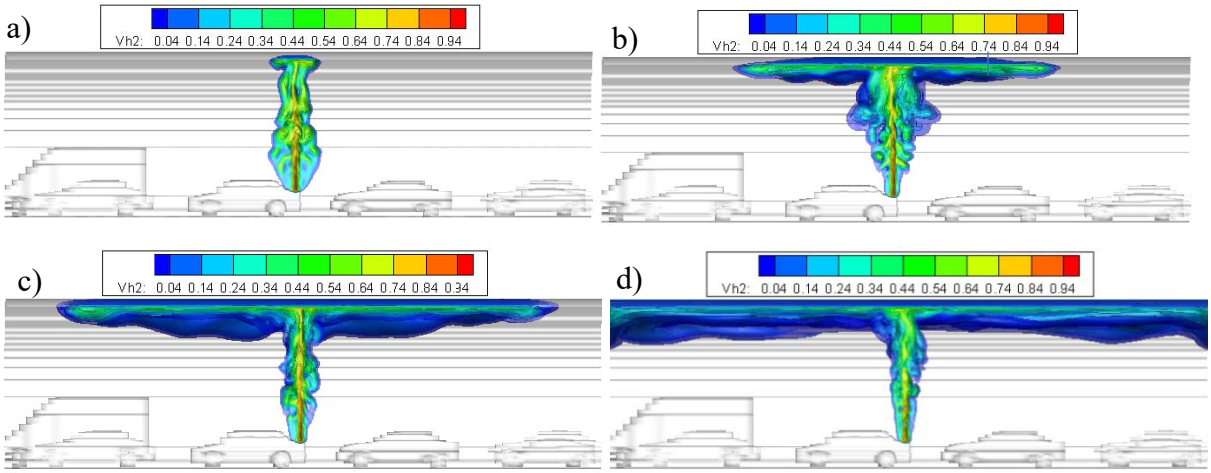


*Figure 25. Hydrogen distribution profiles in a tunnel vs. time after release: a) 1 s; b) 4 s; c) 8s; d) 16 s.*

The model allows the evaluation the possible flame propagation regimes of the hydrogen-air cloud formed by the release of 2.48 kg and 41.64 kg of hydrogen in the four defined cases of hydrogen release and distribution profile in the tunnel. Five levels of average hydrogen mole fraction in the cloud (cases 1 and 2) and five levels of maximum hydrogen mole fraction at the top of the cloud (cases 3 and 4) from 10% to 30% vol. of hydrogen were analysed.

The results of the flame propagation and DDT modelling are summarised as follows:

- The two scenarios (**case 1 and case 4**) for fully filled tunnel cross-section with a hydrogen-air mixture are more likely for a very short release time. In both cases the length of the cloud is not enough for flame acceleration to the speed of sound and transition to detonation. The flame propagates comparatively slow, with maximum combustion overpressure not higher than 0.1-0.2 MPa. Note that this was a preliminary simulation case that assumed a very large TPRD diameter and 0 m/s tunnel air velocity, which may not be representative of reality.
- The two scenarios (**case 2 and case 3**) for formation of a layer of hydrogen-air mixture are more likely for relatively longer release time of the order of 10 s. In both cases the length of the cloud is much longer and can be enough for flame acceleration to the speed of sound and detonation only in the case of bus accident if hydrogen concentration of 20-30% vol. is assumed.
- For all car accidents, there is no scenario of hydrogen release with formation of detonable cloud. The flame propagates comparatively slow with a maximum deflagration overpressure not below 0.1-0.2 MPa.
- If the simulations of release are performed then the realistic hydrogen concentration is likely to be lower than 15-20% vol. Thus, it makes impossible the detonation scenario even for the bus accident. An earlier ignition also prevents elongated cloud formation leading to detonation.
- Ventilation in a tunnel is also facilitate reducing the maximum hydrogen concentration below 15% vol. and thus is preventing the detonation for considered car and bus incident scenarios.

### 7.1.3 Risk evaluation

The individual risk is then calculated by multiplying the frequency of the tank rupture and the probability of fatality along the tunnel length (Figure 26).

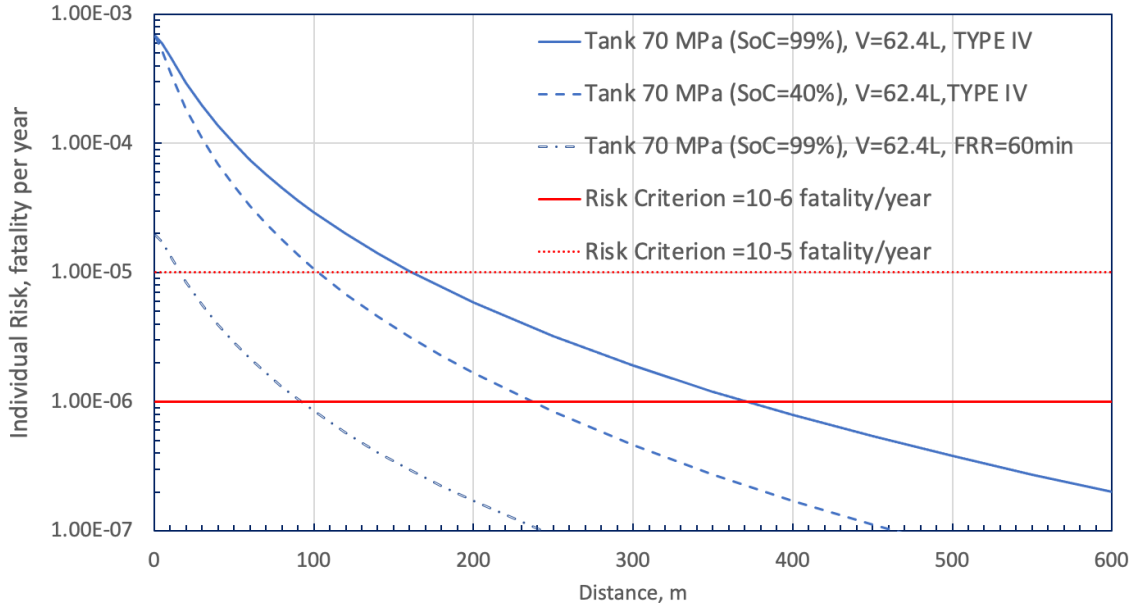


*Figure 26 Individual risk vs distance from the tunnel centre in the case of H2 tank rupture (localised fire) (tank of 62.4 L: SoC=99% and SoC=40%; tank: type IV and with FRR=60 min)*

The individual risk is in the range of $6.8\times10^{-4}$ -$1.0\times10^{-5}$ fatality per year up to a distance from the tunnel centre of 160 m for tank type IV of 62.4L SoC =99%, and of 100 m for SoC=40%.

Assuming a risk acceptance criterion of $10^{-6}$ fatality per year, a fatality hazard distance of 375 m and 240 m is evaluated for SoC=99% and SoC=40%, respectively. On the other hand, using as risk acceptance criterion of $10^{-5}$ fatality per year, hazard distance is reduced to 160 m and 100 m for SoC=99% and SoC=40%, respectively.

As already mentioned, for a 62.4 L tank type IV exposed to a fire the fire resistance rate (FRR) for a SOC of 100% is 8 min (Kashkarov et al., 2021). The increase of the tank FRR for a localised fire reduces the fatality rate, as an example a tank with FRR=60 min (Figure 22) reduces the risk below the acceptable level of $10^{-5}$ fatality per year in all the tunnel except 10 m close to the tunnel centre.

To determine the number of users potentially involved in the event, it is necessary to know the number of vehicles in the queue, their position and size, and the respective occupants. It is here used the vehicle queue formation model for each lane inside the tunnel following an accident reported by Borghetti et al. (2019). The model gives the instantaneous length along which the queue of vehicles extends in each i-th lane from the accident location to the tunnel entrance. The length of the queue is calculated on the basis of the following data: i) the annual average daily traffic is more than 10,000 vehicles per day for each traffic direction and with a percentage of heavy vehicles slightly less than 5% and 95% of light vehicles; ii) the highest speed at which vehicles can legally drive on the road containing the investigated tunnel is 50 km/h; iii) vehicles are forbidden to overtake; iv) the average lengths of the light vehicles, heavy vehicles are for modern vehicles respectively 5 m and 10 m; v) the distance between cars (back front) is 2 m; vi) the average occupancy of car is 2 persons per car. In each lane it is calculated that 83 cars are in the queue, carrying two persons per car, which corresponds in total to 83x2=166 persons.

Assuming a risk acceptance criterion of $10^{-6}$ fatality per year, the fatality hazard distances of 375 m and 240 m (SoC=99% and SoC=40%, respectively) correspond respectively to a queue of 52 and 33 cars for each lane, and assuming an occupancy of 2 people per car, respectively 103 and 66 fatalities. On the other hand, using as risk acceptance criterion of $10^{-5}$ fatality per year, the number of cars in the queue for each lane is 22 and 14 (160 m and 100 m for SoC=99% and SoC=40%, respectively), and the fatalities 44 and 28, respectively.

These hazard distances are significantly higher than the no-harm distance calculated in the case of a hydrogen jet fire from TPRD of 15-25 m for SoC =40-100% (Table 11).

With respect to damage to the equipment and cars in the tunnel, the overpressure reached in the accident location is higher (657 kPa) than the threshold value of 200 kPa to crash cars up to 5 m from the tunnel centre (SoC=99%). The risk of failure of the tunnel structure is $6.8 \times 10^{-4}$ up to a distance of 50 m and 30 m from the tunnel centre for SoC=99% and SoC=40%, respectively, which decreases to $3.4\times10^{-4}$ at a distance of 154 m and 98 m respectively for SoC=99% and SoC=40%.

### 7.1.4 Results and discussion

The results of the frequency analysis (event tree in Figure 20) show that the most likely consequence includes scenarios with no release of hydrogen (3.6 events per year) or hydrogen release without ignition (0.36 events per year). When the hydrogen does ignite, the event chain is most likely a jet fire from the hydrogen system ($4.2 \times10^{-2}$ events per year) than from a TPRD ($1.2 \times10^{-3}$ events per year for SOC=99%). In the presence of a localised fire, if the TPRD fails to open, the catastrophic $H_2$ tank rupture is the most likely scenario ($6.8 \times10^{-4}$ events per year).

For the catastrophic $H_2$ tank rupture, the consequence analysis allows the calculation of the probability of fatality and of tunnel failure as shown in Figure 22 and Figure 23. The individual risk is then calculated by multiplying the frequency of the tank rupture and the probability of fatality along the tunnel length (Figure *26*). The individual risk is in the range of 6.8 $10^{-4}$ -1.0 $10^{-5}$ fatality per year up to a distance from the tunnel centre of 160 m for SoC =99% and of 100 m for SoC=40%.

Assuming risk criteria of $10^{-6}$ per year, a hazard distance of 375 m and of 240 m is evaluated for SoC =99% and SoC=40%, respectively. At these hazard distances correspond respectively 52 and 33 cars in the queue and of 104 and 66 persons involved in the event of for each lane.

Increasing the tank FRR for a localised fire the fatality rate decreases, specifically a tank with FRR higher than 60 min may reduce the individual risk below the acceptable level of $10^{-5}$ fatality per year.

Comparing these results with those obtained for jet fire (Table 11), in the case of tank rupture the hazard distances are significantly higher than no-harm distance calculated in the case of a hydrogen jet fire released from TPRD (from 15 to 23 m for SOC from 40 to 99%).

For all car accidents, there is no scenario of hydrogen release with formation of detonable cloud. The flame propagates comparatively slow with a maximum deflagration overpressure not below 0.1-0.2 MPa. The detonation scenario is impossible even for the bus accident. An earlier ignition also prevents elongated cloud formation leading to detonation.

## 7.2 QRA of hydrogen vehicle in a road tunnel: Dublin tunnel (Ireland) ((Task 5.4; UU)

The suggested for this study hypothetical tunnel is analogous to Dublin Tunnel of 2.89 miles length (4650 m), from the available information on different tunnels in UK and Ireland (RTA, 2019). The tunnel has 2 tubes with 2 lanes each. A tube has the traffic traveling in the same direction on both lanes. In the example of the QRA methodology application, the consequence analysis will be performed for 1 tube. The proposed scenario includes the following assumptions:

- An HFCV is trapped in a severe accident inside the tunnel, which has escalated to a fire. The car has two onboard storage tanks, whereas only the rupture on the larger tank of 62.4 L, NWP=70 Mpa, $m$=2.5 kg of hydrogen (Yamashita et al., 2015) in a fire will be considered.
- The blast wave decay in the tunnel is calculated for a case of stand-alone tank rupture, i.e. without spending mechanical energy of compressed gas on vehicle destruction, body frame translation, etc. (Molkov and Dery, 2020). The reasoning is justified as in the far-field, which is practically the entire tunnel length, the blast wave strengths for a stand-alone or an under-vehicle tank are similar (Molkov and Kashkarov, 2015).
- The car incident location is 50 m away from the tunnel tube exit. Both lanes in the tube for the same direction of traffic are blocked by an incident. This makes all the vehicles that have entered the tunnel, trapped inside and unable to carry on driving to leave the tunnel. This gives the affected tunnel length of (4650–50) m = 4600 m.
- Considering the onboard hydrogen tank's SoC will normally be from 17% to 59% on average before refuelling (Mattelaer, 2020), the value of SoC=59% (the equivalent of storage pressure of 35.5 Mpa and 1.5 kg of hydrogen at 20°C) is selected for the consequence analysis. The tank filled up to NWP=70 Mpa at 20°C would have SoC=99% (or SoC=100% at temperature 15°C).

Table 18 shows mechanical, $E_m$, and chemical, $E_{ch}$, energy fractions contributing to the blast wave strength and calculated using the methodology (Molkov and Kashkarov, 2015).

*Table 18. Fractions of mechanical and chemical energies contributing to the blast wave strength after 62.4 L tank rupture in a fire for two different values of the SoC.*

| Tank SoC, % | Tank $\boldsymbol{P}$, Mpa | $\boldsymbol{E_m}$, MJ | $\boldsymbol{E_{ch}}$, MJ | $\boldsymbol{E_{tot}}$, MJ |
|---|---|---|---|---|
| 99 | 70 | 13.6 | 15.6 | 29.2 |
| 59* | 35.5* | 8.1* | 9.3* | 17.4* |

Note: * will be used for the consequence analysis in the methodology application example.

Table 19 presents the parameters of the tunnel and the assumed for this study number of cars and average number of people per car.

*Table 19. Tunnel and vehicle parameters and the average number of passengers per vehicle.*

| | | |
|---|---|---|
| Overall tunnel length (RTA, 2019) | 4650 | m |
| Tunnel cross-section area (Molkov and Dery, 2020) | 39.5 | $m^2$ |
| Tunnel length used in calculations | 4600 | m |
| Tunnel throughput (RTA, 2019) | 5.5 * | $10^6$ vehicle |
| Car length (calculated average from "What are the average dimensions of a car in the UK?", 2021) | 4.5 | m |
| Length of the gap between cars (assumption) | 5 | m |

| | | |
|---|---|---|
| Average No of passengers per vehicle ("Average car and van occupancy England 2002-2018 statistics") | 1.55 | person/vehicle |

Note: * $5.5\times10^6$ vehicle throughput is for two tubes of the tunnels, for one tube the value $5.5\times10^6/2=2.75\times10^6$, which will be used in our study.

### 7.2.1 Consequence analysis

The rupture of a tank occurs due to exposure of the tank to the initiating fire given that both safety barriers, i.e. TPRD initiation by the fire and the fire extinction by emergency actions, fail. Figure 27 shows the sequence of events for an incident.

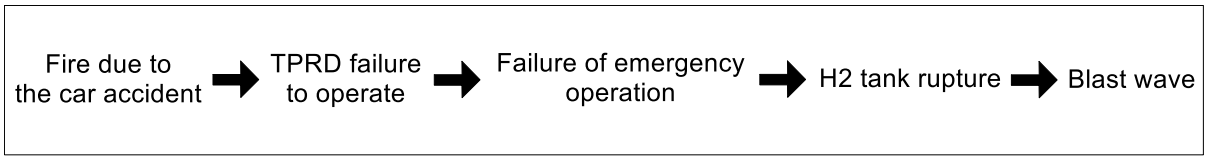


*Figure 27. The sequence of events leading to tank rupture in a fire and resulting in the blast wave.*

The experimental, e.g. (Weyandt, 2006, 2005; Zheng et al., 2010) and numerical, e.g. (Molkov et al., 2021) studies on the performance of hydrogen storage tanks in a fire, consequences of tank rupture and mechanism of the blast waves formation and decay have been carried out for the open atmosphere only. Only partial data is available on high-explosive charges with the mass equivalent to that of trinitrotoluene (TNT). The TNT blast wave, on the other hand, differs from the blast wave generated by a hydrogen tank rupture in a fire, in particular by the process of how the chemical energy is released. The original dimensionless correlation (Molkov and Dery, 2020) is applied in this study to calculate the blast wave decay in the tunnel after the rupture of 62.4 L, 70 Mpa tank at SoC=99% (70 Mpa at 20°C) and SoC=59% (35.5 Mpa at 20°C). The correlation (Molkov and Dery, 2020) allows for consequence assessment for the rupture of any hydrogen tank in a fire inside a tunnel of any cross-section area, aspect ratio and length. The calculated overpressure decay along the hypothetical tunnel is shown in Figure 28 together with three thresholds (fatality, injury and no-harm).

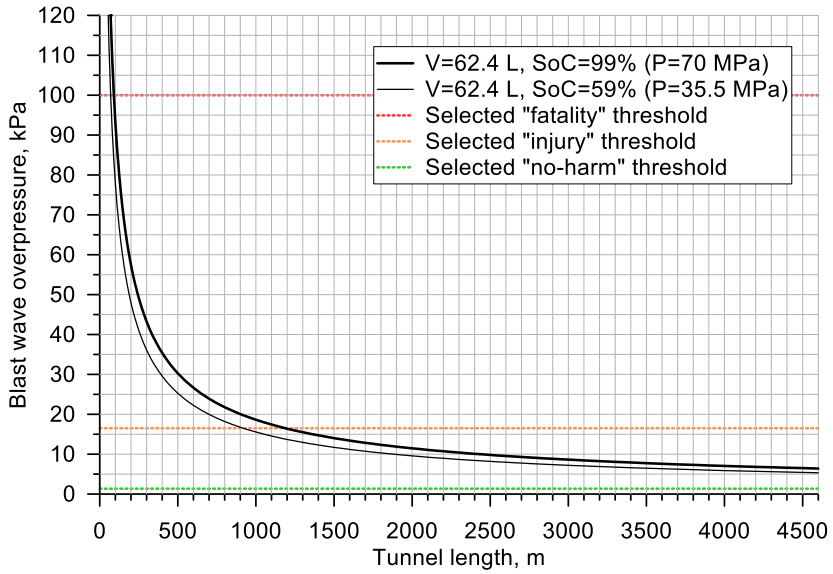


*Figure 28. Blast wave decay in the tunnel for the 62.4 L tank for SoC=99% and SoC=59% (T=20°C).*

The four hazard zones, i.e. fatality, serious injury, slight injury, and no-harm due to a blast wave together with corresponding probabilities are shown in Table 20.

*Table 20. Hazard zones from the blast wave after the tank rupture inside one tube of the tunnel.*

| Harm to people | Blast wave hazard zone for tank rupture at different SoC | |
|---|---|---|
| | For tank SoC=99% (70 Mpa) | For tank SoC=59% (35.5 Mpa) |
| Fatality | 0-90 m | 0-70 m |
| Serious Injury | 90-1150 m | 70-900 m |
| Slight Injury | 1150-4600 m (end of the tunnel) | 900-4600 m (end of the tunnel) |
| No harm | Does not exist | Does not exist |

Therefore, for the tank rupture at SoC=59% (35.5 Mpa) within the first 70 m from the car, the number of people affected is estimated as follows. Given the vehicle length 4.5 m and the assumed gaps between vehicles 5 m, the number of vehicles in 2 lanes within the fatality zone is [70 m/(4.5 m+5 m)]×2 = 15. Given the average number of passengers per vehicle 1.55, the average number of people in the fatality zone is 15×1.55 = 23.25.

The cost of fatality, serious injury, and slight injury are £1,336,800, £207,200, and £300 respectively as introduced by the UK's Health and Safety Executive (HSE). In this study, only the cost of fatality is accounted for in the risk calculations. By multiplying the single fatality cost by the number of fatalities the cost of losses of people due to fatality in an accident involving an HFCV inside the tunnel is calculated as 23.25×£1,336,800=31,080,600 £/accident.

### 7.2.2 Frequency analysis

#### *7.2.2.1 Frequency of the initiating fire event*

The number of hydrogen-powered vehicles is currently very small compared to conventional fuel vehicles. There are no statistics on fire accidents with HFCV. It was assumed here that the parameters relevant to assessing the frequency of initiating fire events associated with HFCVs are the same as for fossil fuels cars. The frequency of fires due to a vehicle accident in the tunnel was estimated using data (Bassan, 2016; LaFleur et al., 2017; NHTSA, 2015) as:

$$F_{fire\ init.} = F_{tunn.accident} \times P_{sev.accident} \times P_{p-crash\ fire}, \quad (1)$$

Using the data available from (Bassan, 2016; Chris Lafleur et al., 2017; NHTSA, 2015), it is calculated as $F_{fire\ init.}$=3.1×10$^{-1}$ accident/10$^{6}$ vehicle-mile/year × 5.94×10$^{-2}$ × 3.17×10$^{-1}$ = 5.84×10$^{-3}$ fire/10$^{6}$ vehicle-mile/year.

#### *7.2.2.2 Failure probability of TPRD*

There is no published data and data on the failure rate of TPRD for hydrogen-powered vehicles. The conservative characteristic value for the random mechanical failure probability of pressure relief devices (PRD) was proposed in the publicly available database NPRD (Reliability Analysis Center, 1991) as $6.04 \cdot 10^{-3}$. This value is used in the calculation of TPRD failure probability similar to (Dadashzadeh et al., 2018). The FireComp project (Saw et al., 2016) suggested the TPRD failure probability in fire conditions as 0 for the engulfed fire and 0.5 for the localised fire. Hence, the failure probability of TPRD in our study can be calculated as (1-0)×(6.04×10$^{-3}$)+0=6.04×10$^{-3}$ for the engulfing fire, and (1-0.5)×(6.04×10$^{-3}$)+0.5=5.03×10$^{-1}$ for the localised fire. Dadashzadeh et al. (2018) demonstrated that the highest risk for a hydrogen-powered vehicle on London roads is due to a localised fire. This study focuses solely on the localised fire scenario being the worst-credible one for tank rupture in a fire.

#### 7.2.2.3 Escalation probability

A probability of failure of emergency operations to extinguish a fire that leads to tank rupture, i.e. the escalation probability, $EP$, could be assessed by implementing a probit function, $Y$ (Landucci et al., 2015, 2009). For avoiding the complications of the integration, the EP was expressed in the following form using the error function ($erf$) following (Papoulis, 1965):

$$EP = \frac{1}{2}\left[1 + erf\left(\frac{Y-5}{\sqrt{2}}\right)\right], \quad (2)$$

where $Y$ is the probit function, previously used as the general equation in the probit analysis (Landucci et al., 2015, 2009; Finney, 1971) which assumes log-normal distribution. The probit function in a scenario of a fire brigade arrival at an accident involving a fire considering a 90% failure probability for 5 mins response time and 10% for 20 mins response time with a hydrogen-powered vehicle can be written as (Dadashzadeh et al., 2018):

$$Y = 9.25 - 1.85 \times ln(FRR), \quad (3)$$

where the $FRR$ is the time from fire initiation until the tank rupture in a fire in case of failed TPRD. For example, for 36 L, 70 Mpa Type IV tank the FRR is 8 min (Makarov et al., 2016; V. Molkov et al., 2021). The use of Eqs. (2) and (3) allow calculation of the EP value as: $Y$=9.25-1.85×ln(8)=5.403, hence $EP$=1/2[1+ $erf\left(\frac{5.403-5}{\sqrt{2}}\right)$]=6.57×10$^{-1}$.

#### 7.2.2.4 Probability of a tank rupture

The tank rupture probability is calculated as:

$$P_{t.rupture} = P_{TPRD\ fail.} \times EP \times P_{no\ leak}. \quad (4)$$

Using the value of 9×10$^{-1}$ (LaFleur et al., 2017) for the "No $H_2$ leak probability", the tank rupture probability is obtained as $P_{t.rupture}$=5.03×10$^{-1}$ × 6.57×10$^{-1}$ × 9×10$^{-1}$ = 2.97×10$^{-1}$.

#### 7.2.2.5 Frequency of a tank rupture

Having already calculated the values of the fire initiation frequency, Eq. (1) and the probability of tank rupture, Eq. (4), the tank rupture frequency can be obtained as follows:

$$F_{t.rupture} = F_{fire\ init.} \times P_{loc.fire} \times P_{t.rupture} \times L_{tunnel} \times TH_{tunnel}. \quad (5)$$

Hence, the tank rupture frequency for the considered accident scenario is:

$F_{t.rupture}$=5.84×10$^{-3}$ fire/10$^6$ vehicle-mile/year ×0.5×2.97×10$^{-1}$×2.89 mile×2.75 10$^6$ vehicle = 6.89×10$^{-3}$ rupture/year.

### 7.2.3 Results and discussion

The risk of fatality is calculated as (see Figure 17a):

$$Risk = P_{fat.} \times F_{t.rupture} \times N, \quad (6)$$

where we assume that the fatality probability, $P_{fat.}$, for people in fatality zone in the tunnel would be taken as 1 (as all the people in this zone would be subject to overpressure equal or above the fatal overpressure threshold), the tank rupture frequency, $F_{t.rupture}$, is obtained from Eq. (5) and the affected individuals (passengers per vehicle), $N$, is presented in Table 20. The fatality probability strongly depends on the tank's $FRR$. The $FRR$ of an unprotected hydrogen tank in a realistic fire, e.g. gasoline/diesel spill fire source of $HRR/A$=1 MW/m$^2$, is as low as 4-6 min. It can reach tens of minutes for the quite low $HRR/A$=0.2 MW/m$^2$ (Molkov et al., 2021). The tank $FRR$ can be significantly increased, e.g. beyond 1 hour, by using intumescent

paint (Makarov et al., 2016). However, it should be noted that this will not guarantee the exclusion of the tank rupture in a fire.

Figure 29a presents the risk of fatality as a function of FRR of the onboard hydrogen storage tank. The risk acceptance criteria value was defined as $10^{-5}$ fatality/vehicle/year which is proposed by (EIHP2, 2003) as an acceptable level of risk for the first responders in a hydrogen refuelling station. Figure 29b shows that the risk in terms of the cost per accident can be as high as about £9.24M for the aforementioned tank with $FRR$=8 min.

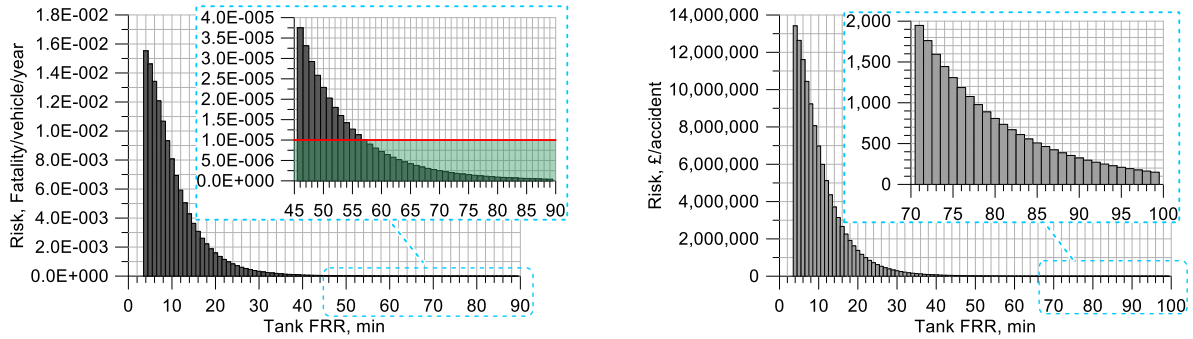


*Figure 29. Risks as a function of hydrogen storage tank FRR in a fire for 62.4 L tank rupture at SoC=59%: (a) Risk (Fatality/vehicle/year), (b) Risk (£/accident).*

It can be seen in Figure 29a that for a hydrogen tank with $FRR$=8 min (Makarov et al., 2016) the risk is $1.07\times10^{-2}$ fatality/vehicle/year, which is 3 orders of magnitude bigger than the acceptable level (shown with a red line with a light green transparent filling under it in the graph insert). The increase of the tank $FRR$ for a localised fire reduces the fatality rate progressively until the risk becomes below the acceptable level at the $FRR$ as long as 58 min. The monetary cost of an incident, however, can be significantly reduced down to as low as only £300, but only if the FRR can be as long as at least 91 min, as can be seen in Figure 29b.

One of the possible solutions to achieve such FRR could be intumescent paint. However, the available experimental studies, e.g. (Makarov et al., 2016), have shown that the increase of FRR beyond 1.5 hours would be possible if the intumescent paint layer thickness is of the order of 1 cm, which is hardly acceptable due to additional volume of storage tanks on board of a vehicle. Fortunately, the breakthrough safety technology of microleak-no-burst (μLNB) explosion free in fire self-venting (TPRD-less) tank is invented and successfully tested for hydrogen storage tanks of type IV (Molkov et al., 2018). The technology allows manufacturing tanks with the same wall thickness as an original tank but with unprecedented safety features to exclude rupture in a fire and avoid TPRD as a potential source of failure.

## 7.3 QRA of hydrogen train in a rail tunnel: the Severn rail tunnel (UK) (Task 5.3; URS)

As an example of QRA methodology application to rail tunnels, the Severn tunnel in the UK is analysed. The Severn Tunnel is a railway tunnel in the United Kingdom, linking South Gloucestershire in the west of England to Monmouthshire in south Wales under the estuary of the River Severn. It was constructed by the Great Western Railway (GWR) between 1873 and 1886 for the purpose of dramatically shortening the journey times of their trains, passenger and freight alike, between South Wales and Western England. The Severn Tunnel is four miles and 624 yards (7.008 km) long, although only 2¼ miles (3.62 km) of the tunnel are under the river. The Severn Tunnel was the longest underwater tunnel in the world until 1987 and, for more than 100 years, it was the longest mainline railway tunnel within the UK. The Severn rail tunnel is a double bore tunnel, 7.0 km long, 7.9 m wide and 6.1 m high. The tunnel has a horseshoe cross-section. The annual average daily traffic (AADT) is 350 trains per day for each traffic direction. A sketch of the tunnel is reported in Figure 30.

*Figure 30. A sketch of Severn Tunnel (source https://www.networkrailmediacentre.co.uk)*

Data for the UK rail network in the year 2018/19 reporting period (01/04/18-31/03/19) indicate that in this period there were 220,711 freight train movements. There were also 7,566,972 passenger trains nationally, giving a total of 7,787,683 trains on the UK rail network (Lipscomb, 2021).

The scenario analysed consider a train accident at the tunnel entrance. It is assumed that the train has different onboard storage tanks, whereas only one tank of 160 L, NWP=35 Mpa ruptures. The tank is considered to be equipped with a TPRD 5 mm-orifice size. The onboard hydrogen tanks may have different SoC, but for a conservative estimation only 99% (immediately after fuelling) is selected for the consequence analysis. Typical passenger occupancy is around 148 passengers per train. The train length is assumed to be three cars (64 m). The peak passenger load at rush hour is around 304 passengers (Lipscomb, 2021).

### 7.3.1 Event tree

Statistics from the International Union of Railways (UIC) is used for the analysis (UIC, 2021). This report is derived from information contained in the UIC Safety Database, which is provided by UIC members on a voluntary basis. This database launched in 2006 with 19 members but has grown over time and now boasts 35 contributing members. Trend of accidents and rates on the last six years (2015-2020) is reported in Table 21 where “Significant accident” means any accident involving at least one rail vehicle in motion, resulting in at least one killed

or seriously injured person, or in significant damage to stock, track, other installations or environment, or extensive disruptions to traffic, excluding accidents in workshops, warehouses and depots.

*Table 21. Trend of accidents and rates on the last six years (2015-2020)*

| ALL RAILWAYS | 2015 | 2016 | 2017 | 2018 | 2019 | 2020 |
|---|---|---|---|---|---|---|
| Number of significant accidents | 1 926 | 2 006 | 1 971 | 4 246 | 4 187 | 3 781 |
| Significant accidents per million train-km | 0,42 | 0,43 | 0,42 | 0,66 | 0,63 | 0,62 |
| Number of accidents with victims | 1 584 | 1 718 | 1 688 | 3 920 | 3 851 | 3 435 |
| Accidents with victims per million train-km | 0,35 | 0,37 | 0,36 | 0,61 | 0,58 | 0,56 |
| Number of victims | 1 803 | 2 119 | 1 919 | 4 319 | 4 137 | 3 670 |
| Victims per million train-km | 0,39 | 0,46 | 0,41 | 0,67 | 0,62 | 0,60 |
| Number of fatalities | 1 029 | 1 181 | 1 086 | 2 687 | 2 608 | 2 329 |
| Fatalities per million train-km | 0,22 | 0,26 | 0,23 | 0,42 | 0,39 | 0,38 |
| Number of million train-kilometres | 4 580 | 4 617 | 4 731 | 6 399 | 6 631 | 6 122 |

In 2020 an average accident rate of 0.62 per $10^6$ train-km is reported for a total number of $6122\times10^6$ train-km, but only 0.4% of the accident occurred in tunnels, hence a tunnel accident rate of $2.3\times10^{-3}$ per $10^6$ train-km is calculated. The probability that an accident in tunnels results in a fire is 7%, i.e. 1 fire in 14 incidents in tunnels (UIC, 2021). For all the other branches the probability values are those described in previous paragraph 5.2.

The event tree for crash scenarios involving a hydrogen train in Severn Tunnel (localized fire) is reported in Figure 31.

It has to be highlighted that for railway tunnel fire information on time required to fire extinguishment are not available in the literature, in our knowledge. Therefore, a null probability that the fire is extinguished on time is assumed as conservative approach.

For train, the tank (V=160 L, P_NWP=350 bar) is considered to be equipped with a TPRD 5 mm-orifice size. If TPRD is activated, $H_2$ is released with an initial mass flow rate of 0.680 kg/s from the tank @350 bar (SoC=100%). It can be then ignited with a probability of 20% according to Aarskog et al. (2020). This provides a complementary 80% chance of not igniting.

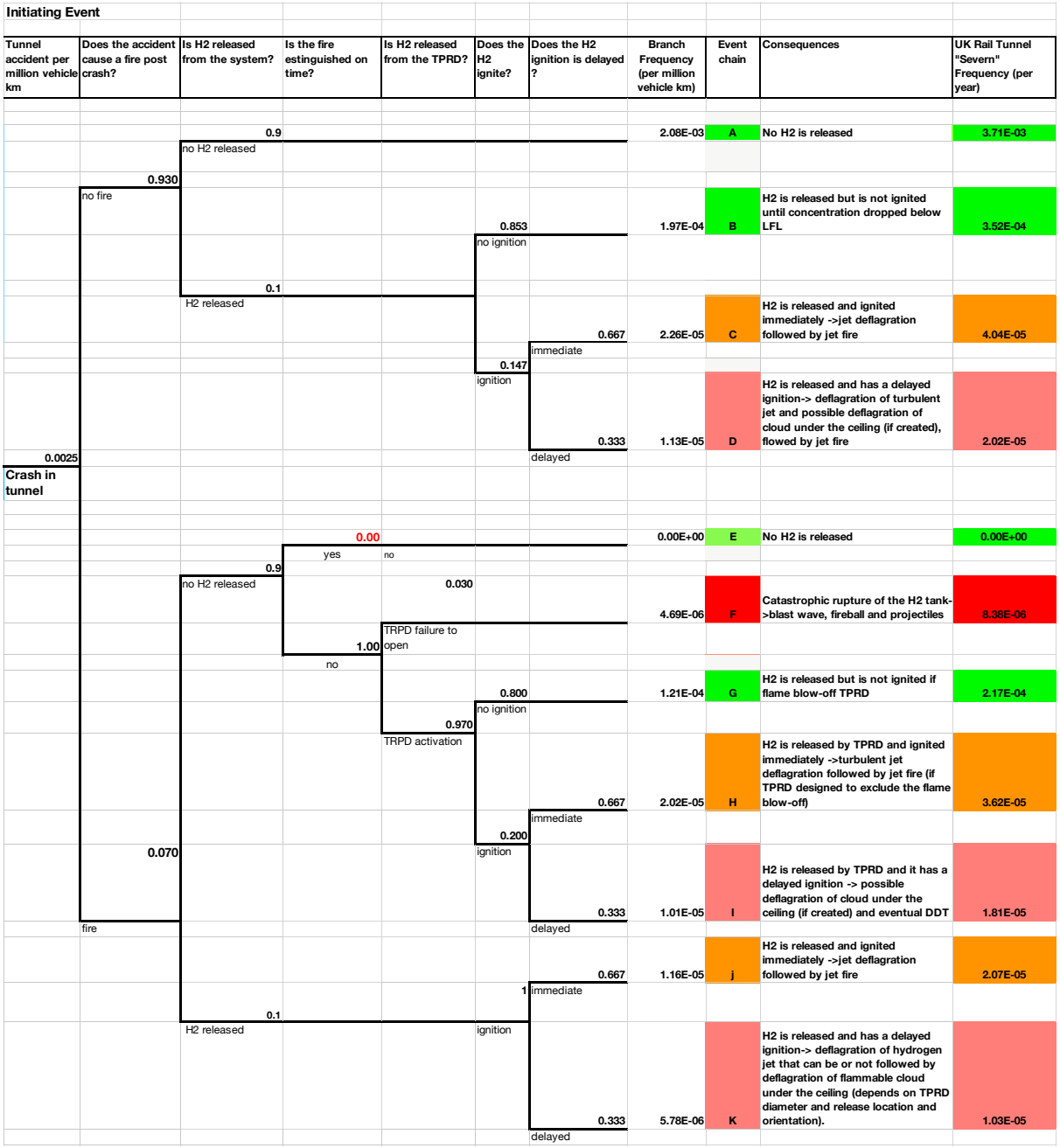


*Figure 31. Event tree for crash scenario involving a hydrogen train (SoC=100%) in Severn railway Tunnel (70localised fire).*

The results of the analysis show that the most likely consequence includes scenarios with no release of hydrogen ($3.7\times10^{-3}$ events per year) or hydrogen release without ignition ($5.7\times10^{-4}$ events per year). When the hydrogen does ignite, it is most likely a jet fire from the hydrogen system ($6.1\times10^{-5}$ events per year) or a TPRD ($3.6\times10^{-5}$ events per year for SoC=99%). In the presence of a localised fire, if the TPRD fails to open, the catastrophic hydrogen tank rupture is the most likely scenario ($8.4\times10^{-6}$ events per year).

### 7.3.2 Consequence analysis

#### *7.3.2.1 Jet fire*

For a jet fire from TPRD, flame length and hazard distances are calculated thanks to the dedicated tool available in hydrogen e-laboratory (https://hyresponder.eu/e-platform/e-laboratory). In Table 22 the input data and the results in terms flame length and hazard distances are reported.

*Table 22. Input data and results of jet fire from 5mm-TPRD*

| **INPUT DATA** | | | | |
|---|---|---|---|---|
| H2 pressure in reservoir (bar) | H2 temperature in reservoir (°C) | Orifice diameter (mm) | Ambient pressure (atm) | Ambient temperature (°C) |
| 350 | 15 | 5 | 1 | 15 |
| **RESULTS** | | | | |
| Flame length (m) | No harm (70°C) separation distance (m) | Pain limit (5 mins, 115°C) separation distance (m) | Third degree burns (20 sec, 309°C) separation distance (m) | |
| 12.98 | 45.42 | 38.94 | 25.96 | |

#### *7.3.2.2 Tank rupture*

For catastrophic tank rupture, the overpressures along the tunnel at different distances from tunnel entrance, where accident occurs, as calculated through the universal correlation for the blast wave decay in a tunnel (Molkov and Dery 2020) are reported in Figure 32.

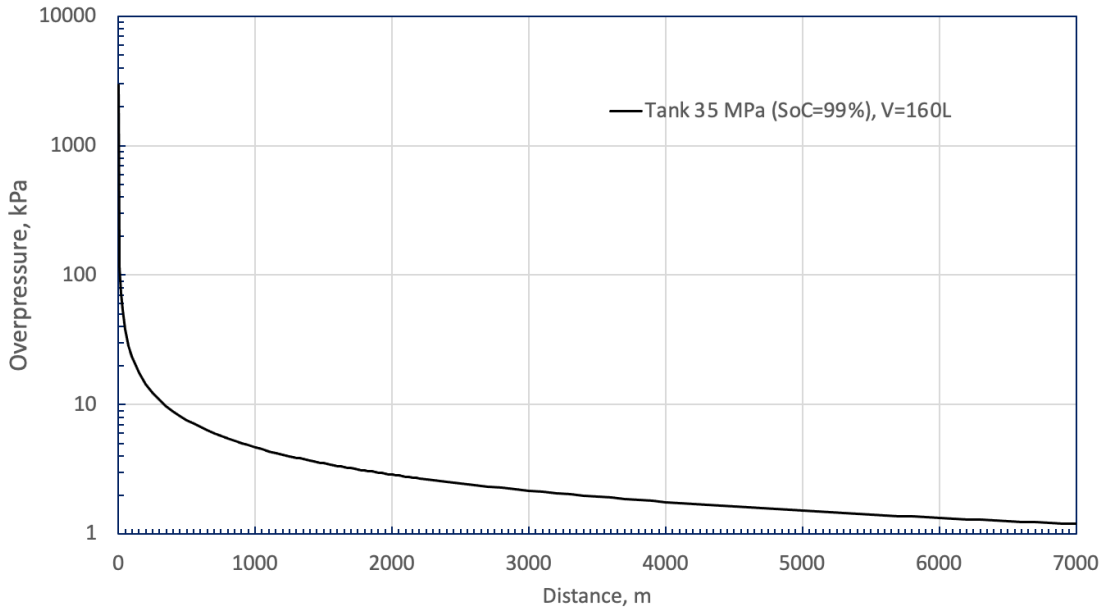


*Figure 32. Blast wave decay vs distance in Severn tunnel for the tank of 160 L: SoC=99%.*

The corresponding fatality rate and failure rate as calculated respectively by the HSE model and Eisenberg model (American Institute of Chemical Engineers, 1998) are reported in Figure 33 and Figure 34.

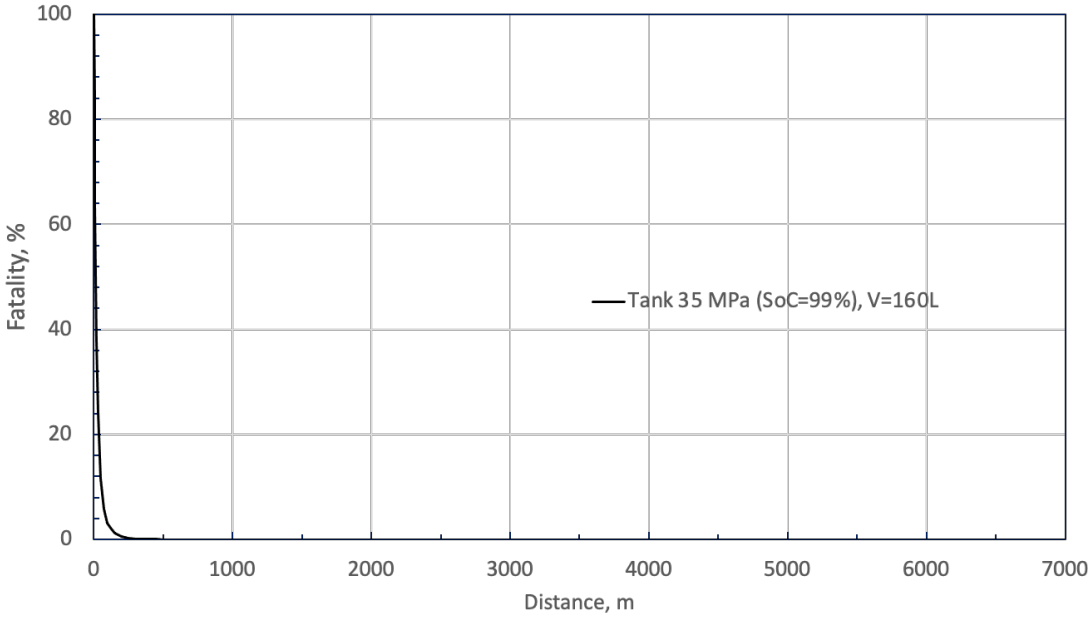


*Figure 33. Probability of fatality along the Severn tunnel at different distances from tunnel entrance as a consequence of catastrophic tank rupture (tank of 160 L: SoC=99%).*

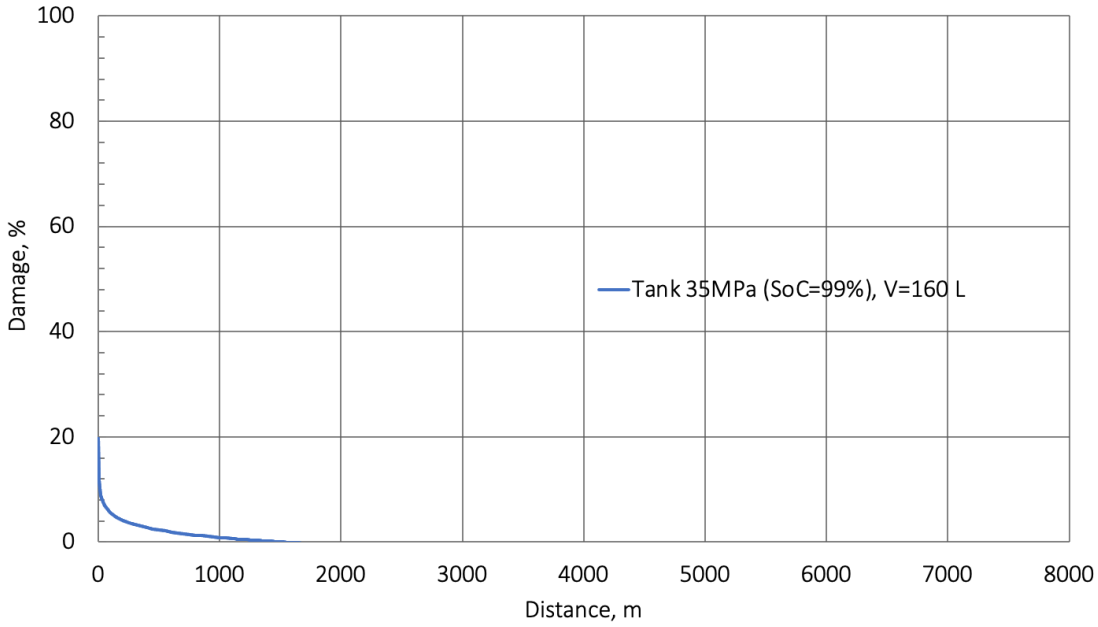


*Figure 34. Probability of tunnel failure along the Severn tunnel at different distances from tunnel entrance as a consequence of catastrophic tank rupture (tank of 160 L: SoC=99%).*

It is observed that the probability of fatality is 100% at the tunnel entrance where the accident occurs and decreases to 1% at 175 m from the tunnel portal. The probability of failure of the

tunnel structure is 20% at the tunnel entrance. It decreases to 1% probability of failure at 900m from the portal.

#### *7.3.2.3 Deflagration/DDT*

In the event that hydrogen is released from the TPRD, but it is not immediately ignited, a cloud can form under the ceiling and if it is ignited with delay, a deflagration or DDT may occur ($1.8\times10^{-5}$ events per year).

The scenario of transition from deflagration to detonation in a narrow space between the train and tunnel was considered. The evaluation of flame propagation and eventual DDT is performed using the flame propagation regime evaluation method developed by KIT. A detailed description of the method is reported in Appendix A3.2.4.

Two UK rail tunnels (i.e. Severn and Channel) with a different cross-section area were analysed (Table 23). The hydrogen inventory of train and of single tank are shown in Table 24.

*Table 23 Dimensions of UK rail tunnels*

| | Tunnel Description | Cross-section Area, CSA ($m^2$) | Real Diameter, D (m) | Equivalent Diameter, D (m) |
|---|---|---|---|---|
| 1 | Severn tunnel, two rail | 60.0 | 7.93 | 8.74 |
| 2 | Channel tunnel single rail | 53.5 | 7.6 | 8.25 |

*Table 24 Initial hydrogen inventory, mass flow rate and discharge time for train*

| **Vehicle** | **Total Vehicle Inventory (kg)** | **Single Tank Inventory (kg)** | **Initial mass flow rate (kg/s)** | **Discharge time (sec)** | **Cross-section area ($m^2$)** |
|---|---|---|---|---|---|
| Train 1 (350 bar) | 96.0 | 4.14 | 7.85 | 67 | 10.7 |
| Train 2 (350 bar) | 105.0 | 5.80 | 5.89 | 97 | 13.9 |

In the analysis the following four cases were considered for different hydrogen clouds (i.e., with uniform hydrogen concentration and linear hydrogen concentration gradient) in a tunnel cross section:

**Case (I):**

- Single rail tunnel of two-tubes tunnel with a circular cross-section 64.3 $m^2$
- Equivalent diameter Deq=8.98 m
- Tunnel roughness equivalent to BR = 1% which is equal to 2.2 cm of roughness.
- Hydrogen inventory 5.8 kg due to the accident, then cloud formation with a late ignition.
- Uniform hydrogen-air mixture of 10 to 30% v/v $H_2$ in air filled a layer of h=0.6 m thick above the train. The cloud is formed in a gap between the roof of the train and the ceiling (Figure 35a).

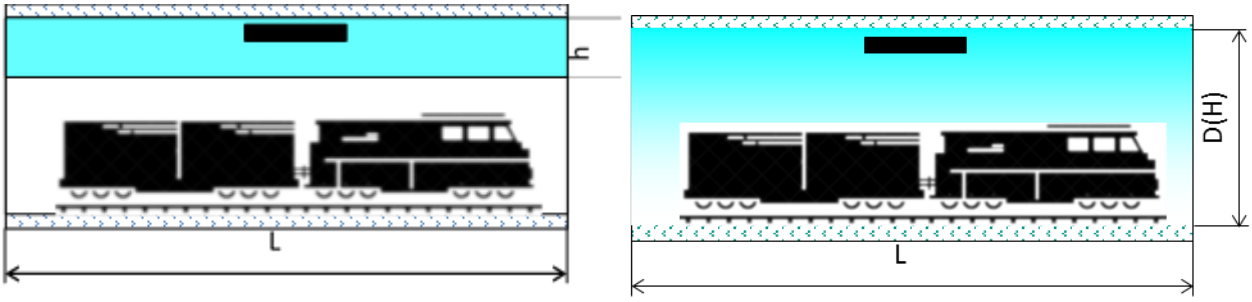


(a) (b)

*Figure 35. Hydrogen cloud geometry: a layer of uniform hydrogen-air mixture (a); fully filled tunnel cross- section with a stratified hydrogen-air mixture (b).*

**Case (II):**

- Single rail tunnel of two-tubes tunnel with a circular cross-section 64.3 $m^2$
- Equivalent diameter Deq=8.98 m
- Tunnel blockage by the train is equivalent to BR = 40%.
- Hydrogen inventory 5.8 kg due to the accident, then cloud formation with a late ignition.
- Stratified hydrogen-air mixture filled the whole tunnel cross-section
- A linear hydrogen concentration gradient with maximum concentration 10, 15, 20, 25, 30% v/v $H_2$ at the ceiling and 0% v/v $H_2$ at the bottom of the tunnel is assumed (Figure 35b).

**Case (III):**

- Single rail tunnel of two-tubes tunnel with a circular cross-section 53.5 $m^2$
- Equivalent diameter Deq=8.25 m
- Tunnel blockage by the train is equivalent to BR = 40%.
- Hydrogen inventory 10 kg due to the accident, then cloud formation with a late ignition.
- Stratified hydrogen-air mixture filled the whole tunnel cross-section
- A linear hydrogen concentration gradient with maximum concentration 10, 15, 20, 25, 30% v/v $H_2$ at the ceiling and 0% v/v $H_2$ at the bottom of the tunnel is assumed (Figure 35b).

**Case (IV):**

- Single rail tunnel of two-tubes tunnel with a circular cross-section 53.5 m2.
- Equivalent diameter Deq=8.25 m
- Tunnel blockage by the train is equivalent to BR = 40%.
- Hydrogen inventory 100 kg due to severe accident, then the cloud formation with a late ignition.
- A stratified hydrogen-air mixture filled the whole tunnel cross-section
- A linear hydrogen concentration gradient with maximum concentration 10, 15, 20, 25, 30% v/v $H_2$ at the ceiling and 0% v/v $H_2$ at the bottom of the tunnel is assumed (Figure 35 b).

In summary, the results show that:

- Independent of hydrogen inventory, for maximum hydrogen concentration of 10 and 11% v/v $H_2$ the flame cannot accelerate to the speed of sound. It will propagate as a slow subsonic flame with a maximum combustion over-pressure 1-2 bar.

- Independent of maximum hydrogen concentration at the ceiling, for hydrogen inventories 5.8 and 10 kg the only slow subsonic flame with a maximum combustion over-pressure 1-2 bar may develop because too small size of the cloud.
- Only in the case **IV** for 100 kg of hydrogen inventory the size of the cloud will be enough for flame acceleration and detonation onset at maximum hydrogen concentration above 15% v/v. Then, it needs the ventilation to keep hydrogen concentration below 15% v/v to prevent the detonation.

### 7.3.3 Risk evaluation

For tank rupture scenario, the individual risk is then calculated by multiplying the frequency of the tank rupture and the probability of fatality along the tunnel length (Figure 36). The individual risk is in the range of $8.4\times10^{-6}$ -$1.0\times10^{-6}$ fatality per year up to a distance from the tunnel portal of 50 m (SoC=99%), which is below the acceptance criterion of $10^{-5}$ fatality per year. On the contrary, assuming a risk criterion of $10^{-6}$ fatality per year a fatality hazard distance of 50 m is evaluated (SoC=99%). This hazard distance is comparable to the no-harm distance calculated in the case of a hydrogen jet fire released from TPRD, i.e. 45 m for SoC=100% (Molkov, 2012).

Assuming the train length is three cars, 64 m long, typical passenger occupancy is around 148 passengers per train, and at peak times the maximum passenger load is around 304 passengers (Lipscomb, 2021), the number of potential victims is 116 with a maximum of 238. Furthermore, if it is assumed that another train is traveling in the tunnel in the opposite lane, the number of fatalities could be double (232 with a maximum of 476). Regarding the probability of failure of the tunnel structure as a result of a catastrophic rupture of the hydrogen tank, it is estimated equal to 20% at the tunnel entrance.

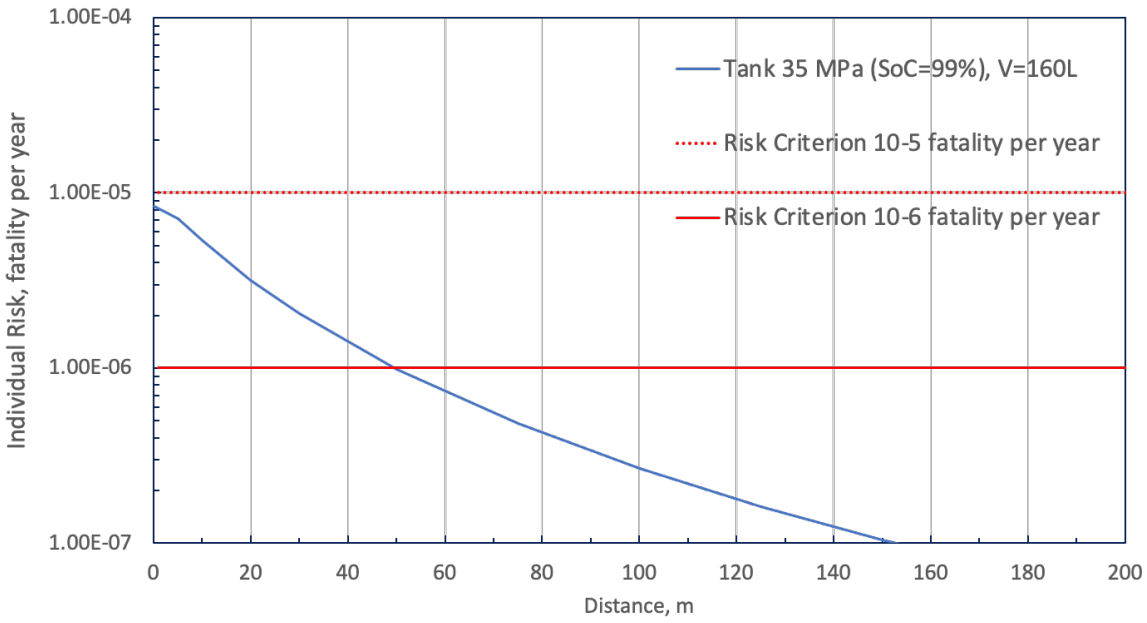


*Figure 36. Individual risk vs distance in Severn Tunnel for the tank of 160 L at 35 Mpa: SoC=99%.*

### 7.3.4 Results and discussion

The results of the analysis show that the most likely consequence includes scenarios with no release of hydrogen ($3.7\times10^{-3}$ events per year) or hydrogen release without ignition ($5.7\times10^{-4}$ events per year). When the hydrogen does ignite, it is most likely a jet fire from the hydrogen

system ($6.1\times10^{-5}$ events per year) or a TPRD ($3.6\times10^{-5}$ events per year for SoC=99%). In the presence of a localised fire, if the TPRD fails to open, the catastrophic hydrogen tank rupture is the most likely scenario ($8.4\times10^{-6}$ events per year).

For this scenario, the individual risk is in the range of $8.4\times10^{-6}$ -$1.0\times10^{-6}$ fatality per year up to a distance from the tunnel portal of 50 m (SoC=99%). Assuming a risk criterion of $10^{-6}$ fatality per year a fatality hazard distance of 50 m is evaluated (SoC=99%). This hazard distance is comparable to the no-harm distance calculated in the case of a hydrogen jet fire released from TPRD, i.e. 45 m for SoC=100.

For a 64 m long and a typical passenger occupancy of about 148 passengers per train, the number of potential victims is 116 with a maximum of 238 in peak time. If another train is traveling in the tunnel in the opposite lane, the number of fatalities could double (232 with a maximum of 476).

## 7.4 QRA of hydrogen vehicles in an underground car park (Task 5.3; DTU)

The risk of hydrogen vehicles in a typical underground car park in Denmark is assessed next. Many different layouts of car parks exist with various geometries and car capacities (Nørregaard, Roed and Skov, 2022). Larger car parks have several decks for parking cars.

The case from the road tunnel scenario is applied with some adaptions to a scenario where hydrogen cars are parked in an underground car park. The road tunnel risks with the largest consequences are shown to be scenarios leading to gas cloud explosions and tank rupture and it is assumed to be the case as well in car park scenarios. The scenario could happen when a thermally activated pressure relieve safety device (TPRD) is opening due to malfunctioning (TPRD activation without demand) and the vessel's hydrogen is released without immediate ignition into a tunnel or carpark. By that ignitable gas clouds may develop with the risk of an explosion. The latter scenario could happen when the same thermally activated safety device does not activate in case of a thermal exposure (TPRD failure of activation on demand). In that case the thermal exposure may lead to a tank rupture followed by a fireball explosion. The initiating event could be a strong heat source like a vehicle fire of the hydrogen vehicle itself, another vehicle in close distance to the hydrogen vehicle, or possibly any external fire source.

While accident scenarios involve severe collisions in road tunnels, the situation in a carpark is different due to the very low speeds of the vehicles in such an infrastructure. Also, only personal cars and smaller vans are expected to park in an ordinary carpark. Nevertheless, vehicles still may self-ignite due to technical defects or be ignited due to arson. In an analysis of cars being ignited in carparks the main causes for car ignition are shown in Figure 37 as being registered in New Zealand during the 8 years period 1995 to 2003, but found to be similar to the causes observed in the USA and UK (Li and Spearpoint, 2007). It is by the authors recognized that the car fleet observed in New Zealand is rather aged and this may increase the number of starting fires.

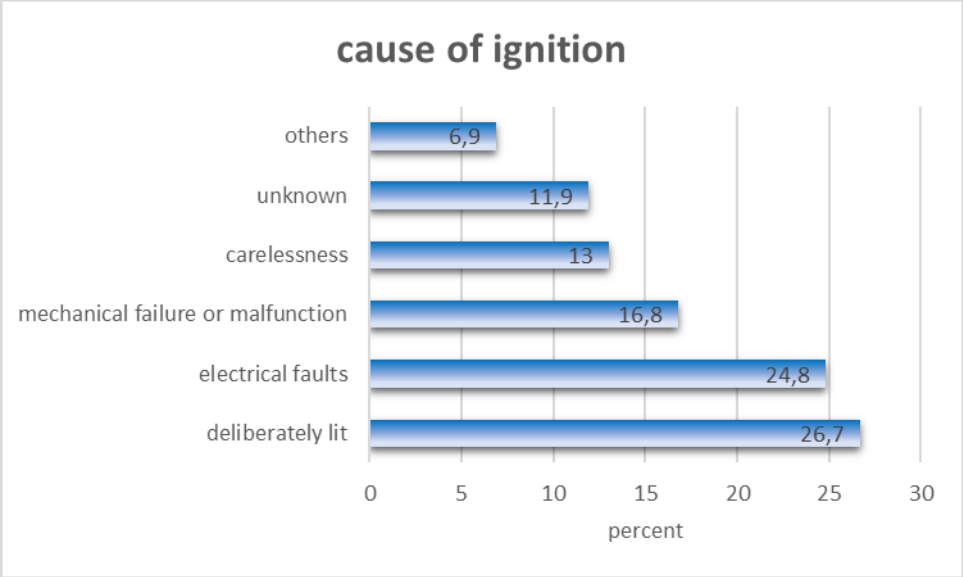


*Figure 37 Causes of car ignition in New Zealand car parks 1995 – 2003* (Li and Spearpoint, 2007).

Fires in car parks are not very frequent and the vast majority is only involving single cars as shown in Table 25 (Tohir and Spearpoint, 2014). It is normally a routine job for the fire brigades to extinguish such car fires within short time.

The mitigation systems that are legally required for carparks are very different from country to country depending on the size of a carpark. In Denmark the requirements are presently that carparks above 1000 $m^2$ need to built-in fire mitigation systems, e.g. sprinkling systems, but it is possible to omit by splitting larger carparks into fire compartments each below the area limit. In a recent report it is recommended to review this limit and to decrease this limit down to 150 $m^2$ (Nørregaard, Roed and Skov, 2022). Mitigation measures are established using e.g., establishing of fire compartments, fire ventilation, and sprinkling. The European regulations in that field based on work by Joyeux et al (Joyeux *et al.*, 2002) are rather old and may not sufficiently cope with the development of modern cars being more lightweight and their dimensions being enlarged, while the parking box space may not be adapted accordingly. Fire spread from car to car is dependent on a number of factors as the parking distance, the heat release rate and ignitability of the car materials, but also on the overall geometry of a car park as ceiling height and wind conditions during a fire as seen in the Stavanger airport fire.

The vehicles are having a certain distance to the neighboring vehicles and only the burning vehicles heat radiation is impinging the potential hydrogen vehicles body, while the pressure vessel is shielded due to the vehicle body. It may be realistic to assume that only in case the fire spreads to the hydrogen vehicle after a certain duration, the hydrogen tank could be exposed to a strong enough thermal impact. Here the reduction of distance between vehicles may be an important factor and may increase the likelihood of fire spread from car to car.

*Table 25 Number of vehicles involved in a fire scenario* (Mohd Tohir and Spearpoint, 2014).

| No. of involved vehicles | No. incidents | Incident probability P |
|---|---|---|
| 1 | 344 | 0.858 |
| 2 | 27 | 0.067 |
| 3 | 21 | 0.052 |
| 4 | 4 | 0.01 |
| 5 | 3 | 0.007 |
| 6 | 0 | 0 |
| 7 | 2 | 0.005 |
| Total incidents / incident probability for 2-7 vehicles ignited | 401 | 0.142 |

The statistics in Table 25 only show the involved vehicles up to 7, which are the most likely number of cars involved. The authors (Mohd Tohir and Spearpoint, 2014) found nevertheless incidents were more than 300 cars got ignited. This is in line with other catastrophic car park fires. Most car park fires involve only very few cars burning at a time – but there are also reported very big car park fires involving many cars (Liverpool, Stavanger airport). The dynamics of these very big and complex fire scenarios have not been analysed yet with regard to the behaviour and potential safety risks for hydrogen vehicles. These big fires may likely simultaneously activate the TPRD's of a number of remote vehicles in the respective carpark and could create an explosive gas cloud. On the other hand, pressure vessels of a number of hydrogen cars will likely be impacted by these large fires and with a failure of activation on demand, likely more than one tank may burst, providing an additional severe explosion scenario to these very large car park fires. Due to the great complexity of the involved scenarios for such big car park fires, in this QRA only single and multiple (1- 7) burning cars are included in the Event Tree analysis.

While in Denmark and many other countries the number of fire events are recorded in incident databases (e.g. DK: Redningsberedskabets Statistikbank – Forside (brs.dk); UK: Fire statistics – GOV.UK (www.gov.uk) . The UK data for underground car park fires during the period 2010 -2020 show a mean of 17 ± 4 fires each of the years with minimum yearly number of 10 fires and a maximum of 22 fires., the relation to the size and number of cars using the car parks is not commonly established.

*Table 26. Number of fires in carparks compared with outhouse /carport /garage fires and all fire incidents in Denmark during the period 2013 – 2020.*

| *[number of fires]* | **2013** | **2014** | **2015** | **2016** | **2017** | **2018** | **2019** | **2020** |
|---|---|---|---|---|---|---|---|---|
| **underground carpark** | 6 | 5 | 12 | 23 | 12 | 15 | 6 | 5 |
| **Outhouse / carport / garage** | 0 | 0 | 79 | 131 | 110 | 90 | 352 | 382 |
| **All fires** | 14392 | 13086 | 12027 | 12381 | 11520 | 13420 | 11224 | 10946 |

A simple approach is made for Denmark. The probability of a car park vehicle fire (Eriksen and Christensen, 2021) may be assessed using the national statistics the Danish Emergency Management Agency (DEMA) (BRS, 2021). In Denmark during the period between 2013 and 2020 on average 12,375 ± 1,188 annual real fire incidents are reported, including an annually average of 11 ± 6 fire incidents within parking garages as shown in Table 26. The total number of parking infrastructures is predicted using the Danish *Central Register of Buildings and Dwellings* (BBR) (Statistics Denmark, 2021). The statistic reports an area and a number count of buildings. Relevant are found buildings categorized as transport and garage facilities, commercial parking and transport facilities as well residential parking and transport facilities. These three categories sum up to 14407 parking and transport facilities in 2021 in Denmark. Thus, the frequency of a fire in a car park is found as:

$$11 \text{ (fires/year)} / 14407 \text{ facilities} = 7.7 \cdot 10^{-4} \text{ (fires/year/facility)},$$

independent on the size of the parking area and thus the number of vehicles frequenting the facilities.

Another more comprehensive approach that also recognizes data from Europe and other countries is made by (Li and Spearpoint, 2007) and refined by (Tohir and Spearpoint, 2013). In the first analysis covering data in the period 1995 – 2003 the probability of a vehicle catching fire in a car parking building in New Zealand was estimated to 4.74 x $10^{-6}$ $year^{-1}$. In a follow up using the same approach as before for the period 2004 – 2012 the frequency was lowered to 1.15 x $10^{-6}$ $year^{-1}$. This gives an overall probability for the period from 1995 – 2012 as 2.76 x $10^{-6}$ $year^{-1}$. The prediction of the fire frequency of a vehicle per year in a car park is mainly based on national fire statistics in New Zealand.

Furthermore, the vehicle exchange rate of a large parking facility is calculated scaled by an estimated total amount of public parking booths of 200,000 in New Zealand. The author determined the frequency f as fires per vehicle visit using a car park and estimated the probability of a vehicle catching fire during a visit in car park buildings in New Zealand as 1.71x$10^{-7}$ fires/visit. In order to calculate the fire incidents the following equation is developed by the authors.

$$F = f \cdot R \cdot \frac{A}{P}$$

*$f$ = 1.71 $10^{-7}$ vehicle fire frequency per vehicle visit*
*$R$ = annual usage ratio or turnover ratio*
*$A$ = total floor area [$m^2$]*
*$P$ = efficiency of parking (assumed 29 $m^2$ /space)*
*$F$ = vehicle fire frequency per year*

The vehicle fire frequency per year F is the fire frequency per year depending on the cars per year using the respective car park. The authors argue that cars possibly ignite only within the first 20 min after arrival in the carpark and by that the number of arrivals and not the duration of parking is the determining parameter for vehicle fires. Nevertheless, arson and starting of the motor while departing may be other contributing parameters to be considered as initiating events.

For the case study a Danish underground car park was selected with a capacity of 58 cars (see Figure 39). Assuming a turnover rate 583 cars per year for every of the 58 parking spaces the total number of cars per year is estimated to 33841 visiting cars per year. This provides a fire frequency of F=0.006 fires per year. This is dependent on the number of visiting cars and in Figure 38 it is shown the linear dependency of F with the number of visiting cars over a year.

### 7.4.1 Event tree

The following event tree is providing the results of a case study for the underground Danish car park Prismet in the town Århus. It has an area of 2144 $m^2$ and 58 parking slots giving a parking efficiency P = 37 $m^2$/car, which is close to the value found by Spearpoint reporting 29 $m^2$/car. It is also in line with the general tendency that car parks are cost-benefit optimized. Assuming a scenario with longer term parking of the cars as it could be typical for company car park, each slot is thought of being used by 583 different cars during a year. This results in 33841 cars using this car park during a year and the corresponding vehicle fire frequency F is 0.006 fires $year^{-1}$.

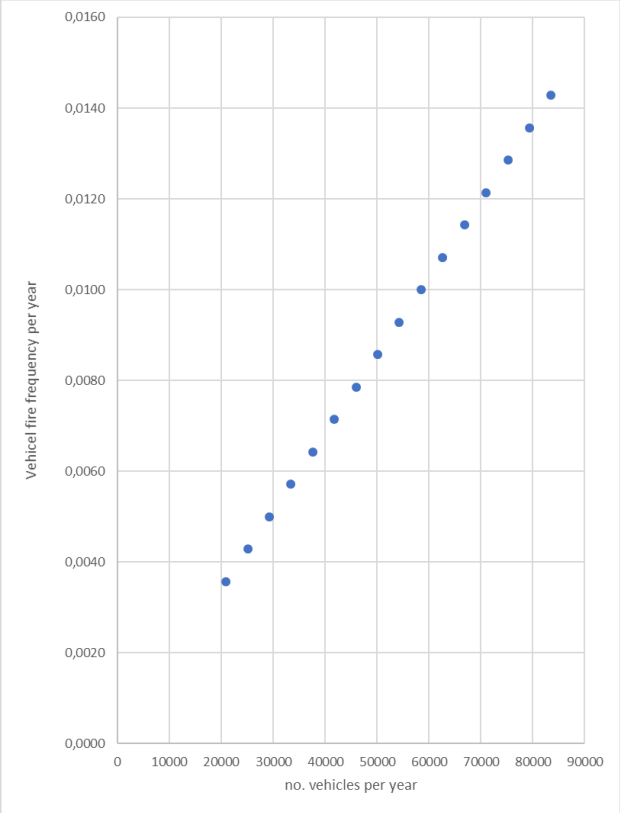


*Figure 38. Vehicle fire frequency, F, as function of visiting vehicles.*

**ETA for FCEV in undergroud car parking**

| smaller car park without sprinklers | Danish example | area [m2] | capacity cars | efficiency P | turn over R | cars per year | F [year-1] |
|---|---|---|---|---|---|---|---|
| | P-kælder under prismet Århus | 2144 | 58 | 37 | 583 | 33841 | 0,0058 |

**Initiating Event**

| Fires per 33841 cars per year in car park | Fire spreads to neighboring cars | Is the fire extinguished in time? | Is H2 released from the TPRD? | Does the H2 ignite? | Is the H2 ignition delayed ? | Frequency | Event chain | Consequences |
|---|---|---|---|---|---|---|---|---|
| | | 0,48 | | | | 3,94E-04 | E | No H2 is released |
| | | yes | no | | | | | |
| | 0,142 | | | | | | | |
| | 2 to 7 cars on fire | | | | 0,333 | 8,99E-06 | I* | H2 from 1 - 7 cars is released by TPRD ignited with a delay -> possible turbulent jet deflagration and/or flammable cloud deflagration under the ceiling (if created) and DDT |
| | | | | 0,08 | delayed | | | |
| | | | | ignition | 0,667 | 1,80E-05 | H* | H2 from 1 -7 cars is released by TPRD and ignited immediately ->turbulent jet deflagration followed by jet fire (if TPRD designed to exclude the flame blow-off) |
| | | | 0,79 | | immediate | | | |
| | | | TPRD activation of a single car out of 7 cars | | | | | |
| | | | | 0,92 | yes | 3,11E-04 | G* | H2 from 1 - 7 cars is released but is not ignited |
| | | 0,52 | | no ignition | | | | |
| | | no | | | | | | |
| 0,006 | | | | | | | | |
| Fires | | | 0,21 | | | 8,97E-05 | F* | Catastrophic rupture of 1 - 7 H2 tanks->blast wave, fireball and projectiles |
| | | | TPRD failure to open of a single car out of seven cars | | | | | |
| | | | OR gate --> sum of P(1) for 7 cars = 0.03 *7 | | | | | |
| | | 0,48 | | | | 2,38E-03 | E | No H2 is released |
| | | yes | no | | | | | |
| | 0,858 | | | | | | | |
| | 1 car on fire | | | | 0,333 | 6,67E-05 | I | H2 is released by TPRD ignited with a delay -> possible turbulent jet deflagration and/or flammable cloud deflagration under the ceiling (if created) and DDT |
| | | | | 0,08 | delayed | | | |
| | | | | ignition | 0,667 | 1,34E-04 | H | H2 is released by TPRD and ignited immediately ->turbulent jet deflagration followed by jet fire (if TPRD designed to exclude the flame blow-off) |
| | | | 0,97 | | immediate | | | |
| | | | TPRD activation | | | | | |
| | | | | 0,92 | | 2,30E-03 | G | H2 is released but is not ignited |
| | | 0,52 | | no ignition | | | | |
| | | no | | | | | | |
| | | | 0,03 | | | 7,75E-05 | F | Catastrophic rupture of the H2 tank->blast wave, fireball and projectiles |
| | | | TPRD failure to open | | | | | |
| | | | | | | | K **) | H2 is released by activated TPRD's in far areas of car park because of heat convectionand (100 C limit). This possibly cause a delayed ignition-> deflagration of hydrogen jet that can be or not followed by deflagration of flammable cloud under the ceiling (depends on TPRD diameter and release location and orientation). |

*) remark: combinations of the event chains I* , H*, G* and F* are likely to occure during a fire involving 3 to 7 cars

**) the typical carpark fires involve only a few cars. There are though reported very large carpark fires involving many more cars. This sceanrio is not modelled in this Event tree It possibly could add scenario K as a consequence.

*Figure 39. Event tree for fires involving hydrogen vehicles in a car park.*

### 7.4.2 Results and discussion

It is found that the most severe scenarios F/F* and I/I* are predicted with a frequency in the range $1 \cdot 10^{-4}$ to $0.9 \cdot 10^{-5}$ per year, which is a rather high occurrence. Usually, the number of people in a carpark is very low as the car is left and people are leaving the carpark immediately. Fire statistics report very few fatalities (BRE, 2010; Tohir and Spearpoint, 2014). Only in very few cases people got harmed and a very low number of emergency personal got injured/fatality affected.

*Table 27 Scenarios ordered by their severity using traffic light approach –green: low severity; yellow: medium severity; red: high severity*

| **Frequency** *[year$^{-1}$]* | **Scenario** | **Consequence** |
|---|---|---|
| 2.38 x $10^{-03}$ | E | No H2 is released |
| 2.30 x $10^{-03}$ | G | H2 is released but is not ignited |
| 3.11 x $10^{-04}$ | G* | H2 from 1 – 7 cars is released but is not ignited |
| 1.34 x $10^{-04}$ | H | H2 is released by TPRD and ignited immediately ->turbulent jet deflagration followed by jet fire (if TPRD designed to exclude the flame blow-off) |
| 1.80 x $10^{-05}$ | H* | H2 from 1 -7 cars is released by TPRD and ignited immediately ->turbulent jet deflagration followed by jet fire (if TPRD designed to exclude the flame blow-off) |
| 8.97 x $10^{-05}$ | F* | Catastrophic rupture of 1 – 7 H2 tanks->blast wave, fireball and projectiles |
| 7.75 x $10^{-05}$ | F | Catastrophic rupture of the H2 tank->blast wave, fireball and projectiles |
| 6.67 x $10^{-05}$ | I | H2 is released by TPRD ignited with a delay -> possible turbulent jet deflagration and/or flammable cloud deflagration under the ceiling (if created) and DDT |
| 8.99 x $10^{-06}$ | I* | H2 from 1 – 7 cars is released by TPRD ignited with a delay -> possible turbulent jet deflagration and/or flammable cloud deflagration under the ceiling (if created) and DDT |

The scenarios with the potential catastrophic rupture and deflagration need more detailed consideration as these may develop in very short time leaving only very little time for safe egress time of people in the car park. It should also be assessed in more detail whether the consequences of such explosions and the resulting blast waves may impact on the carparks structural integrity and possibly could affect the floor separations etc..

The performed QRA Figure 39 shows that the likelihood of explosion and tank rupture scenarios are closely linked with the failure rate on demand for the installed TPRD's. It is established that a localized fire may more often lead to a TPRD failure on demand compared with a fully engulfed vessel fire. This is in the literature explained by the low thermal conductivity of type IV vessels (composite materials) that has the effect that the thermal activation temperature (about 110 C) at the TPRD is not reached before the vessel will burst due to the weakening effect of the thermal exposure. Vessel types that use better thermal

conducting materials (e.g. type I steel tanks) are therefore found more reliable activating the TPRD in time.

The reliability of the TPRD's are not reported sufficiently. There are only very limited literature data available in FireComp risk assessment study (Saw et al., 2016) and in the SANDIA publication (Erhart et al., 2019). These data are also not based on reliability measurements, but on expert judgements comparing the TPRDs with the reliability of burst disc. It is though stated in the same report that the TPRD technology is different. As such validated data on the activation of TPRD's in road vehicle using type IV pressure vessels relevant accident scenarios are of utmost importance. Hereunder, any build-in pressure vessel technology that may improve/assist the TPRD activation due to localized fires should be investigated, as e.g. the concept of "explosion free pressure vessels". Hereunder, one important development is the reduction of the TPRD release diameter as CFD calculations provide evidence that with diameters below 1 mm no extended ignitable clouds are formed (HyTunnel-CS, D3.3, 2022). This has to be analyzed more regarding the fire resistance of vessel in real fire situations to find the optimal diameter. Further, it is recommended that at least generic data for the different types of TPRD systems used for the different vessel types are published.

# 8 Conclusions

Considering previously unavailable knowledge on the risk and hazards of hydrogen vehicles in confined spaces, and especially for catastrophic hydrogen tank rupture, this study carries out the QRA for hydrogen-powered vehicles in confined spaces, i.e., a road tunnel in Italy, a road tunnel analogous to the Dublin Tunnel, a railway tunnel in UK and an underground car park in Denmark. This promotes hydrogen technologies and inherently safer designs of the fuel cell vehicles, informs the stakeholders and the public on the specific hazards and the acceptable risks and elucidates the available solution for prevention and mitigation of the hazards. This supports the significance of our study.

The originality of this study is based on a detailed analysis of the incident scenarios that are unique for hydrogen vehicles, i.e. catastrophic tank rupture and deflagration of flammable cloud under the ceiling and eventual DDT, in terms of both frequency of such events and their consequences. In particular, a novel correlation of the blast wave decay in a tunnel for an incident with a hydrogen-powered vehicle is applied.

The results of the frequency analysis showed that the most likely consequence includes scenarios with no release of hydrogen or hydrogen release without ignition. When the hydrogen does ignite, a jet fire from the hydrogen system is most likely than from a TPRD. In the presence of a localised fire, if the TPRD fails to open, the catastrophic $H_2$ tank rupture is the most likely scenario.

The QRA for the tunnel incident is demonstrated as a holistic analysis of safety and risk reduction measures such as the increase of fire-resistance rating of onboard storage tanks. The "new" hazard to people in a tunnel, i.e. the blast wave after tank rupture in a fire, and associated risks are estimated in terms of fatalities per year and cost per accident were calculated. The risks were assessed for the cases of a 62.4 L, NWP=70 MPa hydrogen tank in a fire with different SoC (SoC=99%, 59% and 40%). The frequency analysis is carried by using existing statistical datasets for road tunnel accidents. The probability analysis resources provided by the Health and Safety Executive (UK) were used to assess the risk in terms of costs per accident.

The risks with the largest consequences are shown to be scenarios leading to hydrogen flammable mixture deflagration (could be eliminated by proper TPRD design) and tank rupture in a fire (could be eliminated by using innovative explosion free in fire self-venting tanks). The former scenario, i.e. deflagration, DDT or detonation, could happen when a TPRD of comparatively large diameter is opening due to malfunctioning (TPRD activation without demand), or due to flame blow-off during release from TPRD, and the vessel's hydrogen is released into a tunnel or underground parking with the formation of flammable cloud that is then ignited. The latter scenario could happen when the same TPRD does not activate in case of a thermal exposure (TPRD failure of activation on demand). In that case, the thermal exposure may lead to a tank rupture followed by catastrophic consequences such as blast waves, fireballs and projectiles. The initiating event could be a strong heat source like a vehicle fire of the hydrogen vehicle itself, another vehicle in close distance to the hydrogen vehicle, or possibly any external fire source, e.g. spill of combustible substances like gasoline or diesel.

As an example, based on the results of the risk analysis for the considered scenario of Dublin Tunnel, the risks for an onboard tank with FRR=8 min are $1.07\times10^{-2}$ fatality/vehicle/year, i.e. 3 orders of magnitude bigger than the acceptable level, and $9.24\times10^{6}$ £/accident. The increase of FRR to 91 min reduces both risks to acceptable levels below $10^{-5}$ fatality/vehicle/year and 300 £/accident.

In the case of the considered rail tunnel scenario, because of the low frequency of fire accident in railway, the individual risk is significantly lower (in the range of $8.4\times10^{-6}$ -$1.0\times10^{-6}$ fatality per year up to a distance from the tunnel portal of 50 m). But on the basis the typical passenger occupancy of about 148 passengers per train the number of potential victims can be as high as 116 with a maximum of 238 in peak time. If another train is traveling in the tunnel in the opposite lane, the number of fatalities can double (232 with a maximum of 476).

The performed QRA shows that the likelihood of deflagration/DDT/detonation of large flammable cloud and tank rupture scenarios are closely linked with the designed parameters and failure rate on demand for the installed TPRD's. It is established that a localised fire may more often lead to a TPRD failure on demand compared with a fully engulfing vessel fire.

Hereunder, any build-in pressure vessel technology that may improve/assist the TPRD activation in a localised fire should be investigated, e.g. the breakthrough safety technology of explosion free in a fire self-venting TPRD-less (a μLNB tank incorporates, by itself, distributed over the whole tank surface "TPRD"). Hereunder, important developments are the reduction of the TPRD release diameter and its proper location and direction of release. The CFD studies provide evidence that with TPRD diameters of fractions of 1 mm, no flammable cloud accumulation under the underground parking ceiling are found, and thus tunnels with higher ceiling heights are preferable.

Naturally, the common measures to prevent tunnel incidents and underground parking fires are crucial for the incident likelihood of all vehicles and the frequency of fires. Some of the common safety measures in any tunnel are, e.g., speed limits, sufficient distance between the vehicles, proper traffic regulations, queue control, and others. Hereunder, tunnels with one-directional traffic in each tube should be considered safer than bidirectional traffic tunnels.

While accident scenarios involve severe collisions in road tunnels, the situation in underground parking is different due to the very low speeds of the vehicles in such an infrastructure. Also, only cars and small vans are expected to use ordinary underground parking. Nevertheless, vehicles still may self-ignite due to technical defects, be ignited by an arsonist, etc. Fires in car parks are not very frequent and the vast majority is extinguished within a short time. The mitigation systems that are required for underground parking are very different from country to country depending on the size of the parking. Mitigation measures are well established and include, e.g. fire compartments, fire ventilation, sprinkling, etc. The European regulations are rather old and may not sufficiently cope with the development of modern cars being more lightweight and their dimensions being enlarged, while the parking box space may not be adapted accordingly. The vehicles are having a certain distance to the neighbouring vehicles and only the burning vehicles heat radiation is impinging the potential hydrogen vehicles body, while the pressure vessel is shielded due to the vehicle body unless the fire of a spill of combustible liquid is involved. It may be realistic to assume that only in case the fire spreads to the hydrogen vehicle after certain duration, the hydrogen tank could be exposed to a strong enough thermal impact. Here the reduction of distance between vehicles may be an important factor and may increase the likelihood of fire spread from car to car.

# 9 References

American Institute of Chemical Engineers (1998). Guidelines for evaluating the characteristics of vapor cloud explosions, flash fires, and BLEVES, center for chemical process safety.

ANAS (2009) Linee Guida per la Progettazione Della Sicurezza nelle Gallerie Stradali Secondo la Normativa Vigente. Circolare n.179431/2009. https://www.stradeanas.it/sites/default/files/pdf/Linee_guida_sicurezza_gallerie_2009.pdf

Aarskog, F. G., Hansen, O.R., Strømgren, T., Ulleberg, Ø (2020) Concept risk assessment of a hydrogen driven high speed passenger ferry. *Int. J. Hydrog. Energy* 45, pp. 1359-1372

Atkinson, G., Cusco, L., Painter, D., Tam, V. (2009) Interpretation of overpressure markers and directional indicators in full-scale deflagrations and detonations. Hazards XXI, IChemE Symposium Series No. 155, pp. 500-506.

Average car and van occupancy England 2002-2018 Statistic [WWW Document], n.d. . Statista. URL https://www.statista.com/statistics/314719/average-car-and-van-occupancy-in-england/ (accessed 10.12.21).

Bassan, S. (2016). Overview of traffic safety aspects and design in road tunnels. *IATSS Res.* 40, pp. 35–46.

Benekos, I. and Diamantidis, D. (2017) On risk assessment and risk acceptance of dangerous goods transportation through road tunnels in Greece, *Safety Science*, 91, pp. 1–10. doi: 10.1016/j.ssci.2016.07.013.

Borghetti, F., Cerean, P., Derudi, M., Frassoldati, A. (2019). Road Tunnels An Analytical Model for Risk Analysis. Springer

BRE (2010). Fire spread in car parks. BD 2552. Department for Communities and Local Government, London.

BRS (2021). Redningsberedskabets Statistikbank År. Available from https://statistikbank.brs.dk/sb#page=43c0171c-0c4f-46c2-b8c3-84a3ece4d33d [Assessed June 18, 2021]

Caliendo, C., Ciambelli, P., De Guglielmo, M.L., Meo, M.G., Russo, P. (2012). Numerical simulation of different HGV fire scenarios in curved bi-directional road tunnels and safety evaluation. *Tunnelling and Underground Space Technology* 31, pp. 33–50.

Caliendo, C., Ciambelli, P., De Guglielmo, M.L., Meo, M.G., Russo, P. (2013). Simulation of fire scenarios due to different vehicle types with and without traffic in a bi-directional road tunnel. *Tunnelling and Underground Space Technology*, 37, pp. 22–36

Caliendo, C. and De Guglielmo, M. L. (2017) Quantitative Risk Analysis on the Transport of Dangerous Goods Through a Bi-Directional Road Tunnel, *Risk Analysis*, 37(1), pp. 116–129. doi: 10.1111/risa.12594.

Caliendo, C. and Genovese, G. (2020) Quantitative Risk Assessment on the Transport of Dangerous Goods Vehicles Through Unidirectional Road Tunnels: An Evaluation of the Risk of Transporting Hydrogen. *Risk Analysis*, p. risa.13653. doi: 10.1111/risa.13653.

Caliendo, C., Guida, M., Postiglione, F., Russo, I. (2022). A Bayesian bivariate hierarchical model with correlated parameters for the analysis of road crashes in Italian tunnels. *Statistical Methods and Applications* 31, pp. 109–131. https://doi.org/10.1007/s10260-021-00567-5

Casey N. (2020). Fire incident data for Australian road tunnels. *Fire Safety Journal,* 111, 102909 doi: 10.1016/j.firesaf.2019.102909.

Cirrone D., Makarov D., Molkov V. (2019), Cryogenic Hydrogen Jets: Calculation of Hazard Distances. International Conference on Hydrogen Safety, 24th-26th September 2019, Adelaide, Australia. Paper ID191.

Dadashzadeh, M., Kashkarov, S., Makarov, D., Molkov, V. (2018). Risk assessment methodology for onboard hydrogen storage. *Int. J. Hydrog. Energy*, 43, pp. 6462–6475.

DOT (U.S. Departmemt of Transportation) (2013). Post-Crash Hydrogen Leakage Limits and Fire Safety Research. Report n. DOT HS 811 816.

DOT (U.S. Departmemt of Transportation) (2015). Crashworthiness Research of Prototype Hydrogen Fuel Cell Vehicles: Task Order 7 Project Report. Report n. DOT HS 812 112E.

Ehrhart, B.D., Brooks, D.M., Muna, A.B. and LaFleur C. B. (2020) Risk Assessment of Hydrogen Fuel Cell Electric Vehicles in Tunnels. *Fire Technol* , 56, pp. 891–912 https://doi.org/10.1007/s10694-019-00910-z

Ekoto, I W, Houf, W G, Ruggles, A J, Creitz, W L, Li, J X. (2012). Large-scale hydrogen jet flame radiant fraction measurements and modeling, Proceedings of the International Pipeline Conference, Calgary, Canada, September 24-28.

Ekoto, I W, Ruggles, A J, Creitz, W L, Li, J X. (2014) Updated jet flame radiation modeling with buoyancy corrections. *Int. J. Hydrog. Energy*, 39, pp. 20570-20577.

EIHP2 (2003). Risk acceptance criteria for Hydrogen Refuelling Stations [WWW Document]. yumpu.com. URL https://www.yumpu.com/en/document/view/29767890/risk-acceptance-criteria-for-hydrogen-refuelling-stations [accessed 10.14.21].

EN 50126 (2000). Railway applications - The specification and demonstration of Reliability, Availability, Maintainability and Safety (RAMS)

Eriksen, D., Christensen, P. (2021) Risk assessment and CFD simulations of fire propagation in enclosed parking facilities, Master Thesis DTU Civil Engineering

European Parliament of the Council of the European Union (2004). Minimum Safety Requirements for Tunnels in the Trans-european Road Network. Directive 2004/54/EC.

Finney, D.J. (1971) Probit analysis (QA276. 8, F6 No. 04).

FireComp (2014). Deliverable D6.6 - Current fire approach for cylinders

Gentilhomme, O., Proust C., Jamois, D., Tkatschenko, I., Cariteau, B., Studer, E., Masset, F., Joncquet, G., Amielh, M., Anselmet, F. (2012) Data for the evaluation of hydrogen risks onboard vehicles: Outcomes from the French project drive, *International Journal of Hydrogen Energy*, 37(22), pp. 17645–17654. doi: 10.1016/j.ijhydene.2012.04.147.

Groethe, M., Merilo, E., Colton, J., Chiba, S., Sato, Y., Iwabuchi, H. (2007) Large-scale hydrogen deflagrations and detonations, *International Journal of Hydrogen Energy*, 32(13), 2125–2133.

Haugom G.P., Rikheim H., Nilsen S., Hydro SA (2003). Hydrogen Applications - Risk Acceptance Criteria and Risk Assessment Methodology, EHEC2003, Grenoble, Sept. 2003. http://www.eihp.org/public/Reports/Final_Report/SubTask_Reports/ST5.2/EHEC%20paper_final.pdf

HyResponder (2021). Deliverable D1.1 Report on hydrogen safety aspects of technologies, systems and infrastructures pertinent to responders.

HyTunnel-CS (2019). Deliverable D1.2 Report on hydrogen hazards and risks in tunnels and similar confined spaces.

HyTunnel-CS (2019). Deliverable D1.3 Report on Selection and Prioritisation of Scenarios

HyTunnel-CS (2022). Deliverable D2.3 Final report on analytical, numerical and experimental studies on hydrogen dispersion in tunnels, including innovative prevention and mitigation strategies

HyTunnel-CS (2022). Deliverable D3.3 Final report on analytical, numerical and experimental studies on fires

HSE (n.d.) Methods of approximation and determination of human vulnerability for offshore major accident hazard assessment. Available from: https://www.hse.gov.uk/foi/internalops/hid_circs/technical_osd/spc_tech_osd_30/spctecosd30.pdf [Accessed 10.7.21].

HSE (n.d.) Risk management: Expert guidance - Cost Benefit Analysis (CBA) checklist [WWW Document]. Health Saf. Exec. Available from https://www.hse.gov.uk/managing/theory/alarpcheck.htm#footnotes [Accessed 10.7.21].

Joyeux, D. *et al.* (2002) Demonstration of real fire tests in car parks and high buildings. EUR 20466. European Communities.

Khalil, J, Mosher, D., Sun, F., Laube, B., Tang, X., Brown, R. (2010) Quantifying & addressing the DOE material reactivity requirements with analysis & testing of hydrogen storage materials & systems. Washington DC: Annual Peer Review; 2010. Project ID ST012.

Kashkarov, S., Li, Z., Molkov, V. (2020). Blast wave from a hydrogen tank rupture in a fire in the open: Hazard distance nomograms. *Int. J. Hydrog. Energy* 45, pp. 2429–2446. https://doi.org/10.1016/j.ijhydene.2019.11.084

Kashkarov, S., Makarov, D., Molkov, V., 2021. Performance of Hydrogen Storage Tanks of Type IV in a Fire: Effect of the State of Charge. Hydrogen 2, 386–398. https://doi.org/10.3390/hydrogen2040021

Kuznetsov, M., Yanez, J., Grune, J., Friedrich, A., Jordan T., Kuznetsov, M. (2015) Hydrogen combustion in a flat semi-confined layer with respect to the Fukushima Daiichi accident, *Nuclear Engineering and Design*, 286, pp. 36–48. doi: 10.1016/j.nucengdes.2015.01.016.

LaChance, J., Houf, W., Middleton, B., Fluer, L. (2009). Analyses to Support Development of Risk-Informed Separation Distances for Hydrogen Codes and Standards, Technical Report No SAND2009-0874

LaChance, J., Tchouvelev, A., Engebo, A. (2011). Development of uniform harm criteria for use in quantitative risk analysis of the hydrogen infrastructure. *Int. J. Hydrog. Energy* 36, pp. 2381-2388

LaFleur, C., Bran-Anleu, G., Muna, A., Ehrhart, B., Blaylock, M., Houf, W. (2017). Hydrogen Fuel Cell Electric Vehicle Tunnel Safety Study, Technical Report No. SAND2017-pp. 11157 674072.

Landucci, G., Argenti, F., Tugnoli, A., Cozzani, V. (2015). Quantitative assessment of safety barrier performance in the prevention of domino scenarios triggered by fire. Reliab. Eng. Syst. Saf., Domino Effects in the Process Industries: fostering innovative approaches and advancing the State-of-the-art 143, 30–43. https://doi.org/10.1016/j.ress.2015.03.023

Landucci, G., Gubinelli, G., Antonioni, G., Cozzani, V. (2009). The assessment of the damage probability of storage tanks in domino events triggered by fire. *Accid. Anal. Prev.,* Accident Modelling and Prevention at ESREL 2006 41, pp. 1206–1215. https://doi.org/10.1016/j.aap.2008.05.006

Li, Y., Xiao, J., Zhang, H., Breitung ,W., Travis, J., Kuznetsov ,M., Jordan ,T. (2021). Numerical analysis of hydrogen release, dispersion and combustion in a tunnel with fuel cell vehicles using all-speed CFD code GASFLOW-MPI. *Int. J. Hydrog. Energy* 46, pp. 12474-12486

Li, Y. Z., 2019. Study of fire and explosion hazards of alternative fuel vehicles in tunnels. *Fire Safety Journal* 110, 102871. doi: 10.1016/j.firesaf.2019.102871.

Li, Y., Spearpoint, M. (2007). Analysis of vehicle fire statistics in New Zealand parking buildings. *Fire Technology*, 43(2), 93–106. https://doi.org/10.1007/s10694-006-0004-2

Lipscomb M., 2021. Private communication. Northern Trains Limited

Makarov, D., Kim, Y., Kashkarov, S., Molkov, V. (2016). Thermal protection and fire resistance of high-pressure hydrogen storage, in: Eight International Seminar on Fire and Explosion Hazards (ISFEH8). Hefei, China.

Makarov D., Shentsov V., Kuznetsov M., Molkov V. (2021). Hydrogen Tank Rupture in Fire in the Open Atmosphere: Hazard Distance Defined by Fireball. *Hydrogen* 2, pp. 134–146. https://doi.org/10.3390/hydrogen2010008

Mattelaer, V. (2020). Private communication.

Molkov, V.V., Cirrone, D.M.C., Shentsov, V.V., Dery, W., Kim, W., Makarov, D.V. (2021). Dynamics of blast wave and fireball after hydrogen tank rupture in a fire in the open atmosphere. Int. J. Hydrog. Energy 46, pp. 4644–4665. https://doi.org/10.1016/j.ijhydene.2020.10.211

Molkov, V., Dadashzadeh, M., Kashkarov, S., Makarov, D. (2021). Performance of hydrogen storage tank with TPRD in an engulfing fire. *Int. J. Hydrog. Energy*. https://doi.org/10.1016/j.ijhydene.2021.08.128

Molkov, V., Dery, W. (2020). The blast wave decay correlation for hydrogen tank rupture in a tunnel fire. *Int. J. Hydrog. Energy* 45, pp. 31289–31302. https://doi.org/10.1016/j.ijhydene.2020.08.062

Molkov, V., Kashkarov, S. (2015). Blast wave from a high-pressure gas tank rupture in a fire: Stand-alone and under-vehicle hydrogen tanks. *Int. J. Hydrog. Energy* 40, pp. 12581–12603. https://doi.org/10.1016/j.ijhydene.2015.07.001

Molkov, V., Makarov, D., Kashkarov, S. (2018). Composite Pressure Vessel for Hydrogen Storage. WO 2018/149772 A1.

Molkov, V., Saffers, J.-B. (2013) 'Hydrogen jet flames', *International Journal of Hydrogen Energy*, 38(19), pp. 8141–8158. doi: 10.1016/j.ijhydene.2012.08.106.

Molkov V. (2012). Fundamentals of Hydrogen Safety Engineering I, vol. 4. bookboon.com

Nørregaard, K., Roed, L. V. and Skov, S. M. (2022) Analyse af brandsikkerhed i garageanlæg, oplag af litium-ion batterier og batterier til solcelleanlæg i bygninger. Copenhagen, Denmark. Available at: https://bpst.dk/sites/default/files/2022-02/Analyse af brandsikkerhed i garageanlæg - Ved batterioplag og BESS 02_2022_01_14.pdf

NHTSA. National Highway Traffic Safety Administration, 2015. Traffic safety facts 2015: a compilation of motor vehicle crash data from the fatality analysis reporting system and the general estimates system. No. DOT HS 812 384.

Otxoterena, P., Björnstig, U. and Lindkvist, M. (2020). Post-collision fires in road vehicles between 2002 and 2015, *Fire and Materials* 44(6), pp. 767–775. doi: 10.1002/fam.2862.

Pape, D., Cox, A. (2015). Compressed hydrogen container fueling option for crash testing. Report No. DOT HS 812 133. Washington, DC: National Highway Traffic Safety Administration

Papoulis, A. (1965). Probability, random variables, and stochastic processes, 3rd ed., New York: McGraw-Hill.

Perrette, L., Wiedemann, H. K. (2007) CNG buses fire safety: learnings from recent accidents in France and Germany. Society of automative engineer world Congress 2007, Apr 2007, Detroit, United States. pp.NC. ineris-00976180

PIARC (2017). World Road Association, Technical Committee C.3.3 Road Tunnel Operation, Experience with Significant Incidents in Road Tunnels, 2017R35EN

PIARC (2016). World Road Association, Technical Committee C.3.3 Road Tunnel Operation, Fixed Firefighting Systems in Road Tunnels: Current Practices and Recommendations, 2016, 2016RO3EN.

PIARC (2012). World Road Association, Technical Committee C.4 Road Tunnel Operations. Current practice for risk evaluation for road tunnels, 2012R23EN, 1-91.

Rattei, G., Lentz, A., Kohl, B. (2014) .How frequent are fires in tunnels – _analysis from Austrian tunnel incident statistics, in: 7th International Conference on Tunnel Safety and Ventilation, Graz, 2014.

Rázga, M., Danišovič, P. and Poledňák, P. (2015) 'Extension of risk analysis model for road tunnels', *Procedia Engineering*, 111, pp. 687–693. doi: 10.1016/j.proeng.2015.07.133.

Reliability Analysis Center, 1991. Non electronic parts reliability data.

Road Tunnel Association (RTA), 2019. UK & Eire Road Tunnel Directory [WWW Document]. URL UK & Eire Road Tunnel Directory (accessed 6.28.19).

RTA, 2019. UK & Eire Road Tunnel Directory [WWW Document]. URL http://www.rtoa.org.uk/Directory.html (accessed 6.28.19).

Ruban, S., Heudier, L., Jamois, D., Proust, C., Bustamante-Valencia L., Jallais S., Kremer-Knobloch K., Maugy C., Villalonga S. (2012). Fire risk on high-pressure full composite cylinders for automotive applications. *Int. J. Hydrog. Energy* 37, pp. 17630-17638.

Russo, P., De Marco, A., Parisi, F. (2020) Assessment of the Damage from Hydrogen Pipeline Explosions on People and Buildings. *Energies*, 13, 5051-5066; doi:10.3390/en13195051

Saw, J., Flauw. Y., Demeestere, E. M, Naudet, V., Blanc-Vannet, P., Hollifield, K., et al. (2016). The EU FireComp Project and risk assessment of hydrogen composite storage applications using bow-tie analysis. In Proceedings of Hazards 26, Edinburgh UK.

Statistics Denmark. (2021). Buildings and their floor area by region, unit and use 20112021. https://www.statistikbanken.dk/BYGB70

Sun, K., Li, Z. (2019). Quantitative risk analysis of life safety and financial loss for road accident of fuel cell vehicle. *Int. J. Hydrog. Energy,* 44, pp. 8791-8798

Tohir, M. Z. M., Spearpoint, M. (2014) Development of Fire Scenarios for Car Parking Buildings using Risk Analysis. *Fire Safety Science*, 11, pp. 944–957. doi: 10.3801/IAFSS.FSS.11-944.

Tohir, M. Z. M., Spearpoint, M. (2013) Distribution analysis of the fire severity characteristics of single passenger road vehicles using heat release rate data. *Fire Science Reviews,* 2(5), pp. 1-26 doi: 10.1186/2193-0414-2-5.

UIC (2021). Safety Report 2021. Avaiklable from: https://safetydb.uic.org/IMG/pdf/uic-safety-public-report_2021.pdf [accessed 11 October, 2021]

UNECE, 2013. Global Registry. Addendum 13: Global technical regulation No. 13. Global technical regulation on hydrogen and fuel cell vehicles.

UNECE (2014) Proposal for a new Regulation on hydrogen and fuel cell vehicles (HFCV). ECE/TRANS/WP.29/2014/78. Availaible from https://unece.org/DAM/trans/doc/2014/wp29/ECE-TRANS-WP29-2014-78e.pdf [Accessed 13.07.21].

U.S. DOT National Highway Traffic Safety Administration (NHTSA) (2015). Traffic safety facts 2015: a compilation of motor vehicle crash data from the fatality analysis reporting system and the general estimates system (No. DOT HS 812 384).

Weyandt, N. (2006). Vehicle bonfire to induce catastrophic failure of a 5,000-psig hydrogen cylinder installed on a typical SUV. Southwest Research Institute report for the Motor Vehicle Fire Research Institute.

Weyandt, N. (2005). Analysis of Induced Catastrophic Failure Of A 5000 psig Type IV Hydrogen Cylinder (No. 01.06939.01.001). Southwest Research Institute report for the Motor Vehicle Fire Research Institute.

What Are The Average Dimensions Of A Car In The UK? [WWW Document] (2021). URL https://www.nimblefins.co.uk/cheap-car-insurance/average-car-dimensions [Accessed 10.12.21].

Willmann, C., Defert, R. (2016). Statistical analyses of breakdowns, accidents and fires in road tunnels in France, in: 7th International Symposium on Tunnel Safety and Security, Canada, Montreal, 2016.

Yamashita, A., Kondo, M., Goto, S., Ogami, N. (2015). Development of High-Pressure Hydrogen Storage System for the Toyota “Mirai.” SAE Tech. Pap., SAE International. https://doi.org/10.4271/2015-01-1169

Zalosh, R. (2008). CNG and hydrogen vehicle fuel tank failure Incidents, testing, and preventive measures. Available from: http://citeseerx.ist.psu.edu/viewdoc/similar?doi=10.1.1.551.4057&type=cc [Accessed 1.7.2021]

Zheng, J., Bie, H., Xu, P., Chen, H., Liu, P., Li, X., Liu, Y., 2010. Experimental and numerical studies on the bonfire test of high-pressure hydrogen storage vessels. Int. J. Hydrog. Energy 35, 8191–8198.

Zulauf, C. *et al.* (2012) *Current practice for risk evaluation for road tunnels*. Edited by World Road Association (PIARC). PIARC.

# Appendix A1

## A1. Flame acceleration and Deflagration-to-Detonation Transition (DDT) in a tunnel (KIT)

### A1.1 Introduction

Evaluation of DDT conditions in a tunnel geometry consists of the four major parameters:

1. Geometry factors:
   - Confinement degree (confined, semiconfined, partially confined), lateral venting, end venting, smooth channel, rough channel, obstructions, fans, natural wind.
   - Scale (characteristic size – cross-section, length of the channel, length of the cloud of the hydrogen-air mixture).
   - The linearity of the channel (straight, bended, T – junction, Y – junction, zigzagging).
2. Mixture characterization:
   - Mixture uniformity/nonuniformity (longitudinal gradient, vertical stratification, vertical gradient).
   - Mixture reactivity (laminar flame velocity, expansion ratio, speed of sound, detonation velocity, detonation pressure, detonation cell size.
3. Ignition source (electric spark, hot surface (glow plug), open flame, local explosion or blast wave)
4. History and dynamics of the process (run-up-distance, runway distance to flame acceleration and DDT)

### A1.2 Nomenclature

| Parameter | Symbol | Unit |
|---|---|---|
| Height of the tunnel | $H$ | m |
| Height of the hydrogen-air layer | $h$ | m |
| Width of the tunnel | $b$ | m |
| Area | $A$ | $m^2$ |
| Blockage ratio | $BR$ | (-) |
| Distance | $x$ | m |
| Diameter | $d, D$ | m |
| Gravity acceleration | $g$ | $m/s^2$ |
| Length | $L$ | m |
| Universal gas constant | $R$ | J/K/kmol |
| Volume fraction of hydrogen | $X$ | (-) |
| Pressure | $p$ | bar |
| Temperature | $T$ | K |
| Molecular mass | $M$ | kg/kmol |
| Density | $\rho$ | $kg/m^3$ |
| Characteristic time | $t$ | s |
| Hydrogen inventory | $m$ | kg |

## A1.3 Model description

The model operates with several basic characteristics for DDT evaluation:

1. The mixture of hydrogen with air should be within the flammability limits 4 – 75 %H2 (vol.). The criterion for flame acceleration is the critical expansion ratio for flame acceleration to speed of sound, σ*=3.75 for hydrogen – air mixtures inside the enclosed channels (Dorofeev et al. 2001). It depends on the scale but not for the tunnel dimensions because the critical Peclet number $Pe = D/\delta >> 100$ for tunnels. For partially confined envelope of hydrogen – air mixture, the critical expansion ratio depends on the opening degree, mixture uniformity and blockage ratio as the ratio of blocked area to the total cross-section area, see Figure 1 (Kuznetsov et al., 2011; Grune et al., 2013; Kuznetsov et al., 2015; Friedrich et al. 2019).

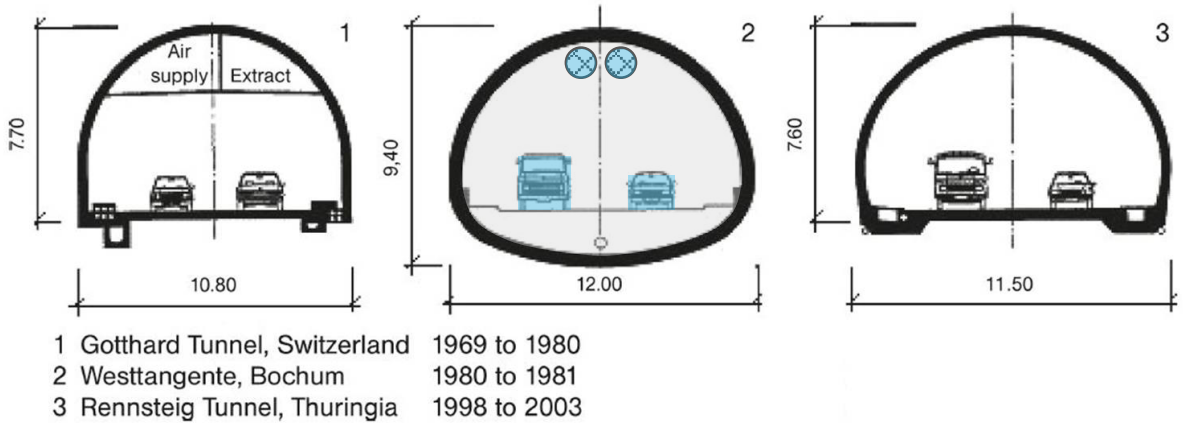


Figure 1. Examples of cross-sections (mined road tunnels). Grey area is the total cross-section, A; blue area is blocked by turbo-fans and/or by cars, $A_i$. BR = $\Sigma A_i/A$.

A linear correlation between the critical expansion ratio σ* and the ratio of the spacing between the obstacles and the layer thickness, *s/h*, was derived by Kuznetsov et al. (2011) for fast flame propagation based on large scale experiments (Figure 2) and theoretical considerations:

$$\sigma^* = \sigma_0^* \left(1 + K \cdot s/h\right) \tag{1.1}$$

where $\sigma_0^* = 3.75$ is the critical expansion ratio for uniform hydrogen-air mixture fully occupied the tunnel cross-section; $K = 0.175$ is a constant depending on the blockage ratio BR = $\Sigma A_i/A$, where $A$ is the tunnel cross-section, $A_i$ is the total visible blockage for cars, busses, trucks ventilators and other supporting equipment inside the tunnel; the spacing $s$ can be a distance between cars in one lane. Eq. (1.1) is true for a layer of stratified hydrogen-air mixture; $h$ is the layer thickness (Figure 4, left, bottom). It is valid for relatively small gradients (less than 30%H2/m) in an assumption that the process of flame propagation governs by the highest hydrogen concentration at the ceiling. For relatively high concentration gradient 40-60%H2/m, efficiently, the only part of the mixture above 8-9%H2 takes part in upward flame propagation. It results in a thinner layer of the mixture pushing the flame. This means that it requires higher hydrogen concentration to provide the flame acceleration to the speed of sound. For instance, it needs the maximum hydrogen concentration of 19%H2 at the ceiling corresponding to 0.24 m of efficient layer thickness compared to 15 %H2 and a layer thickness of 0.6 m for a uniform hydrogen-air composition to provide flame acceleration to speed of sound.

In case of a stratified hydrogen-air mixture fully occupied the cross-section of the system (Kudriakov et al., 2013; Kuznetsov et al., 2019), the process of combustion and flame acceleration is governed

by the maximum hydrogen concentration at the top of the system with $h = H$ in Eq. (1.1).

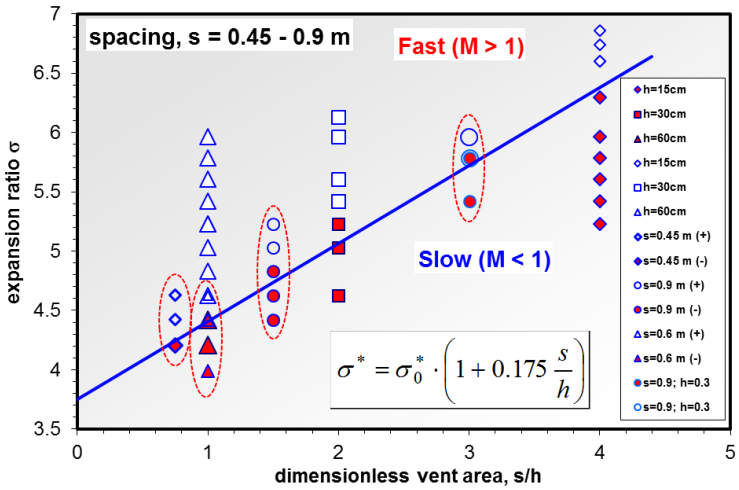


Figure 2. Critical conditions for effective flame acceleration as function of expansion ratio vs. dimensionless vent area: sonic flame and detonations (open points); subsonic flame (solid points). Different spacing is labelled (Kuznetsov et al., 2011).

2. The DDT criterion is based on the ratio of characteristic tunnel dimension (for instance, an equivalent diameter $D = \sqrt{4A/\pi}$ to the detonation cell size, $D/\lambda$. The ratio $D/\lambda$ should exceed the value $N^*$ dependent on geometry, mixture reactivity, uniformity of the mixture (Moen et al., 1981; Teodorczyk et al., 1988; Dorofeev et al. 2001). Critical conditions for uniform or stratified semi-confined layer of hydrogen air mixture are given in terms of the ratio $h/\lambda$, where $h$ is the layer thickness, see Fig. 2, bottom (Kuznetsov et al., 2011; Grune et al., 2013; Kuznetsov et al., 2015; Rudy et al., 2013; Grune et al., 2013b).

The model includes the DDT criterion as dimensionless ratio $L/\lambda$ of the characteristic size $L$ over the detonation cell size $\lambda$ as a measure of detonability of the mixture:

$$\frac{L}{\lambda} > N^* \qquad (1.2)$$

where $N^*$ is the critical value for detonation onset (DDT) or detonation propagation dependent on the geometry of the system. The tunnel relevant critical ratios of $L/\lambda$ for detonation onset in a channel with obstacles fully filled with uniform mixture are summarized in Table **1**.

*Table 1. Dimensionless scale for different processes.*

| Dimensionless scale | Critical value N*, (-) | Detonation relevant phenomenon | References |
|---|---|---|---|
| $D/\lambda$ | $1/\pi$ | Detonation propagation in a smooth channel with diameter $D$ | Moen et al. (1981) |

| | | | |
|---|---|---|---|
| $d/\lambda$ | 1 | Detonation propagation in obstructed tubes with orifice size $d$ (BR*<0.43) | Teodorczyk et al. (1988) |
| $L/\lambda$ | 7 | Detonation onset in obstructed channels | Dorofeev et al. (2000) |
| $L/\lambda$ | 7 | Detonation onset in multi-chamber structure | Dorofeev et al. (2000) |

Most of the practical cases are covered by more universal criterion $L/\lambda > 7$ based on large scale experiments (Dorofeev et al., 2000). Characteristic size $L$ for detonation onset is formulated depending on the size of the channel $D$, dimension of unobstructed passage between obstacle and sidewall $d$ and spacing between repeating obstacles $S$:

$$L = \frac{D+S}{2(1-d/D)} \tag{1.3}$$

For tunnel geometry, it will be more convenient to express the ratio d/D through the blockage ratio BR because d-parameter is not well defined for the complex geometry of obstacles:

$$d/D = \sqrt{1-BR} \tag{1.4}$$

The complex blockage ratio, in turn, can be expressed as follows

$$BR = \sum A_i/A \tag{1.5}$$

where $A_i$ is the area of each visible object which is blocked the tunnel cross-section (a car or cars, a jet fan or ventilator, a truck or trucks). Table 5 has the blockage area $A_i$ for different vehicles. Then, assuming equidistant spacing between vehicles $S = D$, Eq. (1.3) can be derived as a function of blockage ratio BR and an equivalent diameter D keeping constant the DDT condition $L/\lambda = 7$:

$$L = \frac{D}{1-\sqrt{1-BR}} = 7\lambda \tag{1.6}$$

Table **2** summarizes the results of such a practical transformation of Eq. (1.3). It may tell us several conclusions useful for tunnel safety assessment. For very small blockage BR = 0.1 characteristic length for DDT is about 20 calibers ($L/D$ = 19.5). For practically unblocked tunnel (BR=0.1) the critical ratio $D/\lambda$ =0.36 approach to the ratio $D/\lambda$ =1/π found by Moen et al. (1981) for smooth tubes. The critical ratio $d/\lambda$ = 0.96 for BR = 0.3 and $d/\lambda$ = 1.22 for BR = 0.4 are very close to the DDT criterion $d/\lambda$ = 1 found by Teodorczyk et al. (1988) for obstructed tube with BR < 0.43. The higher blockage leads to larger ratios $D/\lambda$ and $d/\lambda$. For the tunnel geometry, we cannot expect the blockage larger than 30% except the rail tunnels where the blockage by the train can reach 50-60 %.

*Table 2. Critical ratios for DDT as function of blockage ratio.*

| Blockage ratio BR | $L/D$ | $D/\lambda$ | $d/\lambda$ |
|---|---|---|---|
| 0.1 | 19.49 | 0.36 | 0.34 |
| 0.2 | 9.47 | 0.74 | 0.66 |
| 0.3 | 6.12 | 1.14 | 0.96 |
| 0.4 | 4.44 | 1.58 | 1.22 |

| | | | |
|---|---|---|---|
| 0.5 | 3.41 | 2.05 | 1.45 |
| 0.6 | 2.72 | 2.57 | 1.63 |

All aforementioned relationships for detonation onset are relevant to the very hypothetical scenario for uniform hydrogen-air mixture fully filled the tunnel cross-section. The most realistic scenario for tunnel geometry is the formation of a stratified layer of the hydrogen-air mixture on top of the channel (Figure 3). It was found by Li et al. (2019, 2021) that due to open boundaries in the axial direction, the cloud grows only in the longitudinal direction with almost constant layer thickness remaining within 0.5-0.6 m.

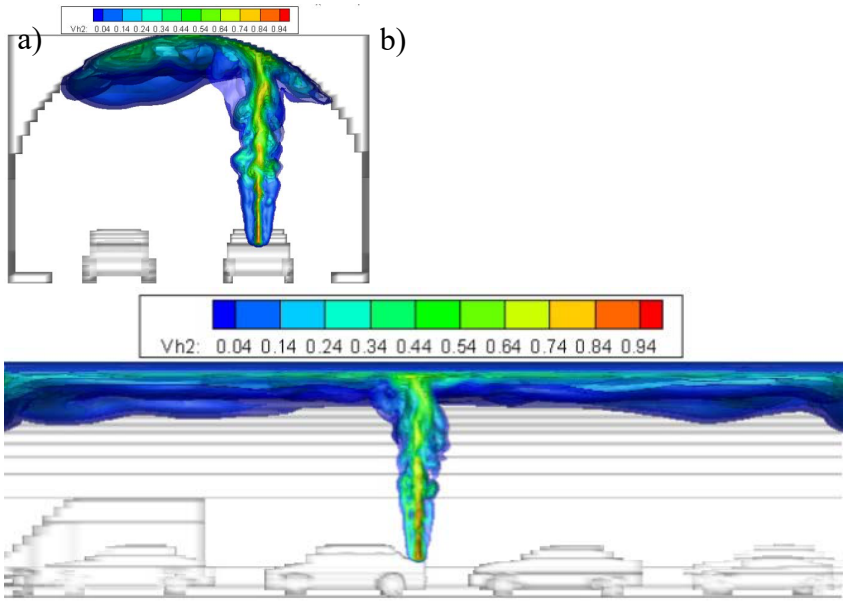


Figure 3. Hydrogen distribution profiles in a tunnel: a) front view; b) side view (Li et al., 2019).

Critical conditions for detonation onset in a semi-confined layer of the uniform hydrogen-air mixture have been experimentally found in a cylinder vessel of 3.5 m ID (Kuznetsov et al., 2011; Kuznetsov et al., 2015):

$$h/\lambda = 13\text{-}14, \quad (1.7)$$

where $h$ is the layer thickness. For the stratified layer, similar to shown in Figure 3, If the hydrogen concentration gradient is not larger than 60%$H_2$/m, the critical condition for a detonation onset is the same (see Eq. 1.7) as for uniform hydrogen composition of the same hydrogen concentration as the maximum concentration of the stratified composition. It happens due to the efficient layer thickness

$$h^* = X_{H2}/\text{grad}(X_{H2}) \quad (1.8)$$

is not less than the corresponding layer thickness for the uniform mixture. For instance the efficient layer thickness $h^*$ = 1.05 m for grad($X_{H2}$) =20%$H_2$/m and $h^*$ = 0.7 m for grad($X_{H2}$) =30%$H_2$/m for stratified compositions which are larger than 0.6 m of detonable uniform composition. In the case of a very steep gradient (more than 60%$H_2$/m) the effective layer thickness $h^*$ = 0.33 m becomes too thin to be detonable. For such a layer thickness the maximum hydrogen concentration should be higher than 23%H2. This value is very close to

experimental one 23.6%H2 (Kuznetsov et al., 2015). Then, for the stratified semiconfined layer the critical DDT condition

$h^*/\lambda$ = 13-14, (1.9)

3. Both of aforementioned criteria for flame acceleration and DDT require the satisfaction of so called "run-up-distance (RUD) criterion", $X$s < $L$, where $L$ is a characteristic length of hydrogen – air cloud along the channel (Veser et al., 2002; Kuznetsov et al., 2005; Ciccarelli et al., 2008). If the cloud dimension $L$ is longer than the run-up-distance to speed of sound $X$s then the detonation may occur.

The run-up-distance to detonation depends on mixture reactivity and the level of turbulence. Both factors can promote flame acceleration and shorten the run-up distance $X$s. A high level of turbulence can be managed by fans or by the obstacles. In particular, in the tunne,l it can be a ventilation system or traffic of the cars. If there are no obstacles and the channel is relatively smooth, then the boundary layer is the only a source of the turbulent motion. Based on the critical thickness of the boundary layer for detonation onset $\delta$ =10λ a run-up-distance to detonation was experimentally evaluated depending on the tube roughness (Kuznetsov et al., 2005):

$X$s = 550 λ, (1.10)

Eq. (1.10) is valid for very thick tubes similar to tunnel with D > 20λ. For relatively narrow tubes with 10λ < D < 20λ the run-up-distance Xs is proportional to tube diameter D depending on roughness Δ:

$X$s = (24-27) D, Δ = 100μ (1.11)

$X$s = (18-19) D, Δ = 1000μ (1.12)

$X$s = (12-14) D, Δ = 5000μ (1.13)

These values fit very well to $X$s = (15-40) D according to papers Bollinger et al. (1961) and Laffitte and Dumanois (1926). To take into account the effect of roughness and involving the boundary layer theory Eqs. (1.11-1.13) have been transformed as follows (Ciccarelli et al., 2008)

$$X_S = D\frac{\gamma}{C}\left[\frac{1}{\kappa}\ln\left(\gamma\frac{D}{h}\right)+K\right] \quad (1.14)$$

where κ, K, and C are the physical constant from turbulent boundary layer theory (Landau and Lifshitz, 1986): κ = 0.4, K = 5.5, and C = 0.2; $D/h$ can be expressed through the blockage ratio:

$$\frac{D}{h}=\frac{2}{1-\sqrt{1-BR}}. \quad (1.15)$$

$$\gamma=\left[\frac{a_p}{\eta S_L(\sigma-1)^2}\left(\frac{\delta}{D}\right)^{1/3}\right]^{\frac{1}{2m+7/3}} \quad (1.16)$$

where *S*L is the laminar flame speed; δ = ν/SL is the laminar flame thickness; *ν* is the kinematic viscosity; η and *m* are two incognita derived from experimental data (Kuznetsov et al., 1999; Kuznetsov et al., 2005; Lindstedt et al., 1989; Kuznetsov et al., 2005b; Kuznetsov et al., 2003): η=2.1 and m=-0.18. Relations Eq. (1.14)-(1.16) consider roughness as a measure of blockage but the relations are valid only up to very small blockage ratio BR < 0.1. There is another relationship to calculate the run-up-distance to supersonic flame within the range BR = 0.3 – 0.75 (Veser et al., 2002):

$$X_S = \frac{a_p D \cdot (1 - BR)}{(1 + 1.5 \cdot BR) \cdot 10 S_L (\sigma - 1)} \tag{1.17}$$

Due to the gap of blockage ratios for the validity of Eq. (1.14) and Eq. (1.17) between BR = 0.1 and BR = 0.3, a linear interpolation between two bounding points Xs/D(BR=0.3) and Xs/D(BR=0.1) can be used (Ciccarelli et al., 2008). For the practical application, we can propose to extend the correlation Eq. (1.17) to blockage ratio BR = 0.1 with 3 times under-prediction compared to Eq. (1.14).

Both relationships Eq. (1.14) and Eq. (1.17) include laminar flame speed SL and laminar flame thickness δ as the measures of reactivity of the mixture. The detonability factor detonation cell size λ is not included in the consideration. Then, it might be a curious result obtained that the distance is enough for the detonation onset but the detonation cell size is too big for the system to make the system detonable. In such a case, a supersonic flame should be considered. One of the disadvantages and also a conservativism of the correlations Eq. (1.14) and Eq. (1.17) is that they cover the cases of uniform mixtures in an enclosed channel. So that that for a semiconfined layer of a stratified hydrogen – air mixture it might be an under-predicted result (a shorten run-up-distance). The under-prediction can be compensated by the existence of local zones enriched with hydrogen in the vicinity of the source and also by some barriers of the tunnel structure or big trucks carried huge cargo reducing the run-up-distance.

4. Characteristic reactivity, geometry, the scale / dimension of the hydrogen – air cloud produced by accidental hydrogen release should be defined depending on the release scenario, total hydrogen inventory, and characteristic time. Characteristic time is the time span between hydrogen release and ignition moments required for hydrogen distribution and cloud formation.

The cloud can be uniform (Figure 4, left, very hypothetical scenario U1 (whole channel) and U2 (a layer)) or a more realistic stratified cloud (Figure 4, right, scenario N1 (full cross-section) and N2 (a layer)). It can be fully filled the tunnel cross-section (Figure 4, top) or formed as a layer on top of the compartment (Figure 4, bottom). The typical layer geometry of the cloud is shown in Figure 3 and Figure 5 based on GASFLOW numerical simulations. The case of uniform hydrogen distribution is more typical for vertical vents from a tunnel to the atmosphere. The case of high pressure hydrogen jet cloud with a radial hydrogen distribution will not be considered in the tool. The average hydrogen concentration in the case of a uniform hydrogen-air cloud and the maximum hydrogen concentration at the ceiling of the tunnel is assumed to be the characteristic concentration of hydrogen to evaluate the reactivity of the cloud.

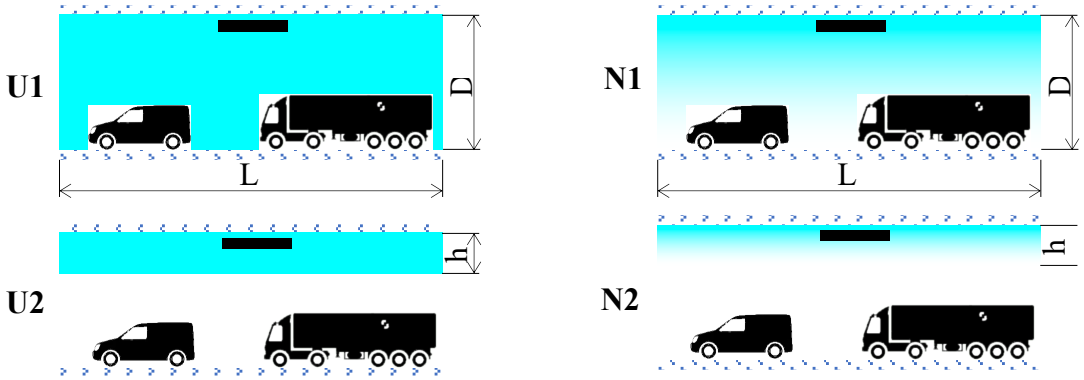


Figure 4. Typical geometry of hydrogen-air cloud inside the tunnel: uniform composition (left); stratified composition (right); fully filled cross-section (top); a semiconfined layer (bottom).

As follows from GASFLOW numerical simulations (Li et al., 2019, 2021) for 3.5 kg of hydrogen distribution from high pressure tank (70 MPa, 5 mm TPRD device) in a tunnel (D = 9.6 m, H = 6.6 m) the most realistic cloud geometry is a semiconfined layer of stratified hydrogen in air along the tunnel (Figure 5). The figure shows the flammable hydrogen cloud ($H_2$ vol >4%) in the tunnel at different times. The hydrogen cloud is gathering at the ceiling and is pushed sidewise along the tunnel by the continuous hydrogen jet. Hence, a layer of combustible hydrogen with thickness of abut 1m is formed at the tunnel ceiling. Figure 5 (d) at 16 s corresponds to the time when hydrogen inventory within the flammability limits has a maximum of about 2.5 kg. The mass flow rate from 0.5 kg/s drops down to 0.1 kg/s at this moment. This time is about a third of the total release time of about 50 s. However, almost 70% of the total hydrogen inventory released during this time. The hydrogen concentration has a strong vertical gradient with the maximum hydrogen concentration near the ceiling around 40% decreasing to 0% at the bottom of the layer. It is supposed to be the most dangerous moment with respect to the severity of the hydrogen explosion. We may take the region of the hydrogen layer (0.6 m below the ceiling) at the time of the third of the total release time to evaluate the hydrogen risk with respect to the flame acceleration and DDT. Such evaluation can be quite conservative because for a smaller nozzle diameter of TPRD device it can be a smaller fraction of total hydrogen inventory as a maximum amount of hydrogen contained within the hydrogen flammability limits.

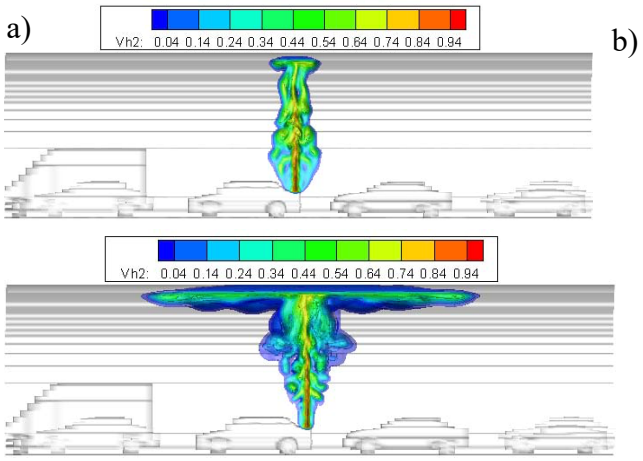

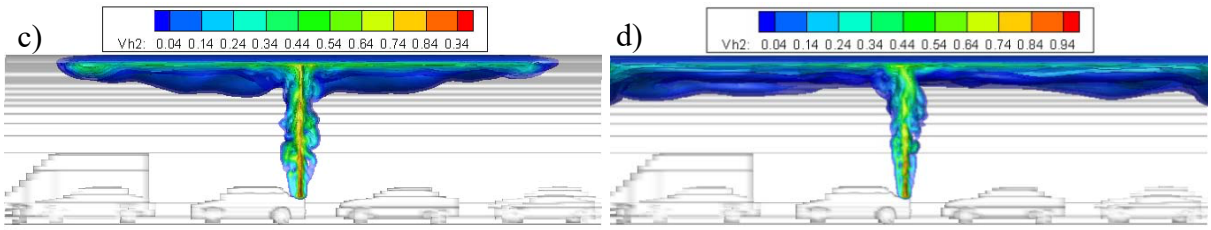


Figure 5. Hydrogen distribution profiles in a tunnel vs. time after release: a) 1 s; b) 4 s; c) 8s; d) 16 s.

Now, we can specify the geometry of hydrogen-air clouds for different tunnel geometries. Three most typical tunnel cross-sections are given in Figure 1. A round shape (4) and a rectangular cross-section (5) can also be introduced as the simplest and the basic ones to be combined to reproduce the real tunnel cross-sections. Within the Hytunnel-CS project (D2.2, Ch. 4.3), typical dimensions for different tunnels and hydrogen inventories for typical vehicles are summarized to be used as input data for safety evaluations (Table 3, Table 4, Table 5, Table 6). Depending on the hydrogen inventory, a volume and dimension of the cloud a characteristic hydrogen concentration can be calculated for a uniform and stratified hydrogen clouds.

The characteristic length of the cloud $L$ for the given average hydrogen concentration $X_{H2}$ is calculated for hydrogen inventory $m$ of uniform hydrogen distribution (Figure 4, left):

$$L = V / A, \tag{1.18}$$

where $V$ is the volume of hydrogen-air mixture as a function of average hydrogen concentration $X_{H2}$

$$V = \frac{1}{X_{H2}} \frac{pM}{mRT}; \tag{1.19}$$

$A$ is the tunnel cross-section area (CSA) (Table 3,Table 4) of a layer cross-section area:

$$A = b \cdot h; \qquad \text{for rectangular tunnel } b * H \tag{1.20}$$

Table 3 Dimensions of European road tunnels

| | Tunnel Description | Cross-section Area, CSA ($m^2$) | Real Diameter, D (m) | Equivalent Diameter, D (m) |
|---|---|---|---|---|
| 1 | Single lane tunnel | 24.10 | | 5.54 |
| 2 | Double lane tunnel | 39.50 | | 7.09 |
| 3 | Gotthard tunnel, double lane | 49.35 | 7.74 | 7.93 |
| 4 | Rennsteig tunnel, double lane | 72.95 | 7.5 | 9.64 |
| 5 | Tyne tunnel (Original), double lane | 48.10 | 7.3 | 7.83 |

Table 4 Dimensions of European rail tunnels

| | Tunnel Description | Cross-section Area, CSA ($m^2$) | Real Diameter, D (m) | Equivalent Diameter, D (m) |
|---|---|---|---|---|
| 1 | High speed traffic, two rail | 92.0 | | 10.82 |

| | | | | |
|---|---|---|---|---|
| 2 | Express traffic tunnel, two rail | 79.2 | | 10.04 |
| 3 | Metro type traffic, single rail | 44.6 | | 7.54 |
| 4 | Rectangular urban rail, two rail | 56.3 | | 8.47 |
| 5 | Severn tunnel, two rail | 60.0 | 7.93 | 8.74 |
| 6 | Channel tunnel single rail | 53.5 | 7.6 | 8.25 |

Table 5 Initial hydrogen inventory, mass flow rate and discharge time for different vehicles

| Vehicle | Total Vehicle Inventory (kg) | Single Tank Inventory (kg) | Initial mass flow rate (kg/s) | Discharge time (sec) | Cross-section area ($m^2$) |
|---|---|---|---|---|---|
| Car (700 Bar) | 5.4 | 2.7 | 0.215 | 168 | 2.8 |
| Bus, truck/lorry (350 bar) | 40.0 | 4.97 | 1.638 | 134 | 7.5 |
| Train 1 (350 bar) | 96.0 | 4.14 | 7.85 | 67 | 10.7 |
| Train 2 (350 bar) | 105.0 | 5.80 | 5.89 | 97 | 13.9 |

Table 6 Hydrogen storage specifications for different car

| Car/Model | Year | No tanks | Vessel pressure (MPa) | Mass per tank / total (kg) | Volume per tank / total (liters) |
|---|---|---|---|---|---|
| Mercedes-Benz GLC F-CELL. | 2018 | 2 | 70 | 2.2 / 4.4 | 57.5 / 115 |
| Hyundai NEXO Fuel Cell | 2018 | 3 | 70 | 2 /6 | 52 / 156 |
| Honda Clarity Fuel Cell | 2016 | 2 | 70 | ? /5.46 | 144 |
| Toyota Mirai | 2015 | 2 | 70 | 2.3 / 4.6 | 60 + 62.4 / 122.4 |
| Hyundai Tucson/ix35 FCEV | 2013 | 2 | 70 | ? / 5. 6 | / 133 |

Table 7 Main properties of hydrogen-air combustible mixtures

| H2 mole fraction* $X_{H2}$ | Expansion ratio** $\sigma$ | Detonation cell size*** $\lambda$, $10^{-3}$ m | H2 mole fraction $X_{H2}$ | Expansion ratio $\sigma$ | Detonation cell size $\lambda$, $10^{-3}$ m |
|---|---|---|---|---|---|
| 0.09 | 3.31 | 18040 | 0.296 | 7.00 | 9.8 |
| 0.1 | 3.54 | 5095 | 0.3 | 7.02 | 9.7 |
| 0.11 | 3.77 | 2319 | 0.35 | 6.90 | 9.7 |
| 0.12 | 3.99 | 1289 | 0.4 | 6.60 | 11.9 |
| 0.13 | 4.21 | 798 | 0.45 | 6.27 | 16.8 |
| 0.14 | 4.42 | 531 | 0.5 | 5.91 | 27.3 |
| 0.15 | 4.63 | 361 | 0.55 | 5.53 | 57.4 |
| 0.16 | 4.83 | 252 | 0.6 | 5.12 | 148 |
| 0.18 | 5.23 | 114 | 0.65 | 4.69 | 362 |
| 0.2 | 5.60 | 44.6 | 0.7 | 4.24 | 930 |
| 0.22 | 5.96 | 24.6 | 0.75 | 3.76 | 2957 |
| 0.25 | 6.45 | 14.5 | 0.8 | 3.25 | 21230 |

* The data for intermediate concentration can be linearly or by spline interpolated.

** Expansion ratios calculated by STANJAN and Cantera codes (Reynolds, 1986; Goodwin, 2001).

*** Detonation cell sizes calculated with CELL_H2 program based on Gavrikov et al. (2000) paper.

Table 8 Laminar flame speed and speed of sound for combustion products

| H2 mole fraction* $X_{H2}$ | Laminar velocity ** SL, m/s | Speed of sound** $a_p$, m/s | Kin. viscosity** v, $cm^2/s$ | H2 mole fraction $X_{H2}$ | Laminar velocity SL, m/s | Speed of sound $a_p$, m/s | Kin. viscosity v, $cm^2/s$ |
|---|---|---|---|---|---|---|---|
| 0.09 | 0.171 | 636 | 0.165 | 0.296 | 2.677 | 980 | 0.202 |
| 0.1 | 0.246 | 659 | 0.167 | 0.3 | 2.719 | 983 | 0.203 |
| 0.11 | 0.334 | 682 | 0.168 | 0.35 | 3.131 | 1024 | 0.214 |
| 0.12 | 0.432 | 703 | 0.170 | 0.4 | 3.333 | 1047 | 0.227 |
| 0.13 | 0.541 | 724 | 0.171 | 0.45 | 3.313 | 1068 | 0.242 |
| 0.14 | 0.657 | 745 | 0.173 | 0.5 | 3.082 | 1087 | 0.258 |
| 0.15 | 0.781 | 765 | 0.175 | 0.55 | 2.672 | 1106 | 0.277 |
| 0.16 | 0.910 | 784 | 0.176 | 0.6 | 2.129 | 1125 | 0.299 |
| 0.18 | 1.180 | 821 | 0.180 | 0.65 | 1.516 | 1145 | 0.325 |
| 0.2 | 1.458 | 855 | 0.183 | 0.7 | 0.905 | 1165 | 0.356 |
| 0.22 | 1.737 | 888 | 0.187 | 0.75 | 0.375 | 1186 | 0.393 |
| 0.25 | 2.139 | 931 | 0.192 | 0.8 | 0.009 | 1206 | 0.441 |

* The data for intermediate concentration can be linearly or by spline interpolated.

** The data calculated by STANJAN and Cantera codes (Reynolds, 1986; Goodwin, 2001).

$$A = \frac{\Theta - \sin\Theta}{2} R^2 \qquad \text{for a circular cross-section of the tunnel,} \qquad (1.21)$$

where $R=D/2$; $\Theta$ is a vision angle for the segment of hydrogen layer of the height $h$:

$$\frac{\Theta}{2} = \arccos\left(\frac{R-h}{R}\right) \qquad \text{for a circular cross-section of the tunnel.} \qquad (1.22)$$

The average hydrogen concentration $X_{H2}$ in Eq. (1.19) and the layer thickness $h$ should be the input parameters. For a stratified hydrogen distribution, the average maximum hydrogen concentration at the top of the tunnel should be an input parameter. A linear gradient of hydrogen concentration from $X_{H2}$ (MAX, AVERAGE) to 0 within the layer thickness $h$ is assumed. Then, the gradient of concentration is calculated as follows

$$grad(X_{H_2}) = X_{H_2} / h. \qquad (1.23)$$

The volume of the cloud of hydrogen – air mixture will be two times larger compared to the uniform cloud with the same hydrogen concentration $X_{H2}$:

$$V = \frac{2}{X_{H2}} \frac{pM}{mRT}; \quad (1.24)$$

The height of the layer in a tunnel geometry with quite large TPRD device (about 5 mm ID) is recommended to be by default $h$ = 0.6 m supported by the natural gravity and density differences.

# A2. Problem formulation: accident in a road tunnel

## A2.1 Tunnel geometry

Table 9 Tunnel geometry

| Title | Value | Units |
|---|---|---|
| Tunnel shape | rectangular | - |
| Tunnel length | 1200 | m |
| Tunnel height | 5.5 | m |
| Tunnel width | 10.5 | m |
| Cross-section area | 57.75 | $m^2$ |
| Tunnel width | 10.5 | m |
| Crash position | 600 | m |

## A2.2 Accident characterization. Car's accident (I).

Table 10 Traffic characterization

| Title | Value | Units |
|---|---|---|
| Cars in queue lane 1 | 125 | - |
| Cars in queue lane 2 | 125 | - |
| Car density | 10000 | vehicles/day |
| car height | 1.7 | m |
| car width | 1.8 | m |
| Car cross-section area | 3.06 | $m^2$ |
| car length | 6 | m |
| parking distance | 2 | m |
| Distance between cars (front to front) | 8 | m |
| Blockage ratio BR (single lane) | 0.052987 | - |
| Blockage ratio BR (double lane) | 0.105974 | - |

Table 11 Hydrogen cloud characterization

| Title | Value | Units |
|---|---|---|
| Tank pressure | 700 | bar |
| Hydrogen inventory cars | 62.4 | Liter |
| Mass of hydrogen | 2.48 | kg |

| | | |
|---|---|---|
| Volume of hydrogen (STP conditions) | 30.0 | $m^3$ |

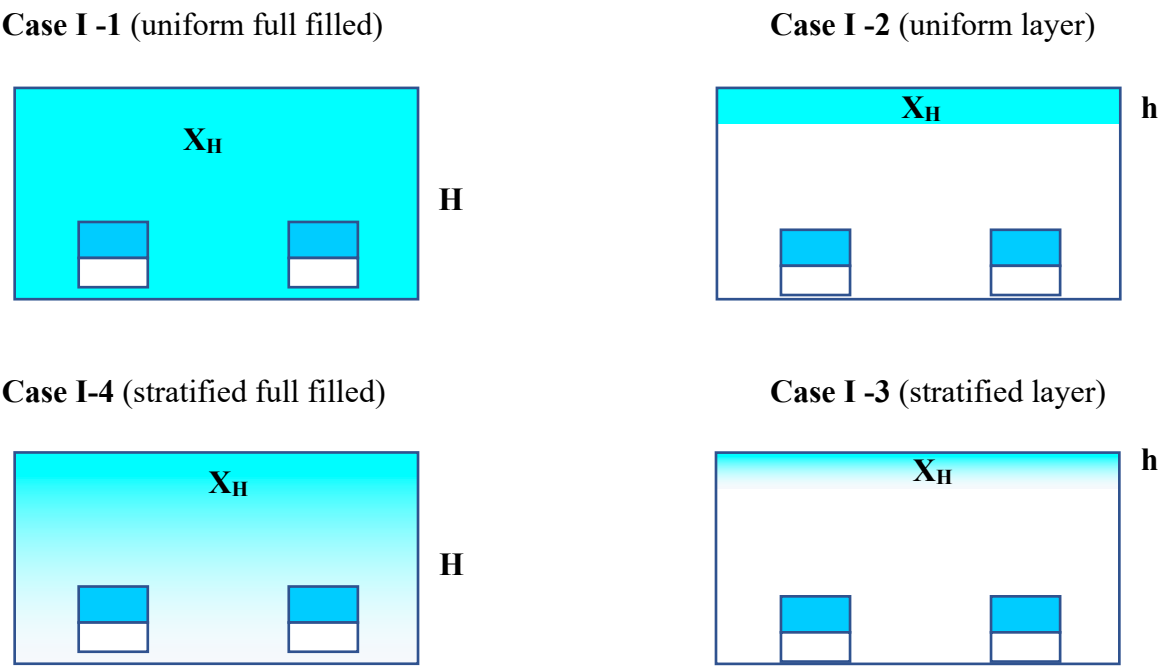


Figure 6. Hydrogen distribution profiles in a tunnel.

According to (Dutton and Coverdill, 1997) in adiabatic assumption, characteristic hydrogen release time can be calculated as follows:

$$t_{ch} = \frac{V}{A \cdot c}, \tag{1.25}$$

Where A is the orifice cross-section area; V=62.4 liter is the hydrogen tank volume; c = 1909 m/s is the speed of sound at chocking conditions. The total release time is four times greater than characteristic time:

$$t \simeq 4t_{ch}. \tag{1.26}$$

Table 12 shows the calculated according Eqs. (1.25-1.26) release time for car accident in a tunnel depending on TPRD orifice diameter from 1 to 5 mm.

Table 12 Calculated hydrogen release time for tank pressure 700 bar and V = 62.4L.

| **Orifice diameter, d, mm** | **1** | **2** | **3** | **5** |
|---|---|---|---|---|
| Characteristic release time, $t_{ch}$, s | 41.6 | 10.4 | 4.6 | 1.7 |
| Total release time, $t$, s | 166 | 42 | 18 | 6.7 |

The case of hydrogen pressurized at 700 bar and released through 5-mm TPRD device was numerically simulated using GASFLOW-MPI CFD code in a tunnel geometry (Li et al., 2019, 2021). A semiconfined layer of hydrogen-air mixture at the ceiling of the tunnel of about 1m thickness is formed in 4 seconds. Then, it develops along the ceiling at almost constant thickness of 1m with longitudinal velocity starting from 2 m/s and approaching the velocity of 0.3 m/s after 8s. I parallel, the average hydrogen concentration reduces inversely proportional to the time. In 16s, a layer of 25-m length will be formed in the tunnel with a maximum hydrogen concentration of 15-20%H2 at the ceiling (Li et al., 2019, 2021).

We consider four cases for hydrogen cloud distribution in a tunnel cross section:

**Case I-1**: Uniform hydrogen concentration distributed over the full tunnel cross-section for the given hydrogen inventory;

**Case I-2**: Uniform hydrogen concentration distributed inside a layer of hydrogen-air mixture for the given hydrogen inventory;

**Case I-3**: Stratified layer of hydrogen-air mixture for the given hydrogen inventory;

**Case I-4**: Stratified hydrogen-air mixture filled the whole tunnel cross-section for the given hydrogen inventory.

For 5 mm TPRD device and 700 bar tank pressure, the cases **I-1** and **I-4** are more typical for the short release time from 1 to 4 s after the TPRD opening (see Figure 7). The cases **I-2** and **I-3** are more typical for longer release time from 8 to 16 s and even more after the TPRD opening (see Figure 8). For 2 mm TPRD device and 700 bar tank pressure the characteristic time for all cases will be roughly 6 times higher. Only late ignition after hydrogen cloud formation is considered.

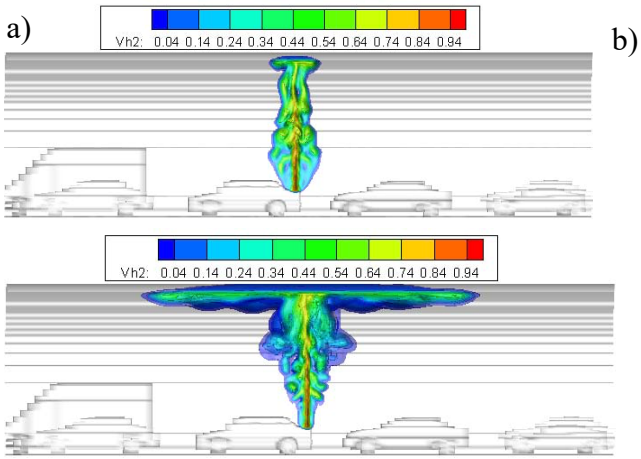


Figure 7. Hydrogen distribution profiles in a tunnel vs. time after release: a) 1 s; b) 4 s.

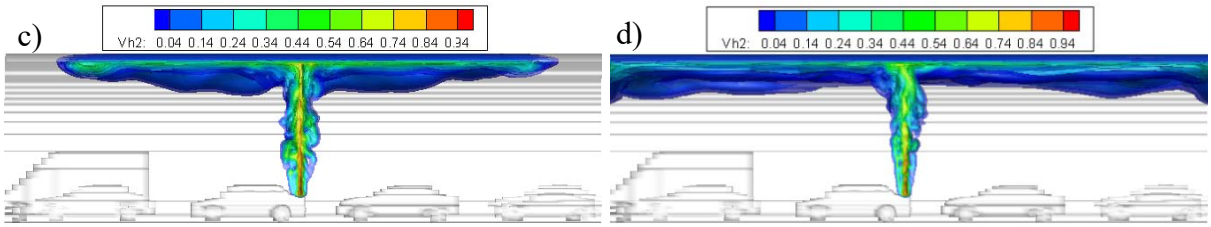


Figure 8. Hydrogen distribution profiles in a tunnel vs. time after release: c) 8s; d) 16 s.

## A2.3 Accident characterization. Buses accident (II).

Table 13 Traffic characterization

| Title | Value | Units |
|---|---|---|
| buses in queue lane 1 | 1 | - |
| buses in queue lane 2 | 1 | - |
| bus height | 3.1 | m |
| bus width | 2.5 | m |
| bus cross-section area | 7.75 | $m^2$ |
| bus length | 12 | m |
| parking distance | 2 | m |
| Distance between buses (front to front) | 14 | m |
| Blockage ratio BR (single lane) | 0.1342 | - |
| Blockage ratio BR (double lane) | 0.2684 | - |

Table 14 Hydrogen cloud characterization

| Title | Value | Units |
|---|---|---|
| Tank pressure | 350 | bar |
| Amount of tanks | 8 | tanks |
| Hydrogen inventory buses | 200 | Liter/tank |
| Mass of hydrogen | 41.64 | kg |
| Volume of hydrogen (STP conditions) | 503.5 | $m^3$ |
| vent size | 5 | mm |

Table 15 Calculated hydrogen release time for tank pressure 350 bar and V=200L. shows the calculated according Eqs. (1.25-1.26) release time for car accident in a tunnel depending on TPRD orifice diameter from 1 to 5 mm. The difference with previous Table 14 was only V=200 liter of the hydrogen tank volume and speed of sound was c = 1614 m/s.

Table 15 Calculated hydrogen release time for tank pressure 350 bar and V=200L.

| **Orifice diameter, d, mm** | **1** | **2** | **3** | **5** |
|---|---|---|---|---|
| Characteristic release time, $t_{ch}$, s | 157.8 | 39.4 | 17.5 | 6.3 |
| Total release time, $t$, s | 631 | 158 | 70 | 25 |

**Case II -1** (uniform full filled)

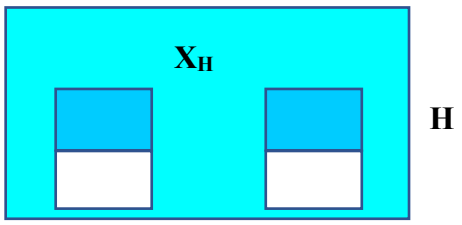


**Case II -2** (uniform layer)

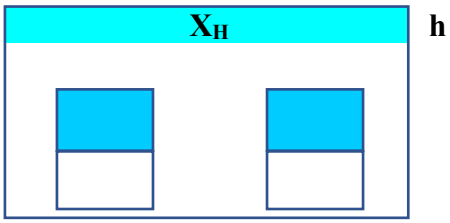


**Case II-4** (stratified full filled layer)

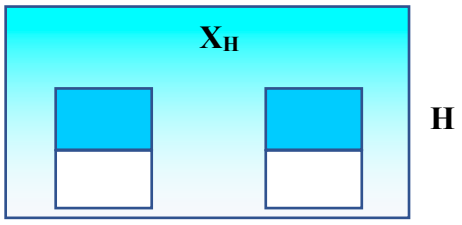


**Case II -3** (stratified layer)

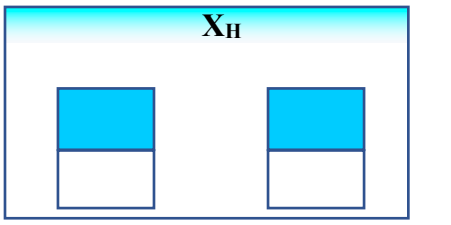


Figure 9. Hydrogen distribution profiles in a tunnel.

We consider four cases for hydrogen cloud distribution in a tunnel cross section:

**Case II-1**: Uniform hydrogen concentration distributed over the full tunnel cross-section for the given hydrogen inventory;

**Case II-2**: Uniform hydrogen concentration distributed inside a layer of hydrogen-air mixture for the given hydrogen inventory;

**Case II-3**: Stratified layer of hydrogen-air mixture for the given hydrogen inventory;

**Case II-4**: Stratified hydrogen-air mixture filled the whole tunnel cross-section for the given hydrogen inventory.

For 5 mm TPRD device and 350 bar tank pressure, the cases **II -1** and **II -4** are more typical for the release time from 6 to 15 s after the TPRD opening (similar to Figure 7). The cases **II 2** and **II -3** are more typical for the long release time more than half a minute after the TPRD opening (similar to Figure 8). Only late ignition after hydrogen cloud formation is considered.

## A2.4 Option 1: Uniform hydrogen concentration distributed over the full tunnel cross-section for the given hydrogen inventory

This option allows user calculating the possible flame propagation regimes of the uniform hydrogen-air cloud formed by the release of 2.48 and 41.64 kg of hydrogen in an assumption of the total tunnel cross-section filled with the cloud. Five levels of average hydrogen mole fraction in the cloud from 10 to 30% H2 are analyzed.

### A2.4.1.Input data

Table 16 Initial properties of the system

| Parameter name | Symbol | Value | | Range | Unit |
|---|---|---|---|---|---|
| Cloud uniformity and geometry | *U, N* | U1 (Figure 4) | | (U1, U2, N1, N2) | (-) |
| Hydrogen inventory* | $m_{H2}$ | 2.48 | 41.64 | 0.1-100 | kg |
| Volume of hydrogen* | $V_{H2}$ | 30 | 503.5 | 0.1-100 | $m^3$ |
| Mole fraction of hydrogen | $X_{H2}$ | 0.1 | | 8-75 | (-) |
| Mole fraction of hydrogen | $X_{H2}$ | 0.11 | | 8-75 | (-) |
| Mole fraction of hydrogen | $X_{H2}$ | 0.15 | | 8-75 | 8-75 |
| Mole fraction of hydrogen | $X_{H2}$ | 0.20 | | 8-75 | (-) |
| Mole fraction of hydrogen | $X_{H2}$ | 0.30 | | 8-75 | (-) |
| Ambient pressure | *p* | 1e5 | | (1-2)e5 | Pa |
| Ambient temperature | *T* | 293 | | 253-313 | K |
| Area of the tunnel cross-section | *A* | 57.75 | | 0.1-100 | $m^2$ |
| Height of the tunnel cross-section | *H* | 5.5 | | 1-15 | m |
| Width of the tunnel cross-section | *D* | 10.5 | | 1-15 | m |
| Equivalent diameter of tunnel cross-section | *D* | 8.575 | | 1-15 | m |
| Spacing between cars (front to front) | *S* | 8 | 14 | 0.1-100 | m |
| Blocked area for one lane occupied | $\Sigma Ai$ | 3.06 | 7.75 | 0.1-100 | $m^2$ |
| Blocked area for two lanes occupied | $\Sigma Ai$ | 6.12 | 15.5 | 0.1-100 | $m^2$ |

* The volume and mass of hydrogen in high pressure tanks calculated as for real gas density using NIST tables.

### A2.4.2.Calculation procedure

Steps 1,2,3…

| | | | |
|---|---|---|---|
| 1 | Hydrogen-air cloud geometry | Figure 4 | (-) |
| 2 | Expansion ratio, σ | Table 17 | (-) |
| 3 | Flame acceleration evaluation | $\sigma > \sigma^* = 3.75$ | Yes / No |
| 4 | Detonation cell size, λ | Table 17 | m |
| 5 | Pre-detonation length, L | $L = \frac{D+S}{2\left(1-\frac{d}{D}\right)}$ or $L = \frac{D}{1-\sqrt{1-BR}}$ if $(S=D)$ | m |
| 6 | Blockage ratio | $BR = \Sigma A_i / A$ | (-) |
| 7 | Ratio d/D | $\frac{d}{D} = \sqrt{1-BR}$ | (-) |
| 8 | Detonation evaluation | $L > 7\lambda$ | Yes/No |
| 9 | DDT run-up-distance, $X_S$ | $X_S = \frac{a_p D \cdot (1-BR)}{(1+1.5 \cdot BR) \cdot 10 S_L (\sigma - 1)}$ | m |
| 10 | $a_p$, $S_L$ evaluation | Table 18 | m/s |
| 11 | Length of hydrogen cloud | $L = V / A$ | m |
| 12 | Volume of hydrogen cloud | $V = \frac{V_{H2}}{X_{H2}}$ | $m^3$ |
| 14 | Primary detonability evaluation | $X_S < L$ | Yes/No |
| 15 | Precise DDT run-up-distance, $X_S$ | $X_S = \frac{\gamma}{C}\left[\frac{1}{\kappa}\ln\left(\gamma\frac{D}{h}\right)+K\right]$ | m |
| 16 | $a_p$, $S_L$ evaluation | Table 18 | m/s |
| 17 | γ evaluation | $\gamma = \left[\frac{a_p}{\eta S_L (\sigma-1)^2}\left(\frac{\delta}{D}\right)^{1/3}\right]^{\frac{1}{2m+7/3}}$ | (-) |
| 18 | D/h evaluation | $\frac{D}{h} = \frac{2}{1-\sqrt{1-BR}}$ | (-) |
| 19 | Kinematic viscosity, ν | Table 18 | $cm^2/s$ |
| 20 | Laminar flame thickness | $\delta = \frac{\nu}{S_L}$ | mm |

| | | | |
|---|---|---|---|
| 21 | Final detonability evaluation | $X_S < L$ | Yes/No |

Eqs. (15)-(20) allow more precise calculations of run-up distance to detonation.

**Algorithm of solution:**

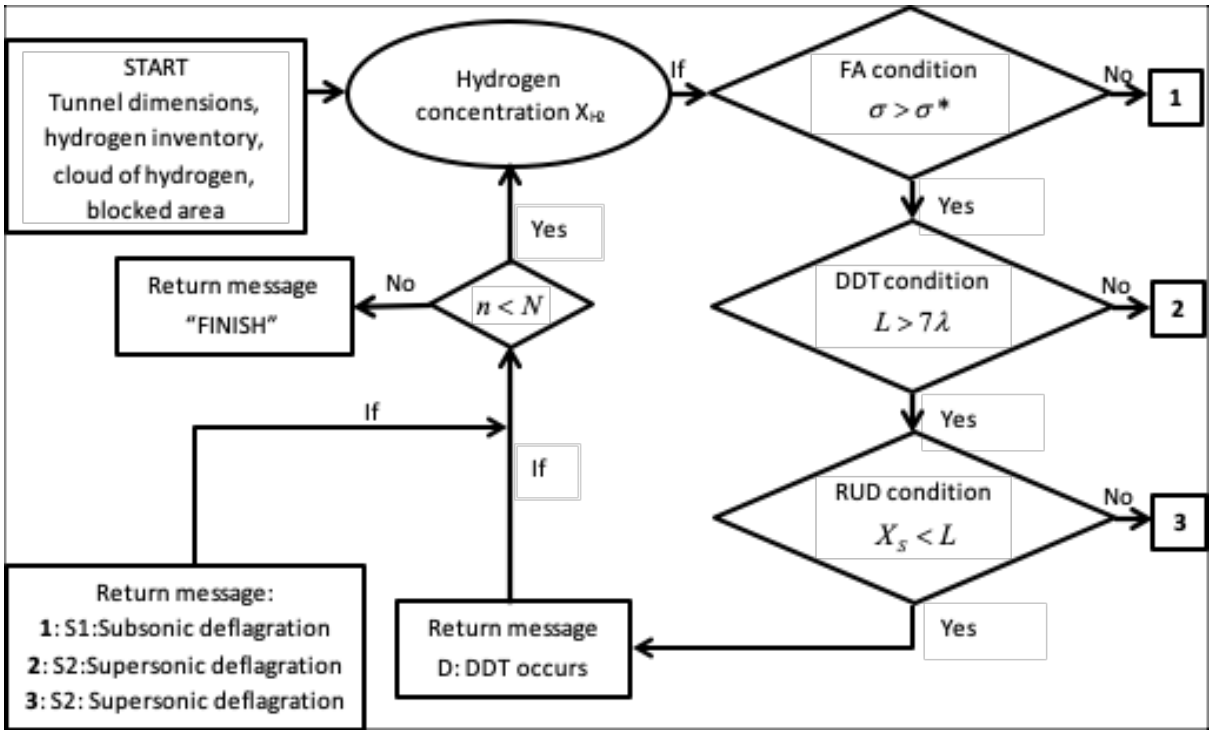


Table 17 Main properties of hydrogen-air combustible mixtures

| H2 mole fraction* $X_{H2}$ | Expansion ratio** σ | Detonation cell size*** λ, $10^{-3}$ m | H2 mole fraction $X_{H2}$ | Expansion ratio σ | Detonation cell size λ, $10^{-3}$ m |
|---|---|---|---|---|---|
| 0.09 | 3.31 | 18040 | 0.296 | 7.00 | 9.8 |
| 0.1 | 3.54 | 5095 | 0.3 | 7.02 | 9.7 |
| 0.11 | 3.77 | 2319 | 0.35 | 6.90 | 9.7 |
| 0.12 | 3.99 | 1289 | 0.4 | 6.60 | 11.9 |
| 0.13 | 4.21 | 798 | 0.45 | 6.27 | 16.8 |
| 0.14 | 4.42 | 531 | 0.5 | 5.91 | 27.3 |
| 0.15 | 4.63 | 361 | 0.55 | 5.53 | 57.4 |
| 0.16 | 4.83 | 252 | 0.6 | 5.12 | 148 |
| 0.18 | 5.23 | 114 | 0.65 | 4.69 | 362 |
| 0.2 | 5.60 | 44.6 | 0.7 | 4.24 | 930 |
| 0.22 | 5.96 | 24.6 | 0.75 | 3.76 | 2957 |
| 0.25 | 6.45 | 14.5 | 0.8 | 3.25 | 21230 |

* The data for intermediate concentration can be linearly or by spline interpolated.

** Expansion ratios calculated by STANJAN and Cantera codes (Reynolds, 1986; Goodwin, 2001).

*** Detonation cell sizes calculated with CELL_H2 program based on Gavrikov et al. (2000) paper.

Table 18 Laminar flame speed and speed of sound for combustion products

| H2 mole fraction* $X_{H2}$ | Laminar velocity ** SL, m/s | Speed of sound** $a_p$, m/s | Kin. viscosity** v, $cm^2/s$ | H2 mole fraction $X_{H2}$ | Laminar velocity SL, m/s | Speed of sound $a_p$, m/s | Kin. viscosity v, $cm^2/s$ |
|---|---|---|---|---|---|---|---|
| 0.09 | 0.171 | 636 | 0.165 | 0.296 | 2.677 | 980 | 0.202 |
| 0.1 | 0.246 | 659 | 0.167 | 0.3 | 2.719 | 983 | 0.203 |
| 0.11 | 0.334 | 682 | 0.168 | 0.35 | 3.131 | 1024 | 0.214 |
| 0.12 | 0.432 | 703 | 0.170 | 0.4 | 3.333 | 1047 | 0.227 |
| 0.13 | 0.541 | 724 | 0.171 | 0.45 | 3.313 | 1068 | 0.242 |
| 0.14 | 0.657 | 745 | 0.173 | 0.5 | 3.082 | 1087 | 0.258 |
| 0.15 | 0.781 | 765 | 0.175 | 0.55 | 2.672 | 1106 | 0.277 |
| 0.16 | 0.910 | 784 | 0.176 | 0.6 | 2.129 | 1125 | 0.299 |
| 0.18 | 1.180 | 821 | 0.180 | 0.65 | 1.516 | 1145 | 0.325 |
| 0.2 | 1.458 | 855 | 0.183 | 0.7 | 0.905 | 1165 | 0.356 |
| 0.22 | 1.737 | 888 | 0.187 | 0.75 | 0.375 | 1186 | 0.393 |
| 0.25 | 2.139 | 931 | 0.192 | 0.8 | 0.009 | 1206 | 0.441 |

* The data for intermediate concentration can be linearly or by spline interpolated.

** The data calculated by STANJAN and Cantera codes (Reynolds, 1986; Goodwin, 2001).

### A2.4.3.Output values

Table 19 Output data for car accident with hydrogen inventory, m = 2.48 kg

| **Hydrogen inventory, m = 2.48 kg** | | | | | | | |
|---|---|---|---|---|---|---|---|
| **Parameter name** | **Symbol** | **Unit** | **Output values** | | | | |
| | | | **Hydrogen mole fraction, $X_{H2}$** | | | | |
| | | | **0.1** | **0.11** | **0.15** | **0.2** | **0.3** |
| Expansion ratio, σ | σ | (-) | **3.54** | **3.77** | **4.63** | **5.6** | **7.02** |
| Detonation cell size, λ | λ | mm | 5095 | 2320 | 361 | 44.6 | 9.7 |
| Blockage ratio, BR | BR | (-) | 0.106 | 0.106 | 0.106 | 0.106 | 0.106 |
| Pre-detonation length, L | L | m | 152 | 152 | 152 | 152 | 152 |
| DDT length | 7λ | m | 35.7 | 16.2 | 2.53 | 0.31 | 0.07 |
| Volume of hydrogen cloud | V | $m^3$ | 300 | 272 | 200 | 150 | 100 |
| Length of hydrogen cloud | L | m | **5.2** | **4.7** | **3.5** | **2.6** | **1.7** |
| Sound speed in products | $a_p$ | m/s | 659 | 682 | 765 | 855 | 983 |
| Laminar velocity | $S_L$ | m/s | 0.25 | 0.33 | 0.78 | 1.46 | 2.7 |
| Run-up-distance (RUD) | Xs | m | **686** | **494** | **179** | **84** | **40** |

| Result | | | S1 | S1 | S1 | S1 | S1 |
|---|---|---|---|---|---|---|---|
| Laminar flame thickness, δ | δ | mm | 0.1342 | 0.1023 | 0.0425 | 0.0203 | 0.0092 |
| γ - parameter | γ | (-) | 2.245 | 1.715 | 0.775 | 0.414 | 0.218 |
| D/h - parameter | D/h | (-) | 36.7 | 36.7 | 36.7 | 36.7 | 36.7 |
| Run-up-distance (RUD) | Xs | m | **1591** | **1166** | **461** | **218** | **100** |
| **Result** | | | **S1** | **S1** | **S1** | **S1** | **S1** |

**Note:** S1– subsonic deflagration ($\sigma < \sigma^* = 3.75$); S1 - subsonic deflagration ($\sigma > \sigma^*$, $X_S > L$); S2 - sonic deflagration ($\sigma > \sigma^*$, $X_S < L$, $7\lambda > L$); D - ($\sigma > \sigma^*$, $X_S < L$, $7\lambda < L$).

Table 20 Output data for bus accident with hydrogen inventory, m = 41.64 kg

| **Hydrogen inventory, m = 41.64 kg** | | | | | | | |
|---|---|---|---|---|---|---|---|
| **Parameter name** | **Symbol** | **Unit** | **Output values** | | | | |
| | | | **Hydrogen mole fraction, $X_{H2}$** | | | | |
| | | | **0.1** | **0.11** | **0.15** | **0.2** | **0.3** |
| Expansion ratio, σ | σ | (-) | **3.54** | **3.77** | **4.63** | **5.6** | **7.02** |
| Detonation cell size, λ | λ | mm | 5095 | 2320 | 361 | 44.6 | 9.7 |
| Blockage ratio, BR | BR | (-) | 0.268 | 0.268 | 0.268 | 0.268 | 0.268 |
| Pre-detonation length, L | L | m | 78 | 78 | 78 | 78 | 78 |
| DDT length | 7λ | m | 35.7 | 16.2 | 2.53 | 0.31 | 0.07 |
| Volume of hydrogen cloud | V | $m^3$ | 5035 | 4578 | 3357 | 2518 | 1678 |
| Length of hydrogen cloud | L | m | **87.2** | **79.3** | **58.1** | **43.6** | **29.1** |
| Sound speed in products | $a_p$ | m/s | 659 | 682 | 765 | 855 | 983 |
| Laminar velocity | $S_L$ | m/s | 0.25 | 0.33 | 0.78 | 1.46 | 2.7 |
| Run-up-distance (RUD) | Xs | m | **464** | **334** | **121** | **57** | **27** |
| **Result** | | | **S1** | **S1** | **S1** | **S1** | **S2, D** |
| Laminar flame thickness, δ | δ | mm | 0.1342 | 0.1023 | 0.0425 | 0.0203 | 0.0092 |
| γ - parameter | γ | (-) | 2.245 | 1.715 | 0.775 | 0.414 | 0.218 |
| D/h - parameter | D/h | (-) | 13.8 | 13.8 | 13.8 | 13.8 | 13.8 |
| Run-up-distance (RUD) | Xs | m | **1356** | **986** | **379** | **175** | **77** |
| **Result** | | | **S1** | **S1** | **S1** | **S1** | **S1** |

**Note:** S1–subsonic deflagration ($\sigma < \sigma^* = 3.75$); S1-subsonic deflagration ($\sigma > \sigma^*$, $X_S > L$); S2 - sonic deflagration ($\sigma > \sigma^*$, $X_S < L$, $7\lambda > L$); D - ($\sigma > \sigma^*$, $X_S < L$, $7\lambda < L$).

### A2.4.4.Comments

The case **I-1** for car accident (5 mm TPRD device and 700 bar tank pressure) is typical for the short release time from 1 to 4 s after the TPRD opening (see Figure 7). The cloud of hydrogen-air mixture is enriched with hydrogen but it is too short (from 1.7 m to 5.2 m) to be enough for flame acceleration to the speed of sound and detonation onset ($X_S > L$). Actually, this case is not realistic and should be more addressed to the case **I-4**. For 2 mm TPRD device and 700 bar tank pressure the characteristic release time will be roughly 6 times higher with higher probability of cases **I-3** and **I-4**.

The case **II -1** for bus accident (5 mm TPRD device and 350 bar tank pressure) is also typical for short release time from 6 to 15 s after the TPRD opening (similar to Figure 7). The cloud of hydrogen-air mixture is enriched with hydrogen but it is still too short (from 29 m to 87 m) to be enough for flame acceleration to the speed of sound and detonation onset ( $X_S > L$).

This case is also not realistic and should be more addressed to the case **II -4**.

## A2.5 Option 2: Uniform hydrogen concentration distributed inside a layer of hydrogen-air mixture for the given hydrogen inventory

This option allows user calculating the possible flame propagation regimes of uniform cloud formed as a layer of hydrogen-air mixture by the release of 2.48 and 41.64 kg of hydrogen corresponding to car and bus accident. Five levels of average hydrogen mole fraction in the cloud from 10 to 30% H2 are analyzed.

### A2.5.1.Input data

Table 21 Initial properties of the system

| Parameter name | Symbol | Value | | Unit |
|---|---|---|---|---|
| Cloud uniformity and geometry | *U, N* | U2 (Figure 4) | | (-) |
| Hydrogen inventory* | $m_{H2}$ | 2.48 | 41.64 | kg |
| Hydrogen inventory* | $V_{H2}$ | 30 | 503.5 | $m^3$ |
| Mole fraction of hydrogen | $X_{H2}$ | 0.1 | | (-) |
| Mole fraction of hydrogen | $X_{H2}$ | 0.11 | | (-) |
| Mole fraction of hydrogen | $X_{H2}$ | 0.15 | | (-) |
| Mole fraction of hydrogen | $X_{H2}$ | 0.20 | | (-) |
| Mole fraction of hydrogen | $X_{H2}$ | 0.30 | | (-) |
| Ambient pressure | *p* | 1e5 | | Pa |
| Ambient temperature | *T* | 293 | | K |
| Area of layer cross-section | *A* | 10.50 | | $m^2$ |
| Height of the tunnel cross-section | *H* | 5.5 | | m |
| Width of the tunnel cross-section | *D* | 10.5 | | m |
| Equivalent diameter of tunnel cross-section | *D* | 8.575 | | m |
| Spacing | *S* | 0.11 | | m |
| Thickness of the layer | *h* | 1 | | m |
| Conventional blockage ratio** | *BR* | 0.05 | | (-) |

**Note:** * Calculated for real gas density using NIST data base.

** Since the vehicles in the tunnel do not block the flame propagation in a layer on top of the tunnel, a conventional blockage ratio of BR = 0.05. Corresponding to the natural roughness of the tunnel surface of about 10 cm is assumed.

### A2.5.2.Calculation procedure

| | | | |
|---|---|---|---|
| 1 | Expansion ratio, σ | Table 17 | (-) |

| | | | |
|---|---|---|---|
| 2 | Critical expansion ratio, σ* | $\sigma^* = \sigma_0 * (1 + K \cdot s/h)$ | (-) |
| 3 | Flame acceleration evaluation | $\sigma > \sigma^*$ | Yes / No |
| 4 | Detonation cell size, λ | Table 17 | mm |
| 5 | Critical layer thickness, h* | $h^* = 13.5\lambda$ | m |
| 6 | Blockage ratio | $BR = 0.05$ | (-) |
| 6 | Spacing, s | $s = \frac{D}{2}\left(1 - \sqrt{1 - BR}\right)$ | (-) |
| 7 | Detonation evaluation | $h > h^* = 13.5\lambda$ | Yes/No |
| 8 | DDT run-up-distance, $X_S$ | $X_S = \frac{\gamma}{C}\left[\frac{1}{\kappa}\ln\left(\gamma\frac{D}{h}\right) + K\right]$ | m |
| 9 | $a_p$, $S_L$ evaluation | Table 18 | m/s |
| 10 | γ evaluation | $\gamma = \left[\frac{a_p}{\eta S_L (\sigma - 1)^2}\left(\frac{\delta}{D}\right)^{1/3}\right]^{\frac{1}{2m+7/3}}$ | (-) |
| 11 | D/h evaluation | $\frac{D}{h} = \frac{2}{1 - \sqrt{1 - BR}}$ | (-) |
| 12 | Kinematic viscosity, ν | Table 18 | $cm^2/s$ |
| 13 | Laminar flame thickness | $\delta = \frac{\nu}{S_L}$ | mm |
| 14 | Length of hydrogen cloud | $L = V / A$ | m |
| 15 | Volume of hydrogen cloud | $V = \frac{V_{H2}}{X_{H2}}$ | $m^3$ |
| 16 | Final detonability evaluation | $X_S < L$ | Yes/No |

### A2.5.3.Output values

Table 22 Output data for hydrogen inventory, m = 2.48 kg, and layer geometry, h = 1 m

| **Hydrogen inventory, m = 2.48 kg** | | | | | | | |
|---|---|---|---|---|---|---|---|
| **Parameter name** | **Symbol** | **Unit** | **Output values** | | | | |
| | | | **Hydrogen mole fraction, $X_{H2}$** | | | | |
| | | | **0.1** | **0.11** | **0.15** | **0.2** | **0.3** |
| Expansion ratio, σ | σ | (-) | 3.54 | 3.77 | 4.63 | 5.6 | 7.02 |
| Critical expansion ratio, σ | σ* | (-) | 3.82 | 3.82 | 3.82 | 3.82 | 3.82 |
| Detonation cell size, λ | λ | mm | 5095 | 2320 | 361 | 44.6 | 9.7 |
| Blockage ratio, BR | BR | (-) | 0.05 | 0.05 | 0.05 | 0.05 | 0.05 |
| Spacing, s | s | m | 0.11 | 0.11 | 0.11 | 0.11 | 0.11 |
| Critical layer thickness, h* | h* | m | **69** | **31** | **4.87** | **0.60** | **0.13** |
| Volume of hydrogen cloud | V | $m^3$ | 300 | 272 | 200 | 150 | 100 |
| Layer cross-section area | A | $m^2$ | 10.50 | 10.50 | 10.50 | 10.50 | 10.50 |
| Layer thickness | h | m | **1** | **1** | **1** | **1** | **1** |

| | | | | | | | |
|---|---|---|---|---|---|---|---|
| Length of hydrogen cloud | L | m | **29** | **26** | **19** | **14** | **10** |
| Sound speed in products | $a_p$ | m/s | 659 | 682 | 765 | 855 | 983 |
| Laminar velocity | $S_L$ | m/s | 0.25 | 0.33 | 0.78 | 1.46 | 2.7 |
| Laminar flame thickness, δ | δ | mm | 0.1342 | 0.1023 | 0.0425 | 0.0203 | 0.0092 |
| γ - parameter | γ | (-) | 2.245 | 1.715 | 0.775 | 0.414 | 0.218 |
| D/h - parameter | D/h | (-) | 79.0 | 79.0 | 79.0 | 79.0 | 79.0 |
| Run-up-distance (RUD) | Xs | m | **1775** | **1307** | **524** | **252** | **118** |
| **Result** | | | **S1** | **S1** | **S1** | **S1** | **S1** |

**Note:** S1 – subsonic deflagration ($\sigma < \sigma^* = 3.82$); S1 - subsonic deflagration ($\sigma > \sigma^*$, $X_S > L$); S2 - sonic deflagration ($\sigma > \sigma^*$, $X_S < L$, $h^* = 13.5\lambda > h$); D - ($\sigma > \sigma^*$, $X_S < L$, $h^* = 13.5\lambda < h$).

Table 23 Output data for hydrogen inventory, m = 41.64 kg, and layer geometry, h = 1 m

| **Hydrogen inventory, m = 41.64 kg** | | | | | | | |
|---|---|---|---|---|---|---|---|
| **Parameter name** | **Symbol** | **Unit** | **Output values** | | | | |
| | | | **Hydrogen mole fraction, $X_{H2}$** | | | | |
| | | | **0.1** | **0.11** | **0.15** | **0.2** | **0.3** |
| Expansion ratio, σ | σ | (-) | 3.54 | 3.77 | 4.63 | 5.6 | 7.02 |
| Critical expansion ratio, σ | σ* | (-) | 3.82 | 3.82 | 3.82 | 3.82 | 3.82 |
| Detonation cell size, λ | λ | mm | 5095 | 2320 | 361 | 44.6 | 9.7 |
| Blockage ratio, BR | BR | (-) | 0.05 | 0.05 | 0.05 | 0.05 | 0.05 |
| Spacing, s | s | m | 0.11 | 0.11 | 0.11 | 0.11 | 0.11 |
| Critical layer thickness, h* | h* | m | **69** | **31** | **4.87** | **0.60** | **0.13** |
| Volume of hydrogen cloud | V | $m^3$ | 5035 | 4578 | 3357 | 2518 | 1678 |
| Layer cross-section area | A | $m^2$ | 10.50 | 10.50 | 10.50 | 10.50 | 10.50 |
| Layer thickness | h | m | **1** | **1** | **1** | **1** | **1** |
| Length of hydrogen cloud | L | m | **480** | **436** | **320** | **240** | **160** |
| Sound speed in products | $a_p$ | m/s | 659 | 682 | 765 | 855 | 983 |
| Laminar velocity | $S_L$ | m/s | 0.25 | 0.33 | 0.78 | 1.46 | 2.7 |
| Laminar flame thickness, δ | δ | mm | 0.1342 | 0.1023 | 0.0425 | 0.0203 | 0.0092 |
| γ - parameter | γ | (-) | 2.245 | 1.715 | 0.775 | 0.414 | 0.218 |
| D/h - parameter | D/h | (-) | 79.0 | 79.0 | 79.0 | 79.0 | 79.0 |
| Run-up-distance (RUD) | Xs | m | **1775** | **1307** | **524** | **252** | **118** |
| **Result** | | | **S1** | **S1** | **S1** | **S1** | **D** |

**Note:** S1 – subsonic deflagration ($\sigma < \sigma^* = 3.82$); S1 - subsonic deflagration ($\sigma > \sigma^*$, $X_S > L$);

S2 - sonic deflagration ($\sigma > \sigma^*$, $X_S < L$, $h^* = 13.5\lambda > h$); D - ($\sigma > \sigma^*$, $X_S < L$, $h^* = 13.5\lambda < h$).

### A2.5.4.Comments

The case **I-2** for car accident (5 mm TPRD device and 700 bar tank pressure) is more typical for the longer release time from 8 to 16 s and even more after the TPRD opening (see Figure

8). The cloud of hydrogen-air mixture is elongated from 10 m to 29 m but still remains too short for flame acceleration to the speed of sound and detonation onset ( $X_S > L$ ). The run-up distance Xs in this case is much longer because the cars do not block the cloud cross-section. The only natural roughness of tunnel surface (about 1 cm) plays a role for flame acceleration. Because of longer release time and high probability of stratification, more realistic case will be the case **I-3.** For 2 mm TPRD device the probability of the case **I-3** will be much higher.

The case **II-2** for bus accident (5 mm TPRD device and 350 bar tank pressure) will be able for release time longer than 15 s after the TPRD opening (similar to Figure 8). The cloud of hydrogen-air mixture is elongated from 160 m to 480 m depending on average concentration. Such length will be enough for flame acceleration to the speed of sound and detonation onset ( $X_S < L$ ) only if the stoichiometric hydrogen-air mixture in the layer is assumed. For leaner hydrogen concentrations the cloud of hydrogen-air mixture will be too short (from 240 m to 480 m) for flame acceleration to the speed of sound and detonation onset ( $X_S > L$ ) because of very long run-up distance to detonation (Xs=250-1775 m) in relatively smooth tunnel ceiling of 1 cm roughness. More realistic is the case **II-3**.

## A2.6 Option 3: Stratified layer of hydrogen-air mixture for the given hydrogen inventory

This option allows user calculating the possible flame propagation regimes of the stratified layer of hydrogen-air mixture by the release of 2.48 and 41.64 kg of hydrogen corresponding to car and bus accidents. Five levels of maximum hydrogen mole fraction at the top of the cloud from 10 to 30% H2 are analyzed.

### A2.6.1.Input values

Table 24 Initial properties of the system

| Parameter name | Symbol | Value | | Unit |
|---|---|---|---|---|
| Cloud uniformity and geometry | $U$, $N$ | N2 (Figure 4) | | (-) |
| Hydrogen inventory* | $m_{H2}$ | 2.48 | 41.64 | kg |
| Hydrogen inventory* | $V_{H2}$ | 30 | 503.5 | $m^3$ |
| Mole fraction of hydrogen* | $X_{H2}$ | 0.1 | | (-) |
| Mole fraction of hydrogen* | $X_{H2}$ | 0.11 | | (-) |
| Mole fraction of hydrogen* | $X_{H2}$ | 0.15 | | (-) |
| Mole fraction of hydrogen* | $X_{H2}$ | 0.20 | | (-) |
| Mole fraction of hydrogen* | $X_{H2}$ | 0.30 | | (-) |
| Ambient pressure | $p$ | 1e5 | | Pa |
| Ambient temperature | $T$ | 293 | | K |
| Area of layer cross-section | $A$ | 10.50 | | $m^2$ |
| Height of the tunnel cross-section | $H$ | 5.5 | | m |
| Width of the tunnel cross-section | $D$ | 10.5 | | m |
| Equivalent diameter of tunnel cross-section | $D$ | 8.575 | | m |
| Spacing | $S$ | 0.11 | | m |
| Thickness of the layer | $h$ | 1 | | m |

| | | | |
|---|---|---|---|
| Conventional blockage ratio** | *BR* | 0.05 | (-) |

**Note:** * Calculated for real gas density using NIST data base.

** Since the vehicles in the tunnel do not block the flame propagation in a layer on top of the tunnel, a conventional blockage ratio of BR = 0.05. Corresponding to the natural roughness of the tunnel surface of about 10 cm is assumed.

### A2.6.2.Calculation procedure

| | | | |
|---|---|---|---|
| 1 | Expansion ratio, σ | Table 17 | (-) |
| 2 | Gradient of concentration, grad($X_{H2}$)* | $grad(X_{H_2}) = X_{H_2} / h$ | (-) |
| 3 | Efficient layer thickness, $h$* | $h^* = X_{H_2} / grad(X_{H_2})^*$ | (-) |
| 4 | Critical expansion ratio, σ* | $\sigma^* = \sigma_0{}^* \left(1 + K \cdot s/h\right)$ | (-) |
| 5 | Flame acceleration evaluation | $\sigma > \sigma^*$ | Yes / No |
| 6 | Detonation cell size, λ | Table 17 | mm |
| 7 | Blockage ratio | $BR = 0.05$ | (-) |
| 8 | Critical layer thickness, h** | $h^* = 13.5\lambda$ | m |
| 9 | Detonation evaluation | $h > h^* = 13.5\lambda$ | Yes/No |
| 10 | DDT run-up-distance, $X_S$ | $X_S = \frac{\gamma}{C}\left[\frac{1}{\kappa}\ln\left(\gamma\frac{D}{h}\right) + K\right]$ | m |
| 11 | $a_p$, $S_L$ evaluation | Table 18 | m/s |
| 12 | γ evaluation | $\gamma = \left[\frac{a_p}{\eta S_L (\sigma - 1)^2}\left(\frac{\delta}{D}\right)^{1/3}\right]^{\frac{1}{2m+7/3}}$ | (-) |
| 13 | D/h evaluation | $\frac{D}{h} = \frac{2}{1-\sqrt{1-BR}}$ | (-) |
| 14 | Kinematic viscosity, ν | Table 18 | $cm^2/s$ |
| 15 | Laminar flame thickness | $\delta = \frac{\nu}{S_L}$ | mm |
| 16 | Length of hydrogen cloud | $L = V / A$ | m |
| 17 | Volume of hydrogen cloud* | $V = \frac{2V_{H2}}{X_{H2}}$ | $m^3$ |
| 18 | Final detonability evaluation | $X_S < L$ | Yes/No |

**Note:** * A linear gradient of concentration from maximum to zero is assumed.

### A2.6.3.Output values

Table 25 Output data for hydrogen inventory, m = 2.48 kg, and stratified layer geometry, h = 1 m

| Hydrogen inventory, m = 2.48 kg | | | | | | | |
|---|---|---|---|---|---|---|---|
| **Parameter name** | **Symbol** | **Unit** | **Output values** | | | | |
| | | | **Hydrogen mole fraction, $X_{H2}$** | | | | |
| | | | **0.1** | **0.11** | **0.15** | **0.2** | **0.3** |
| Expansion ratio, σ | σ | (-) | 3.54 | 3.77 | 4.63 | 5.6 | 7.02 |
| Gradient of concentration | grad($X_{H2}$) | %H2/m | 10.0 | 11.0 | 15.0 | 20.0 | 30.0 |
| Critical expansion ratio, σ | σ* | (-) | 3.82 | 3.82 | 3.82 | 3.82 | 3.82 |
| Detonation cell size, λ | λ | mm | 5095 | 2320 | 361 | 44.6 | 9.7 |
| Blockage ratio, BR | BR | (-) | 0.05 | 0.05 | 0.05 | 0.05 | 0.05 |
| Spacing, s | s | m | 0.11 | 0.11 | 0.11 | 0.11 | 0.11 |
| Critical layer thickness, h* | h* | m | **69** | **31** | **4.87** | **0.60** | **0.13** |
| Volume of hydrogen cloud | V | $m^3$ | 599 | 545 | 399 | 300 | 200 |
| Layer cross-section area | A | $m^2$ | 10.50 | 10.50 | 10.50 | 10.50 | 10.50 |
| Layer thickness | h | m | **1** | **1** | **1** | **1** | **1** |
| Length of hydrogen cloud | L | m | **57** | **52** | **38** | **29** | **19** |
| Sound speed in products | $a_p$ | m/s | 659 | 682 | 765 | 855 | 983 |
| Laminar velocity | $S_L$ | m/s | 0.25 | 0.33 | 0.78 | 1.46 | 2.7 |
| Laminar flame thickness, δ | δ | mm | 0.1342 | 0.1023 | 0.0425 | 0.0203 | 0.0092 |
| γ - parameter | γ | (-) | 2.230 | 1.724 | 0.775 | 0.414 | 0.217 |
| D/h - parameter | D/h | (-) | 79.0 | 79.0 | 79.0 | 79.0 | 79.0 |
| Run-up-distance (RUD) | Xs | m | **1762** | **1315** | **524** | **252** | **117** |
| **Result** | | | **S1** | **S1** | **S1** | **S1** | **S1** |

**Note:** S1 – subsonic deflagration ($\sigma < \sigma^* = 3.82$); S1 - subsonic deflagration ($\sigma > \sigma^*$, $X_S > L$); S2 - sonic deflagration ($\sigma > \sigma^*$, $X_S < L$, $h^* = 13.5\lambda > h$); D - ($\sigma > \sigma^*$, $X_S < L$, $h^* = 13.5\lambda < h$).

Table 26 Output data for hydrogen inventory, m = 41.64 kg, and stratified layer geometry, h = 1 m

| Hydrogen inventory, m = 41.64 kg | | | | | | | |
|---|---|---|---|---|---|---|---|
| **Parameter name** | **Symbol** | **Unit** | **Output values** | | | | |
| | | | **Hydrogen mole fraction, $X_{H2}$** | | | | |
| | | | **0.1** | **0.11** | **0.15** | **0.2** | **0.3** |
| Expansion ratio, σ | σ | (-) | 3.54 | 3.77 | 4.63 | 5.6 | 7.02 |
| Gradient of concentration | grad(XH2) | %H2/m | 10.0 | 11.0 | 15.0 | 20.0 | 30.0 |
| Critical expansion ratio, σ | σ* | (-) | 3.82 | 3.82 | 3.82 | 3.82 | 3.82 |
| Detonation cell size, λ | λ | mm | 5095 | 2320 | 361 | 44.6 | 9.7 |
| Blockage ratio, BR | BR | (-) | 0.05 | 0.05 | 0.05 | 0.05 | 0.05 |
| Spacing, s | s | m | 0.11 | 0.11 | 0.11 | 0.11 | 0.11 |
| Critical layer thickness, h* | h* | m | **69** | **31** | **4.87** | **0.60** | **0.13** |

| | | | | | | | |
|---|---|---|---|---|---|---|---|
| Volume of hydrogen cloud | V | $m^3$ | 10071 | 9155 | 6714 | 5035 | 3357 |
| Layer cross-section area | A | $m^2$ | 10.50 | 10.50 | 10.50 | 10.50 | 10.50 |
| Layer thickness | h | m | **1** | **1** | **1** | **1** | **1** |
| Length of hydrogen cloud | L | m | **959** | **872** | **639** | **480** | **320** |
| Sound speed in products | $a_p$ | m/s | 659 | 682 | 765 | 855 | 983 |
| Laminar velocity | $S_L$ | m/s | 0.25 | 0.33 | 0.78 | 1.46 | 2.7 |
| Laminar flame thickness, δ | δ | mm | 0.1342 | 0.1023 | 0.0425 | 0.0203 | 0.0092 |
| γ - parameter | γ | (-) | 2.230 | 1.724 | 0.775 | 0.414 | 0.217 |
| D/h - parameter | D/h | (-) | 79.0 | 79.0 | 79.0 | 79.0 | 79.0 |
| Run-up-distance (RUD) | Xs | m | **1762** | **1315** | **524** | **252** | **117** |
| **Result** | | | **S1** | **S1** | **S2** | **S2, D** | **D** |

**Note:** S1 – subsonic deflagration ($\sigma < \sigma^* = 3.82$); S1 - subsonic deflagration ($\sigma > \sigma^*$, $X_S > L$); S2 - sonic deflagration ($\sigma > \sigma^*$, $X_S < L$, $h^* = 13.5\lambda > h$); D - ($\sigma > \sigma^*$, $X_S < L$, $h^* = 13.5\lambda < h$).

### A2.6.4.Comments

The case **I-3** for car accident (5 mm TPRD device and 700 bar tank pressure) is the most typical for the longer release time from 8 to 16 s and even more after the TPRD opening (see Figure 8). The cloud of hydrogen-air mixture is elongated from 19 m to 57 m but still remains too short for flame acceleration to the speed of sound and detonation onset ($X_S > L$). Only subsonic deflagration may occur. The run-up distance Xs in this case is much longer (from 117 to 1775 m) because the cars do not block the cloud cross-section. The only natural roughness of the tunnel surface (about 1 cm) plays a role for flame acceleration. For 2 mm TPRD device the case **I-3** will be the most probable scenario.

The case **II-3** for bus accident (5 mm TPRD device and 350 bar tank pressure) will be able for release time longer than 40 s after the TPRD opening (similar to Figure 8). The cloud of hydrogen-air mixture is elongated from 320 m to 960 m depending on average concentration. Such length will be enough for flame acceleration to the speed of sound ($X_S < L$) for hydrogen-air mixtures with a maximum hydrogen concentration at the ceiling from 15 to 30%H2. For 15%H2, the flame accelerates to the speed of sound but the detonability criterion $h^* = 13.5\lambda < h$ is not satisfied. For leaner hydrogen concentrations the run-up distance will be even longer (Xs=1315-1760m) than the cloud of hydrogen-air mixture (from 870 m to 960 m) ($X_S > L$) because of very long run-up distance to detonation in relatively smooth tunnel ceiling of 1 cm roughness. Then, only slow flame propagates with subsonic velocity. The case **II-3** is the most realistic scenario for bus accident at the latest stage, after a minute of release time.

## A2.7 Option 4: Stratified hydrogen-air mixture filled the whole tunnel cross-section for the given hydrogen inventory

This option allows user calculating the possible flame propagation regimes of the stratified hydrogen-air mixture filled the total tunnel cross-section by the release of 2.48 and 41.64 kg of

hydrogen corresponding to car and bus accidents. Five levels of maximum hydrogen mole fraction at the top of the cloud from 10 to 30% H2 are analyzed.

### A2.7.1. Input values

Table 27 Initial properties of the system

| Parameter name | Symbol | Value | | Unit |
|---|---|---|---|---|
| Cloud uniformity and geometry | $U$, $N$ | N1 (Figure 4) | | (-) |
| Hydrogen inventory | $m_{H2}$ | 2.48 | 41.64 | kg |
| Hydrogen inventory | $V_{H2}$ | 30 | 503.5 | $m^3$ |
| Mole fraction of hydrogen at the top | $X_{H2}$ | 0.1 | | (-) |
| Mole fraction of hydrogen at the top | $X_{H2}$ | 0.11 | | (-) |
| Mole fraction of hydrogen at the top | $X_{H2}$ | 0.15 | | (-) |
| Mole fraction of hydrogen at the top | $X_{H2}$ | 0.20 | | (-) |
| Mole fraction of hydrogen at the top | $X_{H2}$ | 0.30 | | (-) |
| Ambient pressure | $p$ | 1e5 | | Pa |
| Ambient temperature | $T$ | 293 | | K |
| Area of the tunnel cross-section | $A$ | 57.75 | | $m^2$ |
| Height of the tunnel cross-section | $H$ | 5.5 | | m |
| Width of the tunnel cross-section | $D$ | 10.5 | | m |
| Equivalent diameter of tunnel cross-section | $D$ | 8.575 | | m |
| Spacing between cars (front to front) | $S$ | 8 | 14 | m |
| Thickness of the layer | $h$ | 5.5 | | m |
| Blockage ratio* | $BR$ | 0.106 | 0.268 | (-) |

**Note:** * The stratified mixture covers total tunnel cross-section. Then, the tunnel will be blocked by cars and trucks.

### A2.7.2.Calculation procedure

| | | | |
|---|---|---|---|
| 1 | Expansion ratio, σ | Table 17 | (-) |
| 2 | Gradient of concentration, grad($X_{H2}$) | $grad(X_{H_2}) = X_{H_2} / h$ | (-) |
| 3 | Layer thickness, $h$ | $h = H$ | (-) |
| 4 | Spacing between cars, $s$ | Table 27 | (-) |
| 5 | Critical expansion ratio, σ* | $\sigma^* = \sigma_0 * (1 + K \cdot s/h)$ | (-) |
| 6 | Flame acceleration evaluation | $\sigma > \sigma^*$ | Yes / No |

| | | | |
|---|---|---|---|
| 7 | Detonation cell size, λ | Table 17 | mm |
| 8 | Critical layer thickness, h* | $h^* = 13.5\lambda$ | m |
| 9 | Detonation evaluation 1** | $H > h^* = 13.5\lambda$ | Yes/No |
| 10 | Pre-detonation length, L | $L = \frac{D+S}{2\left(1-\frac{d}{D}\right)}$ | m |
| 11 | Blockage ratio | Table 27 | (-) |
| 12 | Ratio d/D | $\frac{d}{D} = \sqrt{1-BR}$ | (-) |
| 13 | Detonation evaluation 2* | $L > 7\lambda$ | Yes/No |
| 14 | DDT run-up-distance, $X_S$ | $X_S = \frac{a_p D \cdot (1-BR)}{(1+1.5 \cdot BR) \cdot 10 S_L (\sigma - 1)}$ | m |
| 15 | $a_p$, $S_L$ evaluation | Table 18 | m/s |
| 16 | Length of hydrogen cloud | $L = V / A$ | m |
| 17 | Volume of hydrogen cloud | $V = \frac{2V_{H2}}{X_{H2}}$ | $m^3$ |
| 18 | Primary detonability evaluation | $X_S < L$ | Yes/No |
| 19 | Precise DDT run-up-distance, $X_S$ | $X_S = \frac{\gamma}{C}\left[\frac{1}{\kappa}\ln\left(\gamma\frac{D}{h}\right)+K\right]$ | m |
| 20 | $a_p$, $S_L$ evaluation | Table 18 | m/s |
| 21 | γ evaluation | $\gamma = \left[\frac{a_p}{\eta S_L (\sigma-1)^2}\left(\frac{\delta}{D}\right)^{1/3}\right]^{\frac{1}{2m+7/3}}$ | (-) |
| 22 | D/h evaluation | $\frac{D}{h} = \frac{2}{1-\sqrt{1-BR}}$ | (-) |
| 23 | Kinematic viscosity, ν | Table 18 | $cm^2/s$ |
| 24 | Laminar flame thickness | $\delta = \frac{\nu}{S_L}$ | mm |
| 25 | Final detonability evaluation | $X_S < L$ | Yes/No |

**Note:** * If the gradient is an input parameter then $h = h^*$.

** The most dangerous DDT criterion should be chosen

### A2.7.3.Output values

Table 28 Output data for hydrogen inventory, m = 2.48 kg, and stratified hydrogen-air mixture

| **Hydrogen inventory, m = 2.48 kg** | | | | | | | |
|---|---|---|---|---|---|---|---|
| **Parameter name** | **Symbol** | **Unit** | **Output values** | | | | |
| | | | **Hydrogen mole fraction, $X_{H2}$** | | | | |
| | | | **0.1** | **0.11** | **0.15** | **0.2** | **0.3** |

| | | | | | | | |
|---|---|---|---|---|---|---|---|
| Expansion ratio, σ | σ | (-) | 3.54 | 3.77 | 4.63 | 5.6 | 7.02 |
| Gradient of concentration | grad($X_{H2}$) | %H2/m | 1.8 | 2.0 | 2.7 | 3.6 | 5.5 |
| Critical expansion ratio | σ* | (-) | 4.70 | 4.70 | 4.70 | 4.70 | 4.70 |
| Detonation cell size | λ | mm | 5095 | 2320 | 361 | 44.6 | 9.7 |
| Blockage ratio | BR | (-) | 0.106 | 0.106 | 0.106 | 0.106 | 0.106 |
| Pre-detonation length | L | m | 152 | 152 | 152 | 152 | 152 |
| Spacing | S | m | 8.00 | 8.00 | 8.00 | 8.00 | 8.00 |
| DDT length | 7λ | m | 35.7 | 16.2 | 2.53 | 0.31 | 0.07 |
| Critical layer thickness | h* | m | **68.8** | **31.3** | **4.87** | **0.60** | **0.13** |
| Volume of hydrogen cloud | V | $m^3$ | 599 | 545 | 399 | 300 | 200 |
| Cloud cross-section area | A | $m^2$ | 57.8 | 57.8 | 57.8 | 57.8 | 57.8 |
| Length of hydrogen cloud | L | m | **10.4** | **9.4** | **6.9** | **5.2** | **3.5** |
| Sound speed in products | $a_p$ | m/s | 659 | 682 | 765 | 855 | 983 |
| Laminar velocity | $S_L$ | m/s | 0.25 | 0.33 | 0.78 | 1.46 | 2.7 |
| Run-up-distance (RUD) | Xs | m | **686** | **494** | **179** | **84** | **40** |
| **Result** | | | **S1** | **S1** | **S1** | **S1** | **S1** |
| Laminar flame thickness | δ | mm | 0.1342 | 0.1023 | 0.0425 | 0.0203 | 0.0092 |
| γ - parameter | γ | (-) | 2.230 | 1.724 | 0.775 | 0.414 | 0.217 |
| D/h - parameter | D/h | (-) | 36.7 | 36.7 | 36.7 | 36.7 | 36.7 |
| Run-up-distance (RUD) | Xs | m | **1579** | **1173** | **461** | **218** | **99** |
| **Result** | | | **S1** | **S1** | **S1** | **S1** | **S1** |

**Note:** S1 – subsonic deflagration ($\sigma < \sigma^* = 3.82$); S1 - subsonic deflagration ($\sigma > \sigma^*$, $X_S > L$); S2-sonic deflagration ($\sigma > \sigma^*, X_S < L$, $h^* = 13.5\lambda > H$); D - ($\sigma > \sigma^*$, $X_S < L$, $h^* = 13.5\lambda < H$).

Table 29 Output data for hydrogen inventory, m = 41.64 kg, and stratified hydrogen-air mixture

| **Hydrogen inventory, m = 41.64 kg** | | | | | | | |
|---|---|---|---|---|---|---|---|
| **Parameter name** | **Symbol** | **Unit** | **Output values** | | | | |
| | | | **Hydrogen mole fraction, $X_{H2}$** | | | | |
| | | | **0.1** | **0.11** | **0.15** | **0.2** | **0.3** |
| Expansion ratio, σ | σ | (-) | 3.54 | 3.77 | 4.63 | 5.6 | 7.02 |
| Gradient of concentration | grad(XH2) | %H2/m | 1.8 | 2.0 | 2.7 | 3.6 | 5.5 |
| Critical expansion ratio | σ* | (-) | 5.42 | 5.42 | 5.42 | 5.42 | 5.42 |
| Detonation cell size | λ | mm | 5095 | 2320 | 361 | 44.6 | 9.7 |
| Blockage ratio | h* | m | 0.268 | 0.268 | 0.268 | 0.268 | 0.268 |
| Pre-detonation length | L | m | 78 | 78 | 78 | 78 | 78 |
| Spacing | S | m | 14 | 14 | 14 | 14 | 14 |
| DDT length | 7λ | m | 35.7 | 16.2 | 2.53 | 0.31 | 0.07 |
| Critical layer thickness | h* | m | **69** | **31** | **4.87** | **0.60** | **0.13** |

| | | | | | | | |
|---|---|---|---|---|---|---|---|
| Volume of hydrogen cloud | V | $m^3$ | 10071 | 9155 | 6714 | 5035 | 3357 |
| Cloud cross-section area | A | $m^2$ | 57.8 | 57.8 | 57.8 | 57.8 | 57.8 |
| Length of hydrogen cloud | L | m | **174.4** | **158.5** | **116.3** | **87.2** | **58.1** |
| Sound speed in products | $a_p$ | m/s | 659 | 682 | 765 | 855 | 983 |
| Laminar velocity | $S_L$ | m/s | 0.25 | 0.33 | 0.78 | 1.46 | 2.7 |
| Run-up-distance (RUD) | Xs | m | **464** | **334** | **121** | **57** | **27** |
| **Result** | | | **S1** | **S1** | **S1** | **D** | **D** |
| Laminar flame thickness | δ | mm | 0.1342 | 0.1023 | 0.0425 | 0.0203 | 0.0092 |
| γ - parameter | γ | (-) | 2.230 | 1.724 | 0.775 | 0.414 | 0.217 |
| D/h - parameter | D/h | (-) | 13.8 | 13.8 | 13.8 | 13.8 | 13.8 |
| Run-up-distance (RUD) | Xs | m | **1345** | **993** | **380** | **175** | **77** |
| **Result** | | | **S1** | **S1** | **S1** | **S1** | **S1** |

**Note:** S1 – subsonic deflagration ($\sigma < \sigma^* = 3.82$); S1 - subsonic deflagration ($\sigma > \sigma^*$, $X_S > L$); S2-sonic deflagration ($\sigma > \sigma^*, X_S < L$, $h^* = 13.5\lambda > H$); D - ($\sigma > \sigma^*$, $X_S < L$, $h^* = 13.5\lambda < H$).

### A2.7.4.Comments

The case **I-4** for car accident (5 mm TPRD device and 700 bar tank pressure) is the most typical for the short release time from 1 to 4 s after the TPRD opening (see Figure 7). The cloud of hydrogen-air mixture is elongated from 3.5 m to 10.4 m but still remains too short for flame acceleration to the speed of sound and detonation onset ($X_S > L$). The run-up distance Xs in this case is much longer (from 100 to 1580 m) independent of the cars blocked the cloud cross-section. More conservative run-up distances calculated by Eq. (14) give the values from 40 to 690 m which are still longer than the cloud length.

The case **II-4** for bus accident (5 mm TPRD device and 350 bar tank pressure) will be able for release time longer than 40 s after the TPRD opening (similar to Figure 7). The cloud of hydrogen-air mixture is elongated from 58 m to 175 m depending on average concentration. According to more conservative run-up distance evaluation Eq. (14), such length of the cloud will be enough for flame acceleration to the speed of sound ($X_S < L$) for hydrogen-air mixtures with a maximum hydrogen concentration at the ceiling from 20 to 30%H2. For leaner hydrogen concentrations (10 to 15%H2) the run-up distance will be even longer (Xs=120-464m) than the cloud of hydrogen-air mixture (from 116 m to 174 m) ($X_S > L$). According to more precise run-up distance evaluation Eq. (19), the length of the cloud will be not enough for flame acceleration to the speed of sound ($X_S < L$) for all hydrogen-air mixtures because the run-up distance will be longer (Xs=77-1345m) than the cloud of hydrogen-air mixture (from 58 m to 174 m) ($X_S > L$). The case **II-3** is the most realistic scenario for bus accident at the initial stage, after tenths of second of release time.

## A2.8 Summary

- Four cases of hydrogen cloud formation in a tunnel cross-section are analyzed for car and bus accidents:

**Case 1**: Uniform hydrogen concentration distributed over the full tunnel cross-section for the given hydrogen inventory;

**Case 2**: Uniform hydrogen concentration distributed inside a layer of hydrogen-air mixture for the given hydrogen inventory;

**Case 3**: Stratified layer of hydrogen-air mixture for the given hydrogen inventory;

**Case 4**: Stratified hydrogen-air mixture filled the whole tunnel cross-section for the given hydrogen inventory.

- Different amount of hydrogen inventory from 2.48 kg for car accident and to 41.64 kg for bus accident lead to different size of hydrogen-air cloud.
- The method of flame propagation regime evaluation is based on so called sigma-criterion for flame acceleration, lambda criterion and run-up distance criterion for detonability evaluation.
- Two scenarios (**case 1** and **case 4**) for fully filled tunnel cross-section with a hydrogen-air mixture are more typical for a very short release time. In both cases the length of the cloud is not enough for flame acceleration to the speed of sound and detonation. The flame propagates very slowly, with maximum combustion over-pressure not higher than1-2 bar.
- Two scenarios (**case 2** and **case 3**) for formation of a layer of hydrogen-air mixture are more typical for relatively long release time (order of 10 seconds). In both cases the length of the cloud is much longer and can be enough for flame acceleration to the speed of sound and detonation only in the case of bus accident if hydrogen concentration 20-30%H2 is assumed.
- For all car accidents, there is no scenario of hydrogen release with formation of detonable cloud. The flame always propagates very slowly, with a maximum combustion over-pressure not higher than1-2 bar.
- As Figure 8 shows, the real hydrogen concentration after long time release is usually lower than 15-20%$H_2$. Thus, it makes impossible the detonation scenario even for bus accident. An earlier ignition also prevents elongated cloud formation leading to detonation.
- Of course, a ventilation system reducing the maximum hydrogen concentration below 15%$H_2$ also prevent the detonation.

# A3. Problem formulation: accident in a railway tunnel

**Case (I):**

- Single rail tunnel of two-tubes tunnel with a circular cross-section 64.3 m2 (Figure 10)
- Equivalent diameter Deq=8.98 m
- Tunnel roughness equivalent to BR = 1% which is equal to 2.2 cm of roughness.
- Hydrogen inventory 5.8 kg due to the accident, then cloud formation with a late ignition.
- Uniform hydrogen-air mixture of 10 to 30%H2 in air filled a layer of h=0.6 m thick above the train. The cloud is formed in a gap between the roof of the train and the ceiling (Figure 11 a).

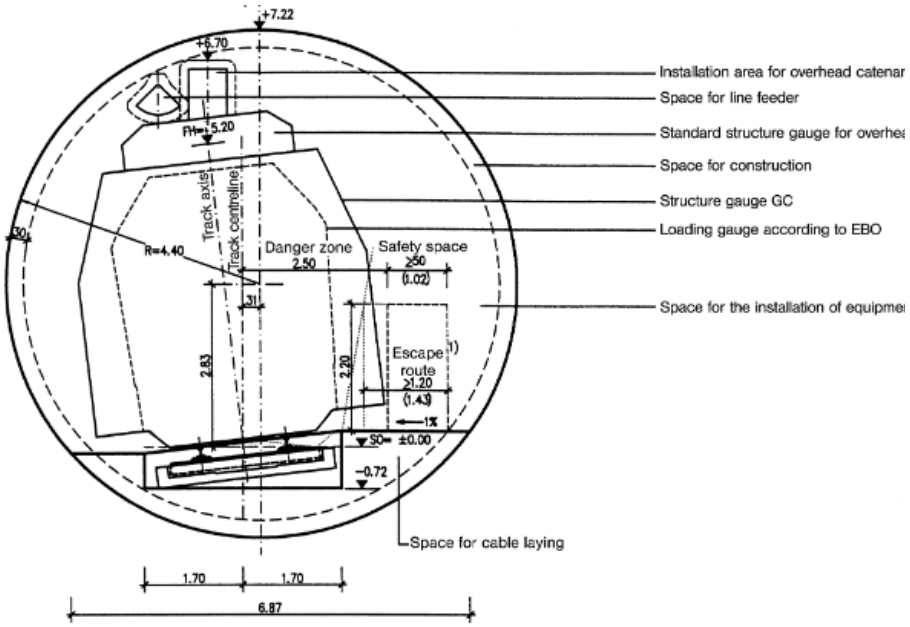


Figure 10. Rail tunnel geometry.

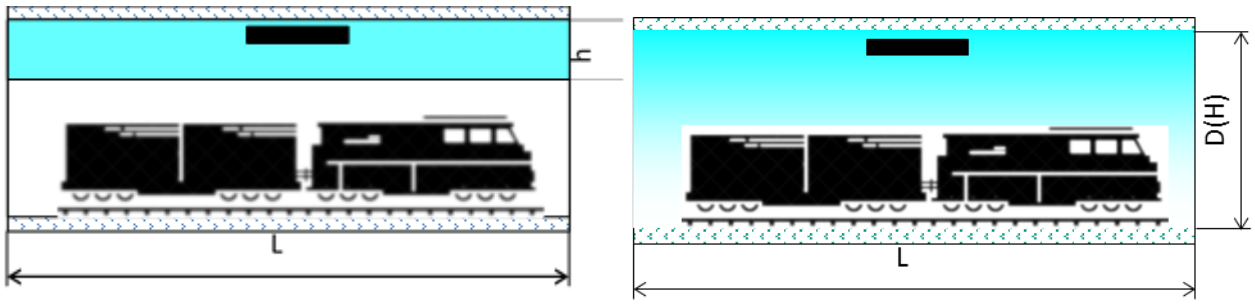


(a) (b)

Figure 11.Hydrogen cloud geometry: a layer of uniform hydrogen-air mixture (left); fully filled tunnel cross- section with a stratified hydrogen-air mixture.

**Case (II):**

- Single rail tunnel of two-tubes tunnel with a circular cross-section 64.3 m2 (Figure 10)
- Equivalent diameter Deq=8.98 m

- Tunnel blockage by the train is equivalent to BR = 40%.
- Hydrogen inventory 5.8 kg due to the accident, then cloud formation with a late ignition.
- Stratified hydrogen-air mixture filled the whole tunnel cross-section
- A linear hydrogen concentration gradient with maximum concentration 10, 15, 20, 25, 30%H2 at the ceiling and 0%H2 at the bottom of the tunnel is assumed (Figure 11 b).

**Case (III):**

- Single rail tunnel of two-tubes tunnel with a circular cross-section 53.5 m2 (Figure 10)
- Equivalent diameter Deq=8.25 m
- Tunnel blockage by the train is equivalent to BR = 40%.
- Hydrogen inventory 10 kg due to the accident, then cloud formation with a late ignition.
- Stratified hydrogen-air mixture filled the whole tunnel cross-section
- A linear hydrogen concentration gradient with maximum concentration 10, 15, 20, 25, 30%H2 at the ceiling and 0%H2 at the bottom of the tunnel is assumed (Figure 11 b).

**Case (IV):**

- Single rail tunnel of two-tubes tunnel with a circular cross-section 53.5 m2 (Figure 10)
- Equivalent diameter Deq=8.25 m
- Tunnel blockage by the train is equivalent to BR = 40%.
- Hydrogen inventory 100 kg due to severe accident, then the cloud formation with a late ignition.
- A stratified hydrogen-air mixture filled the whole tunnel cross-section
- A linear hydrogen concentration gradient with maximum concentration 10, 15, 20, 25, 30%H2 at the ceiling and 0%H2 at the bottom of the tunnel is assumed (Figure 11 b).

We consider four cases for different hydrogen clouds in a tunnel cross section.

## A3.1 Case I: Uniform hydrogen cloud filled a layer of h=0.6 m thick above the train

This option allows user calculating the possible flame propagation regimes of the uniform hydrogen-air cloud formed by the release of 5.8 kg hydrogen in an assumption of hydrogen layer formation. Five levels of average hydrogen mole fraction in the cloud from 10 to 30% H2 are analyzed.

### A3.1.1.Calculation procedure

Combustion regime is evaluated by the expansion ratio σ, detonation cell size λ and run-up-distance $X_S$. Three different regimes may occur: S1 -subsonic deflagration ($\sigma>\sigma^*$); S2-sonic deflagration ($\sigma>\sigma^*$, $X_S >> L_{H2}$); D-detonation ($X_S < L_{H2}$)

If the tunnel is considered as a rough channel with a roughness about 2 cm, the only subsonic deflagration S1 is possible in a layer of 60 cm for hydrogen inventory of 5.8 kg, independent of hydrogen concentration (up to 30%H2). The run-up distance (RUD) is longer than the length of the cloud ($X_S > L_{H2}$)

### A3.1.2.Output values

Table 30 Output data for train accident with hydrogen inventory, m = 5.8 kg (2 cm roughness)

| Hydrogen inventory, m = 5.8 kg | | | | | | | |
|---|---|---|---|---|---|---|---|
| **Parameter name** | **Symbol** | **Unit** | **Output values** | | | | |
| | | | **Hydrogen mole fraction, $X_{H2}$** | | | | |
| | | | **0.1** | **0.11** | **0.15** | **0.2** | **0.3** |
| Expansion ratio, σ | σ | (-) | **3.54** | **3.77** | **4.63** | **5.6** | **7.02** |
| Detonation cell size, λ | λ | mm | 5095 | 2320 | 361 | 44.6 | 9.7 |
| Blockage ratio, BR | BR | (-) | 0.01 | 0.01 | 0.01 | 0.01 | 0.01 |
| Volume of hydrogen cloud | V | $m^3$ | 697 | 634 | 465 | 349 | 232 |
| Length of hydrogen cloud | L | m | **383** | **436** | **320** | **240** | **160** |
| Run-up-distance (RUD) | Xs | m | **2248** | **1666** | **684** | **336** | **162** |
| **Result** | | | **S1** | **S1** | **S1** | **S1** | **S1** |

**Note:** S1 – subsonic deflagration ($\sigma < \sigma^* = 4.49$); S1 - subsonic deflagration ($\sigma > \sigma^*$, $X_S > L$);
S2 - sonic deflagration ($\sigma > \sigma^*$, $X_S < L$, $7\lambda > L$); D - ($\sigma > \sigma^*$, $X_S < L$, $7\lambda < L$).

### A3.1.3.Comments

In case **I** of a train accident, a uniform cloud as a layer of hydrogen-air mixture is formed in a gap of 0.6 m between roof of the train and a tunnel ceiling. We do not consider a blockage of tunnel cross section by the train because the cloud is above the train. The only natural roughness of tunnel inner surface plays a role for a flame acceleration. The calculations show that the required run-up distance for flame acceleration to the speed of sound and detonation onset is always shorter than the length of the cloud ($X_S > L$). Then, the only subsonic flame propagation regimes can occur with characteristic explosion overpressure 1 – 2 bar. This scenario is unrealistic because stratification of the cloud Is not taken into account. A stratification with a linear gradient of hydrogen concentration will increase the length of the clod roughly two times. Then, a detonation of the cloud with 20 and 30%H2 at the top may occur. Strong ventilation is required to avoid the gathering of more than 20% of hydrogen in the cloud.

## A3.2 Cases II-IV: Stratified hydrogen-air mixture filled the whole tunnel cross-section for the given hydrogen inventory

This case consider the calculation of possible flame propagation regimes for the most realistic scenarios of stratified hydrogen-air mixture filled the total tunnel cross-section by the release of 5.8, 10 and 100 kg of hydrogen corresponding to train accidents. Five levels of maximum hydrogen mole fraction at the top of the cloud from 10 to 30% H2 are analyzed.

### A3.2.1.Calculation procedure

Combustion regime is evaluated by the expansion ratio σ, detonation cell size λ and run-up-distance $X_S$. Three different regimes may occur: S1 -subsonic deflagration (σ>σ*); S2-sonic deflagration (σ>σ*, $X_S >> L_{H2}$); D-detonation ($X_S < L_{H2}$)

The tunnel is considered as a channel blocked in 40% by train cross-section. Different flame propagation regimes may occur in the case of hydrogen accident in a rail tunnel depending on hydrogen inventory and on maximum hydrogen concentration at the ceiling of the tunnel (from 10%H2 to 30%H2).

### A3.2.2.Output values

Table 31 Output data for hydrogen inventory, m = 5.8 kg, and stratified hydrogen-air mixture

| **Hydrogen inventory, m = 5.8 kg** | | | | | | | |
|---|---|---|---|---|---|---|---|
| **Parameter name** | **Symbol** | **Unit** | **Output values** | | | | |
| | | | **Hydrogen mole fraction, $X_{H2}$** | | | | |
| | | | **0.1** | **0.11** | **0.15** | **0.2** | **0.3** |
| Expansion ratio, σ | σ | (-) | 3.54 | 3.77 | 4.63 | 5.6 | 7.02 |
| Gradient of concentration | grad($X_{H2}$) | %H2/m | 1.1 | 1.2 | 1.7 | 2.2 | 3.4 |
| Critical expansion ratio | σ* | (-) | 4.49 | 4.49 | 4.49 | 4.49 | 4.49 |
| Blockage ratio | BR | (-) | 0.400 | 0.400 | 0.400 | 0.400 | 0.400 |
| Volume of hydrogen cloud | V | $m^3$ | 1394 | 1268 | 930 | 697 | 465 |
| Cloud cross-section area | A | $m^2$ | 60.5 | 60.5 | 60.5 | 60.5 | 60.5 |
| Length of hydrogen cloud | L | m | **23.0** | **20.9** | **15.4** | **11.5** | **7.7** |
| Run-up-distance (RUD) | Xs | m | **349** | **251** | **91** | **43** | **20** |
| **Result** | | | **S1** | **S1** | **S1** | **S1** | **S1** |

**Note:** S1 – subsonic deflagration ($\sigma < \sigma^* = 4.49$); S1 - subsonic deflagration ($\sigma > \sigma^*$, $X_S > L$);
S2-sonic deflagration ($\sigma > \sigma^*, X_S < L$); D - ($\sigma > \sigma^*$, $X_S < L$).

Table 32 Output data for hydrogen inventory, m = 10 kg, and a stratified hydrogen-air mixture

| **Hydrogen inventory, m = 10 kg** | | | | | | | |
|---|---|---|---|---|---|---|---|
| **Parameter name** | **Symbol** | **Unit** | **Output values** | | | | |
| | | | **Hydrogen mole fraction, $X_{H2}$** | | | | |
| | | | **0.1** | **0.11** | **0.15** | **0.2** | **0.3** |
| Expansion ratio, σ | σ | (-) | 3.54 | 3.77 | 4.63 | 5.6 | 7.02 |
| Gradient of concentration | grad(XH2) | %H2/m | 1.4 | 1.6 | 2.2 | 2.9 | 4.3 |
| Critical expansion ratio | σ* | (-) | 4.53 | 4.53 | 4.53 | 4.53 | 4.53 |
| Blockage ratio | h* | m | 0.400 | 0.400 | 0.400 | 0.400 | 0.400 |
| Volume of hydrogen cloud | V | $m^3$ | 2404 | 2186 | 1603 | 1202 | 801 |
| Cloud cross-section area | A | $m^2$ | 53.5 | 53.5 | 53.5 | 53.5 | 53.5 |
| Length of hydrogen cloud | L | m | **44.9** | **40.9** | **30.0** | **22.5** | **15.0** |
| Run-up-distance (RUD) | Xs | m | **321** | **231** | **84** | **39** | **19** |
| **Result** | | | **S1** | **S1** | **S1** | **S1** | **S1** |

**Note:** S1 – subsonic deflagration ($\sigma < \sigma^* = 4.53$); S1 - subsonic deflagration ($\sigma > \sigma^*$, $X_S > L$);
S2-sonic deflagration ($\sigma > \sigma^*, X_S < L$); D - ($\sigma > \sigma^*$, $X_S < L$).

Table 33 Output data for hydrogen inventory, m = 100 kg, and a stratified hydrogen-air mixture

| Hydrogen inventory, m = 100 kg | | | | | | | |
|---|---|---|---|---|---|---|---|
| **Parameter name** | **Symbol** | **Unit** | **Output values** | | | | |
| | | | **Hydrogen mole fraction, $X_{H2}$** | | | | |
| | | | **0.1** | **0.11** | **0.15** | **0.2** | **0.3** |
| Expansion ratio, σ | σ | (-) | 3.54 | 3.77 | 4.63 | 5.6 | 7.02 |
| Gradient of concentration | grad(XH2) | %H2/m | 1.4 | 1.6 | 2.2 | 2.9 | 4.3 |
| Critical expansion ratio | σ* | (-) | 4.53 | 4.53 | 4.53 | 4.53 | 4.53 |
| Blockage ratio | h* | m | 0.400 | 0.400 | 0.400 | 0.400 | 0.400 |
| Volume of hydrogen cloud | V | $m^3$ | 24041 | 21855 | 16027 | 12021 | 8014 |
| Cloud cross-section area | A | $m^2$ | 53.5 | 53.5 | 53.5 | 53.5 | 53.5 |
| Length of hydrogen cloud | L | m | **449** | **409** | **300** | **225** | **150** |
| Run-up-distance (RUD) | Xs | m | **321** | **231** | **84** | **39** | **19** |
| **Result** | | | **S1** | **S1** | **D** | **D** | **D** |

**Note:** S1 – subsonic deflagration ($\sigma < \sigma^* = 4.53$); S1 - subsonic deflagration ($\sigma > \sigma^*$, $X_S > L$);
S2-sonic deflagration ($\sigma > \sigma^*, X_S < L$); D - ($\sigma > \sigma^*$, $X_S < L$).

### A3.2.3.Comments

The cases **II to IV** for train accident are quite realistic in a tunnel (see Figure 7). The cloud of hydrogen-air mixture is elongated from 7.7 m to 450 m depending on hydrogen inventory and controlled maximum hydrogen concentration at the ceiling. Independent of hydrogen inventory, for maximum hydrogen concentration of 10 and 11%H2 the flame cannot accelerate to the speed of sound because of too small factor of expansion ratio ($\sigma < \sigma^*$). It will propagate as a slow subsonic flame. For hydrogen inventories of 5.8 and 10 kg the cloud remains too short for flame acceleration to the speed of sound and detonation onset ($X_S > L$) and also propagates as a slow flame with maximum combustion pressure 1-2 bar. Only in the case **IV** for 100 kg of hydrogen inventory the size of the cloud will be enough for flame acceleration and detonation onset at maximum hydrogen concentration above 15%. Then, it needs the ventilation to keep hydrogen concentration below 15% to prevent the detonation.

## A3.3 Summary

- Four cases of hydrogen cloud formation in a rail tunnel are analyzed for train accidents:

**Case I**: Uniform hydrogen cloud formation as a layer of h=0.6 m thick above the train (m = 5.8 kgH2);

**Case II**: A stratified hydrogen cloud fully filled the tunnel cross section (m = 5.8 kgH2);

**Case III**: A stratified hydrogen cloud fully filled the tunnel cross section (m = 10 kgH2);

**Case IV**: A stratified hydrogen cloud fully filled the tunnel cross section (m = 100 kgH2)

- Independent of hydrogen inventory, for maximum hydrogen concentration of 10 and 11%H2 the flame cannot accelerate to the speed of sound. It will propagate as a slow subsonic flame with a maximum combustion over-pressure 1-2 bar.
- Independent of maximum hydrogen concentration at the ceiling, for hydrogen inventories 5.8 and 10 kg the only slow subsonic flame with a maximum combustion over-pressure 1-2 bar may develop because too small size of the cloud.
  Only in the case **IV** for 100 kg of hydrogen inventory the size of the cloud will be enough for flame acceleration and detonation onset at maximum hydrogen concentration above 15%. Then, it needs the ventilation to keep hydrogen concentration below 15% to prevent the detonation.

# A4. Conversion units

**Pressure *P***, should be in Pascal (Pa). So whatever unit the user selects (bar, Pa, atm, MPa, kPa or psi), pressure should be converted to Pa:

- $P_{(Pa)} = P_{(atm)} \times 101325$
- $P_{(Pa)} = P_{(bar)} \times 100000$
- $P_{(Pa)} = P_{(psi)} \times 6894.76$
- $P_{(Pa)} = P_{(MPa)} \times 1000000$
- $P_{(Pa)} = P_{(kPa)} \times 1000$

Following the completion of the calculations, for the purposes of the creation of the results table, the units of pressure should be converted back into the units initially chosen by the user:

- $P_{(atm)} = \frac{P_{(Pa)}}{101325}$
- $P_{(bar)} = \frac{P_{(Pa)}}{100000}$
- $P_{(psi)} = \frac{P_{(Pa)}}{6894.76}$
- $P_{(MPa)} = \frac{P_{(Pa)}}{1000000}$
- $P_{(kPa)} = \frac{P_{(Pa)}}{1000}$

**Temperature T,** should be in Kelvin (K). So whatever unit the user selects (C or F), temperature should be converted to K:

- $T_{(K)} = T_{(C)} + 273.15$
- $T_{(K)} = (T_{(F)} + 459.67) * \frac{5}{9}$

Following the completion of the calculations, for the purposes of the creation of the results table, the units of temperature should be converted back into the units initially chosen by the user:

- $T_{(C)} = T_{(K)} - 273.15$
- $T_{(F)} = T_{(K)} * \frac{9}{5} - 459.67$

**Distance (length) L** (in our case height and width H&W), should be in meters (m). Whatever unit the user selects (ft, inch, cm), it should be converted to m:

- $L_{(m)} = L_{(ft)} \times 0.3048$
- $L_{(m)} = L_{(inch)} \times 0.0254$
- $L_{(m)} = L_{(cm)} \times 0.01$

Following the completion of the calculations, for the purposes of the creation of the results table, the units of distance should be converted back into the units initially chosen by the user:

- $L_{(ft)} = \frac{L_{(m)}}{0.3048}$
- $L_{(inch)} = \frac{L_{(m)}}{0.0254}$
- $L_{(cm)} = \frac{L_{(m)}}{0.01}$

# A5. References

Bollinger LE, Fong MC, Edse R. Experimental measurements and theoretical analysis of detonation induction distance. Am Rocket Soc J 1961;31:588.

G. Ciccarelli, S. Dorofeev, Flame acceleration and transition to detonation in ducts, Progress in Energy and Combustion Science, Volume 34, Issue 4, 2008, Pages 499-550

J. Dutton, R. Coverdill, Experiments to study the gaseous discharge and filling of vessels, Int. J. Eng. Ed. 13 (1997) 123–134.

Dorofeev S.B., Kuznetsov M.S., Alekseev V.I., Efimenko A.A., Breitung W. Evaluation of limits for effective flame acceleration in hydrogen mixtures. Journal of Loss Prevention in the Process Industries, 2001, Vol 14/6, pp. 583-589. DOI: http://dx.doi.org/10.1016/S0950-4230(01)00050-X

A. Friedrich, J. Grune, K. Sempert, M. Kuznetsov, T. Jordan, Hydrogen combustion experiments in a vertical semi-confined channel, International Journal of Hydrogen Energy, Volume 44, Issue 17, 2019, Pages 9041-9049

A.I Gavrikov, A.A Efimenko, S.B Dorofeev, A model for detonation cell size prediction from chemical kinetics, Combustion and Flame, Volume 120, Issues 1–2, 2000, Pages 19-33

Goodwin, D.G., Cantera User's Guide, Cal. Institute of Techn., Pasadena, CA, , 2001.

J. Grune, K. Sempert, H. Haberstroh, M. Kuznetsov, T. Jordan, Experimental Investigation of Hydrogen-Air Deflagrations and Detonations in Semi-Confined Flat Layers, Journal of Loss Prevention in the Process Industries, Volume 26, Issue 2, March 2013, Pages 317-323, ISSN 0950-4230

J. Grune, K. Sempert, M. Kuznetsov, T. Jordan, Experimental investigation of fast flame propagation in stratified hydrogen–air mixtures in semi-confined flat layers, Journal of Loss Prevention in the Process Industries, Volume 26, Issue 6, November 2013b, Pages 1442-1451

Dorofeev S.B., Sidorov V. P., Kuznetsov M. S., Matsukov I. D., Alekseev V. I. Effect of scale on the onset of detonations. Shock Waves, 2000, v. 10, pp. 137-149

S. Kudriakov, E. Studer, M. Kuznetsov, J. Grune, Experimental and numerical investigation of hydrogen-air deflagration in the presence of concentration gradients. Submitted to ICONE21, July 29- August 2, 2013, Chengdu, China. https://doi.org/10.1115/ICONE21-16910

Kuznetsov M, Alekseev V, Bezmelnitsyn A, Breitung W, Dorofeev S, Matsukov I, Veser A, Yankin Yu. Effect of obstacle geometry on behavior of turbulent flames, Report No. FZKA-6328, Forschungszentrum Karlsruhe/Preprint No. IAE-6137/3, RRC ''Kurchatov Institute,'' 1999.

Kuznetsov M., Alekseev V., Matsukov I., Dorofeev S. DDT in a Smooth Tube filled with Hydrogen-Oxygen Mixtures. Shock Waves, vol. 14, No 3, pp 205 - 215 (2005)

M. Kuznetsov, J. Grune, A. Friedrich, K. Sempert, W. Breitung and T. Jordan, Hydrogen-Air Deflagrations and Detonations in a Semi-Confined Flat Layer, In: Fire and Explosion Hazards, Proceedings of the Sixth International Seminar (Edited by D. Bradley, G. Makhviladze and V. Molkov), 2011, pp 125-136, http://dx.doi.org/10.3850/978-981-08-7724-8_02-05

Kuznetsov M, Matsukov I, Alekseev V, Breitung W, Dorofeev S. Effect of boundary layer on flame acceleration and DDT. In: Proceedings of 20th international colloquium on the dynamics of explosions and reactive systems, Montreal, Canada, 2005b.

Kuznetsov M, Singh RK, Breitung W, Stern G, Grune J, Friedrich A, Sempert K, Veser A. Evaluation of structural integrity of typical DN15 tubes under detonation loads. Report Forschungszentrum Karlsruhe, December, 2003.

Kuznetsov M., Xiao J., Hu P., Stratified Hydrogen Combustion and Water Spray Mitigation Tests in a Containment of 220 m3, Proc. of the Ninth International Seminar on Fire and Explosion Hazards (ISFEH9), Edited by Snegirev A., Liu N.A., Tamanini F., Bradley D., Molkov V., and Chaumeix N., Published by Saint-Petersburg Polytechnic University Press, ISBN: 978-5-7422-6498-9, DOI: 10.18720/spbpu/2/k19-129, pp. 1293-1305 (2019)

M. Kuznetsov, J. Yanez, J. Grune, A. Friedrich, T. Jordan, Hydrogen Combustion in a Flat Semi-Confined Layer with Respect to the Fukushima Daiichi Accident, Nuclear Engineering and Design, Volume 286, May 2015, Pages 36-48

M. Kuznetsov, J. Grune, S. Kobelt, K. Sempert, T. Jordan, Experiments for the hydrogen combustion aspects of ITER LOVA scenarios, Fusion Engineering and Design, Vol. 86, Issues 9–11, October 2011, Pages 2747-2752.

Laffitte P, Dumanois P. Influence of pressure on the formation of the explosive wave. Compt Rend Acad Sci Paris 1926;183:284.

L. D. Landau and E. M. Lifshiz, Hydrodynamics, Edition 3, Nauka, Moscow, 1986, 736 p

Y. Li, J. Xiao, H. Zhang, W. Breitung, J. Travis, M. Kuznetsov, T. Jordan. Analysis of transient hydrogen release, dispersion and explosion in a tunnel with fuel cell vehicles using all-speed CFD code GASFLOW-MPI. Proc. of the 8th International Conference on Hydrogen Safety (ICHS 8th) September 24-26, 2019, Adelaide (Australia), paper ID: #169, p. 1-12

Y. Li, J. Xiao, H. Zhang, W. Breitung, J. Travis, M. Kuznetsov, T. Jordan, Numerical analysis of hydrogen release, dispersion and combustion in a tunnel with fuel cell vehicles using all-speed CFD code GASFLOW-MPI, International Journal of Hydrogen Energy, Volume 46, Issue 23, 2021, Pages 12474-12486

Lindstedt RP, Michels HJ. Deflagration to detonation transitions and strong deflagrations in alkane and alkene air mixtures. Combust Flame 1989;76:169–81.

Moen, I. O., Donato, M., Knystautas, R., Lee, J. H. S. (1981) The influence of confinement on the propagation of detonations near the detonability limit. Symp. (Int.) Combust., 18th, pp. 1615--23. Pittsburgh, Pa : Combust. Inst.

Teodorczyk, A., Lee, J.H., Knystautas, R. (1988) Propagation mechanism of quasi-detonations. 22nd Symposium (Int.) on Combustion. The Combustion Institute, Pittsburgh, pp 1723–1731

Reynolds, W.C., The Element Potential Method for Chemical Equilibrium Analysis: Implementation in the Interactive Program STANJAN Version 3, Dept. of Mechanical Engineering, Stanford University, Palo Alto, California, January 1986.

W. Rudy, M. Kuznetsov, R. Porowski, A. Teodorczyk, J. Grune, K. Sempert, Critical conditions of hydrogen–air detonation in partially confined geometry. Proceedings of the Combustion Institute, Volume 34, Issue 2, 2013, Pages 1965-1972, ISSN 1540-7489

A. Veser, W. Breitung, S. B. Dorofeev, Run-up distances to supersonic flames in obstacle-laden tubes, J. Phys. IV France, 12, No 7, 2002, pp333-340, https://doi.org/10.1051/jp4:20020301